

# The Matching Principle: A Geometric Theory of Loss Functions for Nuisance-Robust Representation Learning

Vishal Rajput  
vishal.stark42@gmail.com  
KU Leuven

## Abstract

Robustness, domain adaptation, photometric and occlusion invariance, compositional generalisation, temporal robustness, alignment safety, and classical anisotropic regularisation are usually treated as separate problems with separate method families. This paper argues that much of their shared structure is one statistical problem: estimate the covariance  $\Sigma_{\text{task}} = \text{Cov}_{Q_n}(n)$  of *label-preserving* deployment nuisance, then regularise the encoder Jacobian along a matrix  $\Sigma'$  whose range *covers*  $\text{range}(\Sigma_{\text{task}})$ —the *matching principle*. CORAL, adversarial training, IRM, augmentation, metric learning, Jacobian penalties, and alignment-style constraints are different estimators of that object, not independent robustness tricks. In the linear-Gaussian model we prove closed-form optimality (Theorem A), including cube-root water-filling within the matched range; necessity of range coverage for quadratic Jacobian penalties (Theorem G); the same range dichotomy at deep global minima (Theorem  $A_{\text{global}}^*$ ); and two falsification controls (Lemma C; Corollaries E/E\*), with seven conditional consistency lemmas (D1–D7) for estimation under standard identifiability assumptions. We introduce the *Trajectory Deviation Index* (TDI), a label-free probe of embedding sensitivity when task accuracy or  $\|J\|_F$  is insufficient. Thirteen pre-registered blocks from classical ML through Qwen2.5-7B test the predicted matched->-isotropic->-wrong- $W$  ordering on geometry and deployment drift; twelve pass, and the sole exception (Office-31) is a Lemma D1 eigengap failure named before the run; at that largest scale, in a controlled alignment regime, matched style-PMH improves selective honesty and preserves Style TDI where standard DPO degrades it (§8). The contribution is naming  $\Sigma_{\text{task}}$ , stating what  $\Sigma'$  must do, and supplying a closed-form, falsifiable theory once that object is identified—not universality on every leaderboard.

## 1 Introduction

**How to read this paper.** **Act I (§2–3):** name  $\Sigma_{\text{task}}$ , the PMH loss, and why ERM cannot remove deployment drift. **Act II (§4–5):** what  $\Sigma'$  must look like (Fig. 2:  $G \rightarrow A \rightarrow B \rightarrow A^*$ ; Lemmas C, Cor. E/E\*; D1–D7). **Act III (§6–8):** geometry (TDI,  $D_N/D_S$ ), the five-step recipe, and thirteen blocks—including failures named in advance. Definitions: §2; proofs: Appendix A; headline block T7A (Qwen2.5-7B): §8.

Since 2018 the field has catalogued adversarial fragility, texture and corruption bias, domain shift, sensor and accent drift, and alignment sycophancy as *separate* problems, each with its own methods and ablations [2, 7–9, 11–13, 15]. Prior unifications (domain bounds, transfer surveys, metric learning, information bottleneck) clarify patterns but do not name a single optimal regulariser matrix, falsifiable controls, or failure modes fixed before experiments run (§3, Table 1).

## The matching principle in plain terms

**Object.**  $\Sigma_{\text{task}}$  is the covariance of ways inputs can change at deployment *without* changing the label (domain shift, noise, style, adversarial directions, ...). **Loss.** Train with task loss plus a penalty that discourages the encoder Jacobian along a matrix  $\Sigma'$  (Eq. (4) in §2). **Match.** Choose  $\Sigma'$  so its column space *covers*  $\Sigma_{\text{task}}$ ; then deployment representations stop drifting under  $Q_n$ . Wrong  $\Sigma'$  (random, isotropic-only, or signal-aligned) fails in ways the theory names *before* you run the experiment. **Thesis.** CORAL, PGD-AT, IRM, augmentation, metric learning, and Jacobian penalties are not independent methods—they are different estimators of the same  $\Sigma_{\text{task}}$ , with a single optimum once  $A_k$  is fixed.

**Why this is non-obvious.** Theorem 4.2 makes range coverage *necessary* in the full quadratic Jacobian family; Theorem 4.9 extends the dichotomy to deep global minima (Lemma 4.10 verifies expressivity); Lemmas 4.12 and Corollaries 4.13/4.14 turn the claim into falsifiable controls tested in §8.

### 1.1 The problem the field had

The post-2018 literature accumulated three structural difficulties at once. First, methods proliferated faster than the theory could organise them, leaving comparison reduced to leaderboard-driven empirical horse races. Second, every method came with its own ablation conventions—random projections, label shuffling, signal masking—without any shared understanding of why one ablation falsifies a hypothesis and another does not. Third, the *loss function* was treated as background: cross-entropy or MSE or InfoNCE was assumed, and innovation took place in architectures, data, and compute. The matching principle reorganises all three. It identifies the common population object the methods are estimating, turns ablations into named falsification tests with predicted outcomes, and promotes the loss function to a first-class design variable parametrised by one PSD matrix per nuisance type.

### 1.2 The principle, stated

Deployment variation is a law  $Q_n$  with covariance  $\Sigma_{\text{task}} = \text{Cov}_{Q_n}(n)$ ; drift is measured by  $D_Q$  and its Jacobian linearisation  $\tilde{D}_Q$  (Eqs. (3) and surrounding definitions in §2). Training adds a trace penalty along a chosen  $\Sigma' \succeq 0$  (Eq. (4)). The *matching principle* is threefold: (i) matched range  $\text{range}(\Sigma') \supseteq \text{range}(\Sigma_{\text{task}})$  drives  $\tilde{D}_Q \rightarrow 0$  in the linear model (Theorem 4.1); (ii) no other quadratic Jacobian penalty can do so without covering that range (Theorem 4.2); (iii) the same dichotomy holds at the global minimum of deep encoders under (R)–(I), with (E) verified constructively (Theorem 4.9, Lemma 4.10). When regressor energy is uniform on  $\text{range}(\Sigma_{\text{task}})$ , the optimal allocation simplifies to  $\Sigma' \propto \Sigma_{\text{task}}$ ; otherwise cube-root water-filling applies (§4.1).

**What the paper claims, in two sentences.** The thirteen empirical blocks collectively reject the null hypothesis that the matched, isotropic, and wrong-direction arms have the same effect on deployment-drift metrics, in the direction the theory predicts, across modalities (vision, speech, code, molecules, language) and scales (linear models to 7B-parameter transformers). The single failure of the matched arm to outperform a competing method (Office-31, where CORAL beats matched PMH) is itself a failure mode the framework predicts when the estimator’s eigengap is near the Wedin bound.

**What the paper does not claim.** We do not claim universality. Causal/spurious-correlation problems (Colored MNIST, Waterbirds) violate the label-preservation hypothesis that defines  $\Sigma_{\text{task}}$  and remain out of scope. We do not claim that matched PMH beats every competing method on every leaderboard; PGD-trained networks remain stronger than PMH at very large adversarial radii, and supervised accent adaptation can outperform matched PMH on WER while leaving the geometric problem un-repaired. We do not claim that the one-epoch DPO result at 7B replaces multi-epoch full-scale RLHF; it shows the mechanism in a controlled regime. These boundaries are the discipline of the framework, not its embarrassments; the framework’s main theoretical open question (optimisation reachability of the global minimum by gradient descent on a non-convex PMH loss) is named explicitly in §10 as Open Question 1.

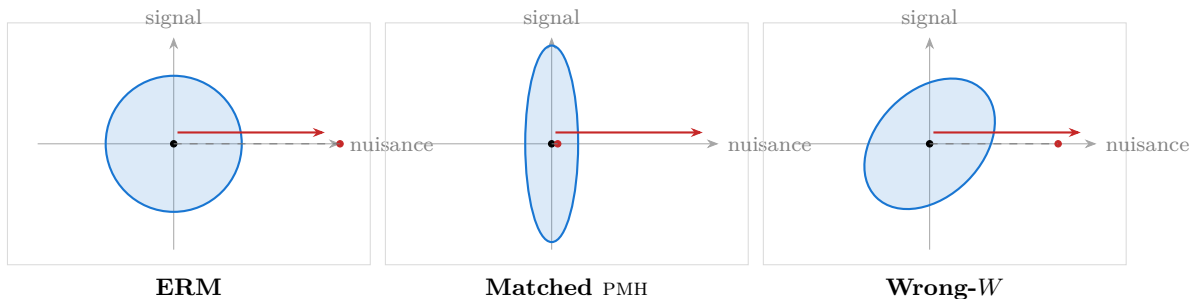


Figure 1: **The matching principle, geometrically.** Axes: signal (vertical) vs. deployment nuisance (horizontal). Blue ellipses: regions of Jacobian sensitivity; red arrow: the *same* nuisance perturbation in all panels; red dot: where the embedding moves. *Left (ERM)*: sensitivity in all directions  $\Rightarrow$  shift. *Centre (matched PMH)*: sensitivity suppressed along nuisance  $\Rightarrow$  no shift. *Right (wrong-W)*: suppression at  $45^\circ \Rightarrow$  shift remains. The theory is the choice of which directions the ellipse covers.

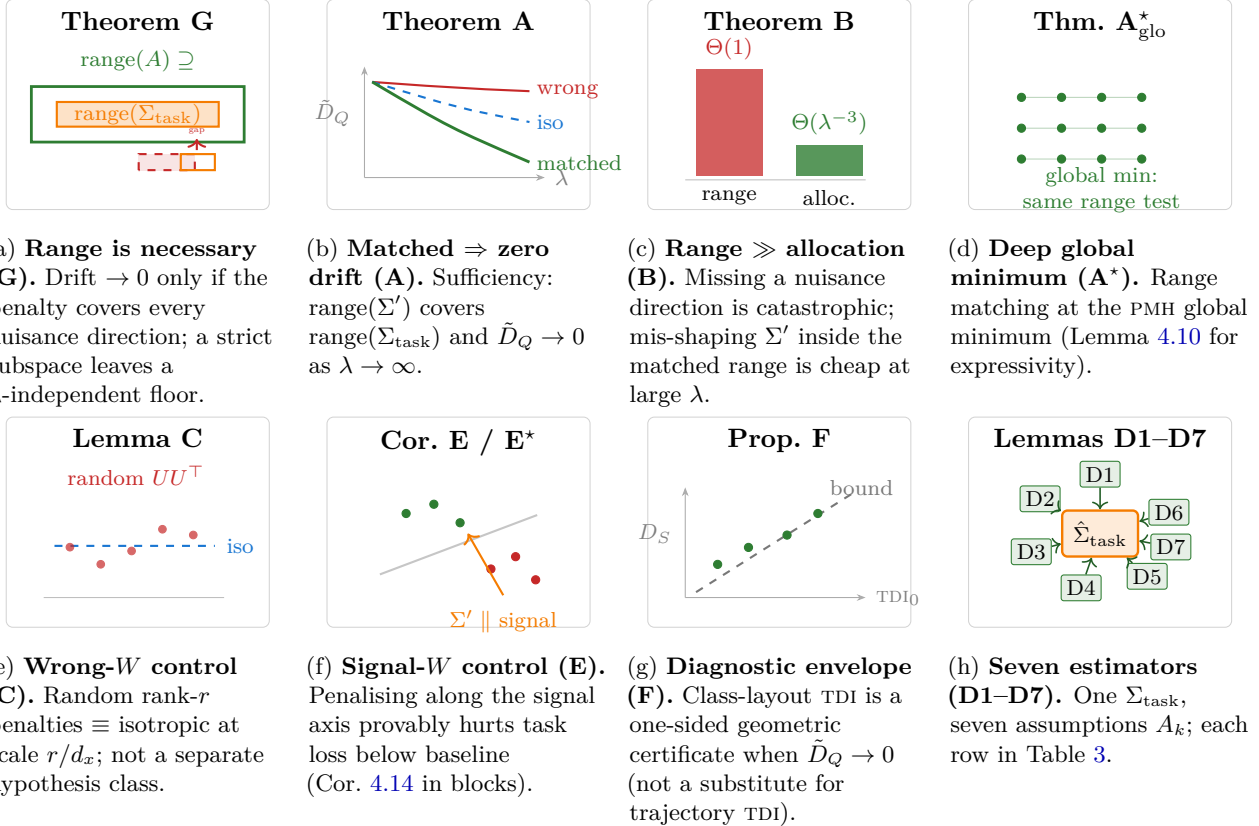


Figure 2: **Theorem map (one page)**. Row 1 (read left to right): **G** (range necessity)  $\rightarrow$  **A** (matched sufficiency)  $\rightarrow$  **B** (range vs. allocation cost)  $\rightarrow$  **A\*<sub>global</sub>** (deep global minimum). Row 2: Lemma C and Cor. E/E\* (falsification controls), Prop. F (diagnostic envelope), Lemmas D1–D7 (estimators of  $\Sigma_{\text{task}}$ ). Panel letters (a)–(h) follow this layout. Statements: §4–§6; proofs: Appendix A. Training-time  $A_{\text{train}}^*$  needs assumption (O) (§10).

## 2 Setup and definitions

We work in the Perturbation Matching Hypothesis (PMH) framework: a task loss plus a trace penalty on the encoder Jacobian, with an explicit deployment-nuisance law  $Q_n$ .

**Spaces and maps.**  $x \in \mathcal{X} = \mathbb{R}^{d_x}$ ;  $y \in \mathcal{Y}$  (discrete or continuous); encoder  $\phi_\theta : \mathcal{X} \rightarrow \mathcal{Z} = \mathbb{R}^{d_\phi}$  differentiable a.e.;  $L$ -Lipschitz decoder  $h_\theta : \mathcal{Z} \rightarrow \mathcal{Y}'$ ; predictor  $f_\theta = h_\theta \circ \phi_\theta$ ; task loss  $\mathcal{L}_{\text{task}}$  a strictly proper scoring rule throughout.

**Training distribution.**  $P(x, y)$  on  $\mathcal{X} \times \mathcal{Y}$  satisfies a *correlated-nuisance* condition: either screening confounding ( $I(n(x); y | s(x)) = 0$ ) or direct nuisance influence ( $p(y | x) \neq p(y | s(x))$  on positive measure). This is the structural precondition for the ERM blind-spot lower bound of Theorem 3.1.

**Deployment-nuisance law.** Think of  $n$  as a random *input displacement* (not a separate latent variable): noise, domain shift, style rewrite, or adversarial step. A law  $Q_n$  on  $\mathcal{X}$  has  $\mathbb{E}_{Q_n}[n] = 0$  and

$$\Sigma_{\text{task}} := \text{Cov}_{Q_n}(n) \in \mathbb{S}_{\geq 0}^{d_x} \quad (1)$$

finite.  $\Sigma_{\text{task}}$  is the paper’s central object: which directions in input space move at deployment *without changing the label*. The deployment distribution is  $P_{\text{deploy}}(x, y) = \int P(x - n, y) dQ_n(n)$ .

**Definition 2.1** (Label-preserving vs. label-changing deployment).  $Q_n$  is *label-preserving* for a training law  $P(x, y)$  if, for  $P_X$ -almost every  $x$  and  $Q_n$ -almost every  $n$ ,

$$p(y | x + n) = p(y | x) \quad (\text{equivalently } y \perp n | x \text{ when } y \text{ is deterministic}).$$

The matching principle applies to  $\Sigma_{\text{task}} = \text{Cov}_{Q_n}(n)$  under this regime. A shift is *label-changing* (out of scope) when there exists a set of positive measure with  $p(y | x + n) \neq p(y | x)$ —e.g. colour predicts  $y$  on the training distribution (Colored MNIST, Waterbirds). Then no label-preserving  $\Sigma_{\text{task}}$  exists; causal / multi-environment tools are required (§7.3, Table 8, Causal).

**Worked example (domain shift).** If training images come from source domain  $S$  and deployment images from target  $T$  with the same labels, a natural  $Q_n$  is  $n = x_T - x_S$  for paired domains. Then  $\Sigma_{\text{task}} = \text{Cov}(x_T - x_S)$  is the cross-domain Gram matrix estimated by CORAL or Lemma A.11; matched PMH penalises  $J_\phi^\top J_\phi$  along that matrix so embeddings move less when the input shifts like a real deployment shift. Table 3 (§5) lists six other instantiations.

**Drift functionals.** The embedding drift is

$$D_Q(\phi) = \mathbb{E}_{x \sim P_X, n \sim Q_n} [\|\phi(x + n) - \phi(x)\|_2^2], \quad (2)$$

and its first-order linearisation around zero-mean  $Q_n$  is

$$\tilde{D}_Q(\phi) = \mathbb{E}_x \left[ \text{Tr} \left( J_\phi(x)^\top J_\phi(x) \Sigma_{\text{task}} \right) \right] = \mathbb{E}_x \left[ \langle J_\phi(x)^\top J_\phi(x), \Sigma_{\text{task}} \rangle_F \right], \quad (3)$$

where  $\langle A, B \rangle_F = \text{Tr}(A^\top B)$  and  $J_\phi(x) = \partial\phi/\partial x|_x$  is the encoder Jacobian. The linearisation remainder is controlled by Lemma A.3 ( $|D_Q - \tilde{D}_Q| = O(\sigma^4)$  at small  $\sigma$  under a Jacobian envelope). Throughout the theory we work with  $\tilde{D}_Q$  (Jacobian-weighted, easier to optimise and bound); the

full nonlinear  $D_Q$  is what we measure in trajectory diagnostics (§6) when reporting embedding drift after training.

### Two drift quantities (do not conflate)

$\tilde{D}_Q$  (Eq. (3)): theory and PMH training—“how sensitive is the Jacobian along  $\Sigma_{\text{task}}$ ?”  $D_Q$  / TDI: post-hoc measurement on a trained model—how far do embeddings move under probe noise? They align at small  $\sigma$  (Lemma A.3) but can diverge when geometry and accuracy decouple (§7.2).

**The PMH loss family.** For any  $\Sigma' \succeq 0$  and  $\lambda > 0$ ,

$$\mathcal{L}_{\text{PMH}(\Sigma')}(\theta) = \mathcal{L}_{\text{task}}(\theta) + \lambda \mathbb{E}_x \left[ \text{Tr} \left( J_\phi(x)^\top J_\phi(x) \Sigma' \right) \right]. \quad (4)$$

Any minimiser is denoted  $\phi^{\text{PMH}(\Sigma')}$ . The *matched-PMH minimiser*  $\phi^{\text{PMH}(\Sigma_{\text{task}})}$  is the central object. In practice the trace is estimated by Hutchinson / Rademacher / paired-view surrogates; see §7 for implementation details.

**Population vs. sample.** All theoretical statements are at the population level. Finite-sample versions follow by standard concentration; empirical sections name the sample size explicitly.

**Proof map.** All proofs are in Appendix A: foundation (A.1), matching theorems, and Lemmas A.8–A.14. §8 reports thirteen *observational* blocks, not one joint inference theorem.

## 2.1 What “nuisance law” means in practice

Table 3 (§5) instantiates  $Q_n$  and  $\Sigma_{\text{task}}$  for seven nuisance families. Despite different modalities, all seven are the same statistical object with one loss template when  $\Sigma'$  is chosen to match.

**Estimability.**  $\Sigma_{\text{task}}$  is never observed directly; each block supplies  $\hat{\Sigma}_{\text{task}}^{(k)}$  under assumption  $A_k$ . When  $A_k$  is wrong or the spectrum has no gap (Office-31), the estimator is misaligned and matched PMH need not win—that is a *predicted* failure, not noise in the method. Formal rates: Lemmas A.8–A.14 (§5).

**Matched training (one recipe).** Specialising Eq. (4) with  $\Sigma' = \hat{\Sigma}_{\text{task}}^{(k)}$  from row  $k$  of Table 3 gives the *matched* loss used in every block:  $\mathcal{L}_{\text{task}} + \lambda \text{Tr}(J_\phi^\top J_\phi \hat{\Sigma}_{\text{task}}^{(k)})$ . Seven estimators, one loss template, one population object  $\Sigma_{\text{task}}$ . §4 governs match vs. mismatch; §5 governs estimation; §8 tests all seven families.

## 3 Background: correlated nuisance, isotropic PMH, and the blind spot

We begin from the *geometric blind spot* of supervised learning under label-correlated nuisance: ERM cannot drive deployment drift to zero even at infinite capacity. Within the quadratic Jacobian penalty family, isotropic noise is the unique deployment-*agnostic* choice; standard adversarial training does not implement it. The five results below are proved in Appendix A.1; the Gaussian model is Remark A.1.

**Notation bridge.** Table 1 maps CORAL, augmentation, VAT/Jacobian  $L_2$ , PGD-AT, IRM/-GroupDRO, and RLHF-style constraints to  $(A_k, \Sigma')$  rows. In every case the design question is whether  $\text{range}(\Sigma')$  covers  $\text{range}(\Sigma_{\text{task}})$  (§4, §5).

**How to read the five results.** Think of four layers: (i) ERM must keep sensitivity along nuisance-like directions (Theorems 3.1/3.2); (ii) if you do not know which directions matter, the only fair isotropic probe is  $\Sigma_\delta = \sigma^2 I$  (Proposition 3.3); (iii) PGD does not implement that probe and can distort geometry (Corollary 3.4); (iv) training can cap the penalty without tuning  $\lambda$  (Proposition 3.5). The matching principle (§4) is layer (v): when  $\Sigma_{\text{task}}$  is identifiable, set  $\Sigma' = \hat{\Sigma}_{\text{task}}$ .

**Theorem 3.1** (ERM geometric incompleteness (Gaussian)). *In the linear-Gaussian model with nuisance-label correlation  $\rho > 0$ , any minimiser  $\phi_\theta^*$  of population MSE with  $L$ -Lipschitz decoder satisfies*

$$\tilde{D}_Q(\phi_\theta^*, \sigma) \geq \frac{\sigma^2 \rho^2}{L^2},$$

*independent of model capacity and dataset size.*

**Corollary 3.2** (Strictly proper losses). *For any strictly proper scoring rule  $\mathcal{L}$ , correlated-nuisance distribution  $P$ , and Lipschitz constant  $L$ ,  $\tilde{D}_Q(\phi_\theta^*, \sigma) \geq \sigma^2 C'(P, \mathcal{L})/L^2$ , where  $C'$  is the Bregman-gap constant  $\Delta(P, \mathcal{L}) = \mathbb{E}_x[d_\psi(p(y|x) \| p(y|s(x)))]$ .*

**Proposition 3.3** (Isotropy and uniform Frobenius control). *Among zero-mean  $\delta$  with  $\text{Cov}(\delta) = \Sigma_\delta$ , the identity  $\text{Tr}(J_\phi^\top J_\phi \Sigma_\delta) = \sigma^2 \|J_\phi\|_F^2$  holds if and only if  $\Sigma_\delta = \sigma^2 I$ .*

**Corollary 3.4** (PGD training remains anisotropic). *Adversarial training under bounded PGD shrinks  $\|J_\phi \hat{\delta}^*\|$  but does not enforce isotropic Jacobian shrinkage; trajectory TDI@0 can worsen even as  $\|J\|_F$  drops (T7B: PGD-AT TDI 1.506 vs. matched 0.870; §6, §8.7).*

**Proposition 3.5** (Capped PMH fixed point). *If the PMH penalty is capped at  $\text{cap} \cdot \mathcal{L}_{\text{task}}$ , the steady-state PMH fraction is  $f = \text{cap}/(1 + \text{cap})$  with no  $\lambda$  tuning required.*

Together, these results are the floor: ERM has unavoidable drift (Theorem 3.1); isotropic noise is the unique direction-agnostic penalty (Proposition 3.3); PGD is not a substitute for matched geometry (Corollary 3.4); the cap fixes the training balance (Proposition 3.5).

**What this paper adds.** When  $\Sigma_{\text{task}}$  is estimable, *which*  $\Sigma'$  to use is no longer a modelling choice but a closed-form matching problem (§4–5), tested on thirteen blocks (§8; protocols in Appendix B).

### 3.1 Prior methods and unification attempts

Prior work unifies domain adaptation [4–6], transfer surveys [10, 17], metric learning [3], and information bottlenecks [1, 16]—but typically with bounds or narratives, not a matrix-valued training prescription, pre-registered falsification controls, or failure modes named before experiments. Table 1 maps seven standard methods to an implicit  $\Sigma'$ , the matching assumption  $A_k$ , a predicted failure when  $A_k$  fails, and the block that tests it (§4 develops the theory; §4.8 fixes three quantitative checks).

**Reading the table.** Each row is a structural identification: CORAL’s moment matching is the  $A_4$  Gram estimator; augmentation modes yield  $A_3$ ; PGD deltas yield  $A_7$ . Theorem 4.2 upgrades this from analogy to necessity: any quadratic Jacobian penalty that zeros deployment drift on all task directions must cover  $\text{range}(\Sigma_{\text{task}})$ . Rewrites for CORAL, PGD-AT, and augmentation appear in §4.3.

Table 1: Seven methods as implicit estimators of  $\Sigma_{\text{task}}$ . Columns: regularised directions, assumption  $A_k$ , predicted failure when  $A_k$  is violated, and empirical block.

Method	Implicit $\Sigma'$	Matched under	Predicted failure mode	Block
Adversarial training (PGD)	$\text{Cov}(\hat{\delta}_{\text{PGD}}^*)$	$A_7$ , PGD-delta nuisance	Range too narrow; clean accuracy collapses	T7B
CORAL	Cross-domain feature Gram	$A_4$ , hierarchical domain shift, low rank	Marginal eigengap (Wedin); fails when shift is high-rank	T1 (Office-31), T4A
IRM / Group-DRO	Per-environment penalty cov.	$A_4$ with environment labels	Spurious relation (label-changing); out of scope	cor- (scope)
Data augmentation	$\frac{1}{K} \sum_k \beta_k \beta_k^\top$ (aug. delta cov.)	$A_3$ , finite-mixture photometric/occlusion	Test-time corruption outside family	corrup- aug. T2A, T3A, T3B
Mahalanobis metric learning	Within-class scatter $S_W$	$A_1$ , low-rank subspace nuisance	Signal contamination of $\hat{W}$ at low eigengap	T1 (oracle Office-31)
Jacobian reg. / VAT	$I$ or random rank- $r$ proj.	$A_2$ , isotropic acquisition (Lemma 4.12)	Wrong- $W$ collapses to isotropic; no win over iso	T7B, T6B
RLHF style / KL-anchored DPO	Style-pair representation Gram	$A_7$ , stylistic alignment nuisance	Preference aligned with style (sycophancy)	signal T7A

## 4 The matching principle

This section states the matching-principle results (Theorems 4.1, 4.2, 4.9, 4.11; Lemmas 4.12, 4.10; Corollaries 4.13/4.14). Each has a short **intuition** paragraph before the formal statement; proofs are in Appendix A. Figure 2 summarises the map (row 1:  $G \rightarrow A \rightarrow B \rightarrow A^*$ ; row 2: falsification controls C, E, diagnostic F, estimators D1–D7).

**Reading order.** Logic:  $\mathbf{G} \rightarrow \mathbf{A} \rightarrow \mathbf{B} \rightarrow \mathbf{A}_{\text{global}}^*$  (Fig. 2); we state A before G so the optimum is concrete first. Alongside: Lemma 4.12, Corollaries 4.13/4.14. Worked identifications (CORAL / PGD-AT / augmentation) and §8 follow.

### 4.1 Theorem A: the matched penalty is the right answer

**Reader map.** Part (i): cover  $\text{range}(\Sigma_{\text{task}})$  or drift stays  $\Theta(1)$ . Part (ii): within the matched range, allocate via cube-root water-filling (QM9 tradeoff when  $\lambda$  is finite). Proof: Appendix A.2.

**Intuition.** Imagine the deployment nuisance moves your input along a small set of directions in input space. If the encoder’s Jacobian has energy along those directions, deployment perturbations shift the embedding and the model’s prediction drifts. Theorem A says: in the linear-Gaussian model, the way to eliminate this drift is to penalise the Jacobian along exactly those directions, and the penalty has to cover all of them or it fails completely.

**Theorem 4.1** (Matched- $\Sigma$  optimality; linear-Gaussian). *For the linear-Gaussian regression model (Remark A.1) with deployment-nuisance covariance  $\Sigma_{\text{task}}$ , the PMH-regularised minimiser  $w(\Sigma') = (I + 2\lambda\Sigma')^{-1}v$  satisfies*

$$\tilde{D}_Q(w(\Sigma')) \xrightarrow{\lambda \rightarrow \infty} 0 \iff \text{range}(\Sigma') \supseteq \text{range}(\Sigma_{\text{task}}).$$

When this range condition fails,  $\tilde{D}_Q(w(\Sigma'))$  converges to a constant independent of  $\lambda$ . Within the range-matched class, the trace-constrained optimum is the cube-root water-filling allocation  $\mu_i^* \propto (\tilde{v}_i^2 \lambda_i)^{1/3}$ , with the proportional rule  $\Sigma' \propto \Sigma_{\text{task}}$  recovering it under rotation-invariant regressor energy.

**What this rules out.** Missing a nuisance direction in  $\text{range}(\Sigma_{\text{task}})$  cannot be fixed by increasing  $\lambda$ ; the drift floor is structural (same geometry as the centre panel of Figure 1).

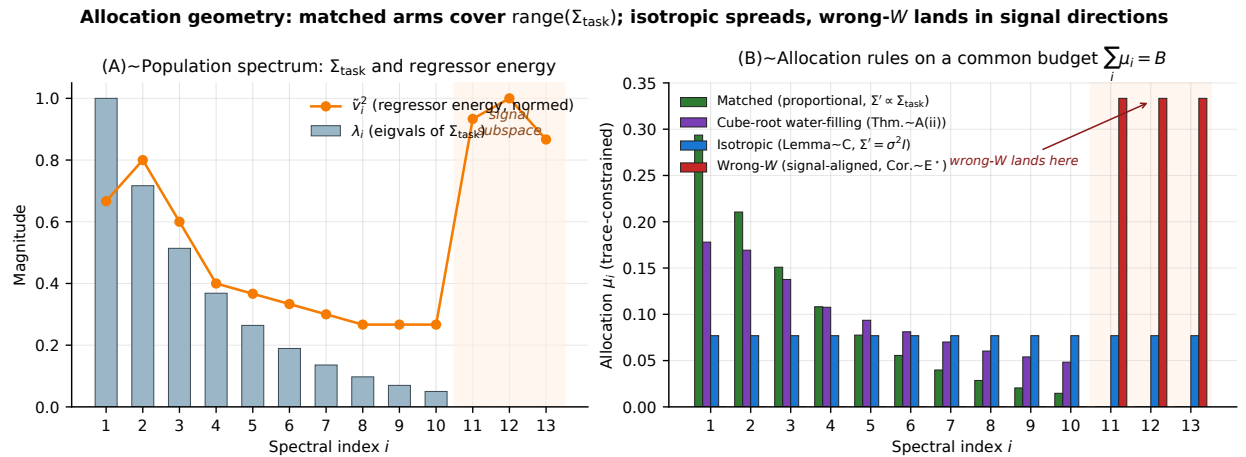


Figure 3: **Theorem 4.1(ii): where to put trace budget  $\sum_i \mu_i = B$ .** *Top:* eigenvalues of  $\Sigma_{\text{task}}$  (blue) vs. regressor energy (orange); peach band = signal outside the nuisance subspace. *Bottom:* proportional  $\Sigma' \propto \Sigma_{\text{task}}$  (default recipe), cube-root optimum, isotropic PMH, wrong- $W$  on signal (Cor. 4.14). **Range** must cover nuisances; **shape** within range matters less (Theorem 4.11).

## 4.2 Theorem G: the range condition is not optional

**Intuition.** Theorem A says range matching is *sufficient*. Theorem G says no other quadratic Jacobian penalty can succeed without doing the same thing. Across all of CORAL, adversarial training, Mahalanobis metric learning, augmentation, and Jacobian regularisation, the only way to drive deployment drift to zero on *every* task-relevant direction is to cover  $\text{range}(\Sigma_{\text{task}})$ .

**Theorem G 4.2** (Necessity of  $\text{range}(\Sigma_{\text{task}})$ ). Let  $A \succeq 0$  define any quadratic Jacobian regulariser  $\mathcal{R}_A(\phi) = \mathbb{E}_x[\text{Tr}(J_\phi^\top J_\phi A)]$ . If  $\tilde{D}_Q(w_\lambda(A)) \rightarrow 0$  for every effective regressor  $v \in \text{range}(\Sigma_{\text{task}})$ , then  $\text{range}(A) \supseteq \text{range}(\Sigma_{\text{task}})$ .

**What this rules out.** No quadratic Jacobian penalty can zero drift without covering  $\text{range}(\Sigma_{\text{task}})$ .

### 4.3 Three consequences of Theorem G: CORAL, PGD-AT, and augmentation as matched PMH

**Why this subsection exists.** Readers often treat CORAL, PGD-AT, and heavy augmentation as unrelated tricks. The point of the rewrites below is *not* to claim we invented them, but to show they already estimate different  $\hat{\Sigma}_{\text{task}}^{(k)}$  and add a Jacobian penalty along it—so disagreements between methods in §8 are disagreements about *estimator quality and eigengap*, not about whether a shared principle exists.

Theorem G says every successful quadratic Jacobian regulariser covers  $\text{range}(\Sigma_{\text{task}})$ . We make that claim concrete on the three most-cited methods: rewrite each loss until its implicit  $\Sigma'$  is visible, then read off the Lemma Dk failure mode that block tests.

**Deep CORAL is matched PMH along the cross-domain Gram.** The Deep CORAL objective [15] adds a feature-level term  $\mathcal{L}_{\text{CORAL}} = \|C_S^\phi - C_T^\phi\|_F^2$  where  $C_S^\phi, C_T^\phi$  are source and target feature covariances. Linearise the encoder around the source mean:  $\phi(x) \approx \phi(\mu_S) + J_\phi(\mu_S)(x - \mu_S)$ . Then  $C_S^\phi - C_T^\phi \approx J_\phi(\text{Cov}_S(x) - \text{Cov}_T(x)) J_\phi^\top = J_\phi \Sigma_{\text{dom}} J_\phi^\top$ , with  $\Sigma_{\text{dom}} = \text{Cov}(x_T - x_S)$  the cross-domain Gram — which is exactly the Lemma D4 estimator  $\hat{\Sigma}_{\text{task}}^{(4)}$ . By cyclic invariance of the trace and the operator-norm bound,

$$\|J_\phi \Sigma_{\text{dom}} J_\phi^\top\|_F^2 = \text{Tr}((J_\phi \Sigma_{\text{dom}} J_\phi^\top)^2) \leq \|J_\phi\|_{\text{op}}^2 \|\Sigma_{\text{dom}}\|_{\text{op}} \text{Tr}(J_\phi^\top J_\phi \Sigma_{\text{dom}}).$$

Up to bounded operator-norm factors, CORAL minimises the matched-PMH penalty along  $\Sigma_{\text{dom}}$ —a second-moment surrogate of matched PMH under  $A_4$  (Lemma A.11). When the cross-domain spectrum is nearly rank-deficient (Office-31, §8.1), the  $A_1$ /D1 eigengap condition fails and both CORAL and matched PMH degrade, as predicted.

**PGD adversarial training is matched PMH along the gradient-direction Gram.** PGD-AT [9] samples  $\hat{\delta}^*(x) = \Pi_{\|\delta\| \leq \epsilon} [\alpha \text{sign}(\nabla_x \mathcal{L})]^K$  at each step and trains on  $\mathcal{L}(\theta; x + \hat{\delta}^*)$ . Taylor-expand the per-sample loss along  $\delta$ :

$$\mathcal{L}(\theta; x + \delta) = \mathcal{L}(\theta; x) + \delta^\top \nabla_x \mathcal{L} + \frac{1}{2} \delta^\top J_\phi^\top H_\phi J_\phi \delta + O(\|\delta\|^3),$$

where  $H_\phi$  is the Hessian of the decoder. Averaging over  $\hat{\delta}^*$  at adversarial radius  $\epsilon$  gives an expected loss whose first non-trivial Jacobian term is  $\frac{\epsilon^2}{2} \mathbb{E}_x[\text{Tr}(J_\phi^\top H_\phi J_\phi \hat{\Sigma}_{\text{PGD}})]$  with  $\hat{\Sigma}_{\text{PGD}} = \text{Cov}(\hat{\delta}^*)$  — the  $A_7$  / D7 estimator. PGD-AT therefore implements matched PMH along  $\hat{\Sigma}_{\text{PGD}}$  (Lemma A.14), with two caveats: (i) decoder weighting via  $H_\phi$  is not the proportional allocation of Theorem 4.1(ii) — the Cor. 3.4 dissociation (T7B: −14.8 pp clean vs. baseline, worse TDI than PGD-delta PMH). (ii)  $\hat{\Sigma}_{\text{PGD}}$  is low-rank; explicit PMH with a full PGD-delta estimator (T7B matched arm) can match robustness with better clean accuracy.

**Data augmentation is matched PMH along the augmentation delta Gram.** A label-preserving augmentation pipeline  $\mathcal{A} = \{a_1, \dots, a_K\}$  trains on  $\mathcal{L}(\theta; a_k(x))$  for  $k \sim \text{Unif}\{1, \dots, K\}$ . Define the augmentation delta  $\delta_k = a_k(x) - x$  and its mixture covariance  $\hat{\Sigma}_{\text{aug}} = \frac{1}{K} \sum_k \mathbb{E}_x[\delta_k \delta_k^\top]$ . A second-order Taylor expansion gives the expected loss

$$\mathbb{E}_{x,k}[\mathcal{L}(\theta; a_k(x))] = \mathbb{E}_x[\mathcal{L}(\theta; x)] + \frac{1}{2} \mathbb{E}_x[\text{Tr}(J_\phi^\top H_\phi J_\phi \hat{\Sigma}_{\text{aug}})] + O(\|\delta\|^3).$$

The leading regularisation term is matched PMH along  $\hat{\Sigma}_{\text{aug}}$  (Lemma A.10). Augmentation wins when test corruptions lie in  $\text{span}\{\delta_k\}$  (T2A: +4.3 pp on ImageNet-C) and fails when they are orthogonal—the scope condition of  $A_3$ .

**Takeaway.** CORAL, PGD-AT, and augmentation are not separate mechanisms once linearised; they are matched PMH along different  $\hat{\Sigma}_{\text{task}}^{(k)}$ . Theorem 4.2 says every successful quadratic Jacobian penalty must do the same. Empirical differences reduce to estimator quality and eigengap (§8).

#### 4.4 Theorem A\*: the same dichotomy holds for deep encoders

**Intuition.** Theorems 4.1 and 4.2 are linear-Gaussian. Theorem 4.9 lifts the same range dichotomy to deep encoders at the *global* minimum under four assumptions (R, C<sup>b</sup>, E, I) below. (E) sounds abstract—“there exists  $\theta_0$  with zero PMH penalty”—but Lemma 4.10 constructs it for MLPs, CNNs, ViTs, Transformers, and GNNs (Table 2).

**Assumption 4.3** ((R) Regularity). The encoder  $\phi_\theta$  is differentiable a.e. with  $\|J_\phi(x)\|_{\text{op}} \leq M$  for all  $x$  in the support of  $P_X$ , and the regularised loss  $\mathcal{L}_{\text{PMH}(\Sigma')}^\lambda$  attains a global minimum  $\theta_\lambda^{\text{glob}}$ .

**Assumption 4.4** ((C<sup>b</sup>) Directional encoding necessity). Along any  $q \in \text{range}(\Sigma_{\text{task}})$  with label correlation, the global minimiser cannot suppress  $J_\phi$  along  $q$  below the blind-spot scale  $\rho_q^2/(2L^2)$  (Theorem 3.1, directional form).

**Proposition 4.5** ((C<sup>b</sup>) in the linear model). *In the linear-Gaussian correlated-nuisance model (Remark A.1), at any population minimiser  $\phi_\theta^*$  of a strictly proper task loss with  $\rho > 0$ , and for every unit  $q \in \text{range}(\Sigma_{\text{task}})$ ,*

$$\mathbb{E}_x \left[ q^\top J_{\phi_\theta^*}(x)^\top J_{\phi_\theta^*}(x) q \right] \geq \frac{\rho_q^2}{L^2},$$

so (C<sup>b</sup>) holds before any PMH regularisation is applied. The same bound holds for any strictly proper loss via Corollary 3.2.

**Remark 4.6** (When to expect (C<sup>b</sup>) for deep encoders). Theorem 4.9 uses (C<sup>b</sup>) only in the *necessary* direction: if  $\text{range}(\Sigma') \not\supseteq \text{range}(\Sigma_{\text{task}})$ , the global PMH minimiser cannot eliminate drift along a missing direction by an unpenalised Jacobian shortcut. For deep networks we treat (C<sup>b</sup>) as the directional lift of Theorem 3.1/Corollary 3.2: it is expected when (i) the task loss is strictly proper, (ii) deployment nuisance is label-correlated in the sense of §2, and (iii) the encoder Jacobian along  $q \in \text{range}(\Sigma_{\text{task}})$  is not already driven to zero by the task loss alone. A full characterisation of (C<sup>b</sup>) on non-convex landscapes is Open Question (O) (Table 8); experiments are consistent with the linear prediction (e.g. T7B PGD-AT: high robustness, poor isotropic TDI).

**Assumption 4.7** ((E) Expressivity). For the encoder class under study, there exists  $\theta_0$  with  $\mathbb{E}_x[\text{Tr}(J_{\phi_{\theta_0}}^\top J_{\phi_{\theta_0}} \Sigma')] = 0$  and finite task loss  $\mathcal{L}_{\text{task}}(\theta_0) < \infty$ .

**Assumption 4.8** ((I) Identifiability on  $\text{range}(\Sigma_{\text{task}})$ ). Every direction in  $\text{range}(\Sigma_{\text{task}})$  that carries regressor energy in the linearised model has non-zero coupling to the deployment drift functional: if  $q \in \text{range}(\Sigma_{\text{task}})$  and  $q^\top \Sigma_{\text{task}} q > 0$ , then  $\tilde{D}_Q$  cannot vanish along  $q$  unless the Jacobian is suppressed along  $q$ .

**Theorem A\*<sub>global</sub> 4.9** (Range-matching dichotomy for deep encoders). Under (R), (C<sup>b</sup>), (E), (I) and at the global minimum  $\theta_\lambda^{\text{glob}}$  of  $\mathcal{L}_{\text{PMH}(\Sigma')}^\lambda$ :

$$\text{range}(\Sigma') \supseteq \text{range}(\Sigma_{\text{task}}) \implies \tilde{D}_Q(\theta_\lambda^{\text{glob}}) = O(1/\lambda) \rightarrow 0,$$

$$\text{range}(\Sigma') \not\supseteq \text{range}(\Sigma_{\text{task}}) \implies \tilde{D}_Q(\theta_\lambda^{\text{glob}}) = \Theta(1) \text{ along the missing direction.}$$

Table 2:  $\mathcal{C}_{\text{NRP}}$ : architectures with constructive (E) via Lemma 4.10.

Family	First-layer map $W^{(1)}$
MLP / ConvNet / ResNet	Linear or <code>conv1</code> on inputs
ViT / Transformer LLM	Patch or token embedding
GNN + input MLP; Whisper stem	Feature projection; spectrogram conv

**Lemma 4.10** (D-ML; constructive verification of (E)). *If  $\phi_\theta(x) = \psi(W^{(1)}x + b; \theta_{\text{rest}})$  with non-residual input projection  $W^{(1)}$ , there exists  $\theta_0$  with zero PMH trace along  $\Sigma'$  and finite task loss. Class  $\mathcal{C}_{\text{NRP}}$  (Table 2) includes MLPs, CNNs, ResNets, ViTs, Transformers, GNNs, and Whisper-style encoders.*

**Open endpoint (O).** Theorem 4.9 is a *global*-minimum statement. Whether gradient descent reaches it is assumption (O); experiments are consistent but a proof is open (§10, Appendix A.5).

#### 4.5 Theorem B: missing the range is catastrophic; mis-allocating is cheap

**Intuition.** Theorem A asks two separate questions: (1) “Did you penalise the *right subspace*?” and (2) “Given the right subspace, did you put enough penalty mass on each nuisance direction?” **Wrong range** means  $\Sigma'$  misses a direction of  $\Sigma_{\text{task}}$ —drift stays  $\Theta(1)$  no matter how large  $\lambda$  is (Figure 1, right). **Wrong allocation** means the range is correct but  $\Sigma'$  is poorly shaped inside it—extra drift is only  $\Theta(\lambda^{-3})\|\Sigma' - \Sigma^*\|_F^2$  and vanishes relative to  $\Theta(\lambda^{-2})$  drift as  $\lambda \rightarrow \infty$  (Figure 3).

**Theorem 4.11** (Mismatch cost). *For range mismatch,  $\tilde{D}_Q(w(\Sigma')) - \tilde{D}_Q(w(\Sigma^*)) = \Theta(1)$ , independent of  $\lambda$ . For allocation mismatch within the range-matched class, the excess drift is at least  $\Theta(\lambda^{-3})\|\Sigma' - \Sigma^*\|_F^2$ , vanishing relative to the absolute drift  $\Theta(\lambda^{-2})$  as  $\lambda \rightarrow \infty$ .*

**Practice.** Estimate  $\text{range}(\Sigma_{\text{task}})$  first; use  $\Sigma' \propto \Sigma_{\text{task}}$  as default (all blocks do).

#### 4.6 Lemma C: random penalty directions reduce to isotropic

**Intuition.** The usual wrong- $W$  ablation (random rank- $r$  projector) is isotropic PMH at scale  $r/d_x$  in expectation (Lemma 4.12), not a separate hypothesis class.

**Lemma 4.12** (Stiefel-manifold equivalence). *If  $U \in \mathbb{R}^{d_x \times r}$  is uniform on the Stiefel manifold, then  $\mathbb{E}_U[UU^\top] = (r/d_x)I$ . The deviation  $\|UU^\top - (r/d_x)I\|_{\text{op}}$  concentrates at rate  $O(\sqrt{r \log d_x/d_x})$ .*

**Practice.** Matched must beat *both* isotropic and wrong- $W$ ; beating only wrong- $W$  is inconclusive.

#### 4.7 Corollaries E and E\*: penalising along the signal hurts

**Intuition.** The wrong- $W$  control is the random-direction ablation. The signal- $W$  control is the wrong-direction ablation: deliberately penalise along the signal axis (the directions that the label depends on). Corollaries E/E\* say this provably increases task risk—at rate  $\Omega(\rho^4)$  when the loss is smooth at its minimum, and  $\Omega(\rho^2)$  when the loss has a non-vanishing subgradient (SVM hinge, finite-horizon cross-entropy, max-margin segmentation). This is why the keyword-PMH arm in T5B and the isotropic-pixel arm in T4B fail; in both cases the regulariser is incident on signal directions.

**Corollary 4.13** (Smooth task loss). *If  $R(\phi)$  is smooth at  $\phi^*$  with positive Hessian along signal  $s$  and  $s^\top \Sigma' s \geq \rho_{\text{signal}}^2 > 0$ , then  $R(\phi^{\text{PMH}(\Sigma')}) - R(\phi^*) \geq c_R \rho_{\text{signal}}^4$ .*

**Corollary 4.14** (Margin-active task loss). *Under a non-vanishing subgradient along  $s$  (hinge, finite-horizon cross-entropy, max-margin segmentation), the leading penalty is  $\Omega(\rho_{\text{signal}}^2)$ .*

**Mapped failures (§8.8).** Not every negative result is a surprise: Office-31 is a Lemma A.8 eigengap failure; Cityscapes iso-pixel and T5B keyword-PMH are Corollary 4.14 signal penalties; QM9 at large noise is a Theorem 4.1(ii) clean-robust tradeoff when the allocation cannot be monotone in both.

## 4.8 Three quantitative predictions, three verifications

A claim is falsifiable only if the wrong ablations are specified in advance. We use three controls on every block: **isotropic** PMH (no directional information), **wrong- $W$**  (random rank- $r$  subspace), and **signal-aligned** PMH (penalise the label direction). Lemma 4.12 predicts wrong- $W$  should track isotropic; Corollary 4.14 predicts signal-PMH should *hurt*; Corollary 3.4 predicts PGD-AT should not sit on the same geometry-accuracy curve as matched PMH. The box below records the sharpest numerical checks (full tables: Appendix B).

### Three predictions fixed before experiments

1. **Wrong- $W \approx$  isotropic** (Lemma 4.12, T7B). Predicted  $D_N/D_S$  gap  $\leq 5\%$ ; observed 2.98 vs. 3.11 (**4.2%**).
2. **Signal-PMH hurts** (Cor. 4.14, T5B). Predicted below B0; observed `rename_bacc_ratio` 0.830  $\rightarrow$  **0.738**.
3. **PGD-AT off the geometry-accuracy Pareto** (Cor. 3.4, T7B). PGD@4 **44.8%** but clean **64.6%** vs. B0 **79.4%** (**-14.8 pp**); PGD-delta PMH TDI **0.870** vs. PGD-AT **1.506**.

## 5 Seven estimators of $\Sigma_{\text{task}}$

Given  $\Sigma_{\text{task}}$ , the remaining design choice is *how to estimate it* from data. **Implementers:** choose  $A_k$  via §5.1, pick the row in Table 3, follow §7, run wrong- $W$  and signal- $W$  controls. **Readers of results:** §8 and Appendix B. If the eigengap is small, expect the Office-31 pattern (Lemma D1) rather than a silent bug. Formal statements and rates: Appendix A.9. When several nuisances co-occur, compose penalties additively (e.g. T2A + T3B).

### 5.1 Practitioner guide: choosing $A_k$ and pre-flight checks

**Choosing  $A_k$  (symptom  $\rightarrow$  row).** Use Table 4 after inspecting how deployment shifts inputs *without relabelling*. When two stories apply, use the dominant deployment shift for the matched arm and add the second penalty additively (Step 2' below).

**Multiple nuisances.** When acquisition noise *and* photometric modes both move deployment inputs (Type 2+Type 3), use

$$\mathcal{L} = \mathcal{L}_{\text{task}} + \lambda_2 \text{Tr}(J^\top J \hat{\Sigma}^{(2)}) + \lambda_3 \text{Tr}(J^\top J \hat{\Sigma}^{(3)}),$$

with separate caps (Prop. 3.5) per term. T2A+T3B is the canonical composition in the programme.

**Eigengap pre-flight (rank- $r$  estimators, Lemmas D1/D3/D4/D7).** Let  $\hat{C}$  be the sample second-moment matrix your estimator targets (cross-domain deltas, aug. Gram, style Gram, etc.)

Table 3: Master index: nuisance family, deployment law, assumption  $A_k$ , Lemma  $Dk$  estimator, and test blocks. Rates and proofs: Appendix A.9.

Family	$A_k$	D	$Q_n / \Sigma_{\text{task}}$	Estimator $\hat{\Sigma}_{\text{task}}$	Blocks
Subspace	1	1	$n=W\eta; WW^\top$	Top- $r$ SVD	cross-domain T1
Isotropic	2	2	$\mathcal{N}(0, \sigma^2 I)$	$\hat{\sigma}^2 I$	T2A, T2B
Photometric	3	3	aug. modes $\beta_k$	$\frac{1}{K} \sum_k \mathbb{E}[\beta_k \beta_k^\top]$	T3A, T3B
Domain	4	4	paired $x_T - x_S$	Per-layer Gram	cross-domain T4A, T4B
Compositional	5	5	coord. spike on $\mathcal{V}_n$	Cov. on nuisance block	T5A, T5B
Temporal	6	6	$\Delta h$ along sequence	Content-residual / sensor scatter	T6A, T6B
Adv. / align.	7	7	PGD $\hat{\delta}^*$ or style shift	PGD-delta / Gram	style-pair T7A, T7B

and  $\gamma_r := \lambda_r(\hat{C})/\lambda_{r+1}(\hat{C})$  the rank- $r$  ratio gap. Lemma A.8 (Appendix A.9) gives  $\|\Pi_{\hat{W}} - \Pi_W\|_F \lesssim 2\|\hat{C} - C\|_{\text{op}}/\gamma$  with  $\gamma = \lambda_r(C) - \lambda_{r+1}(C)$  at population. *Practical rule* (before training):

1. Compute  $\gamma_r$  on held-out deployment pairs / nuisance samples.
2. **Pass** if  $\gamma_r \geq 1.2$  and  $\lambda_{r+1}/\lambda_r \leq 0.95$ .
3. **Marginal** if  $1.0 < \gamma_r < 1.2$  (Office-31 used  $\gamma_r \approx 1.03$  at rank 32): expect Lemma D1 failure—report CORAL/second-moment baselines, do not treat a matched-arm loss as definitive.
4. **Fail** if  $\gamma_r \approx 1$ : fall back to  $A_2$  isotropic PMH or a non-subspace baseline; wrong- $W$  should track isotropic (Lemma 4.12).

**Sample size.** Require  $N \gtrsim cr/\gamma^2$  deployment pairs for  $c \approx 4$  when using the Lemma A.8 rate  $\|\hat{C} - C\|_{\text{op}} = O_P(\sigma_1/\sqrt{N})$ .

**D1 ( $A_1$ , subspace).** Requires  $n \approx W\eta$  with signal orthogonal to  $\text{range}(W)$ . Recovery needs a spectral gap (Wedin/Davis–Kahan); marginal gap  $\Rightarrow \hat{W}$  unreliable and matched penalty may lose to a stronger second-moment method (Office-31 pattern). Verdicts: §8.1.

**D2 ( $A_2$ , isotropic).** When deployment noise has no preferred direction, the matched penalty is  $\hat{\sigma}^2 I$ —the only fair direction-agnostic choice (Proposition 3.3), not a fallback. Wrong- $W$  should track isotropic (Lemma 4.12). Verdicts: §8.2.

**D3 ( $A_3$ , photometric/occlusion).** Finite label-preserving modes  $\{\beta_k\}$ ; estimator is their empirical second moment. Fails when test corruptions lie outside  $\text{span}\{\beta_k\}$ . Verdicts: §8.3.

**D4 ( $A_4$ , hierarchical domain).** Shift acts at multiple representation depths; per-layer cross-domain Gram is the matched object (pixel-level isotropic PMH is a mis-specified estimator). Verdicts: §8.4.

**D5 ( $A_5$ , compositional).** Known coordinate partition into signal vs. nuisance blocks; estimator is empirical covariance on the nuisance block only. Penalising the signal block is Corollary 4.14 (keyword-PMH arm). Verdicts: §8.5.

Table 4: Heuristic map from deployment symptoms to assumption  $A_k$  (confirm with wrong- $W$  / signal- $W$  controls).

Deployment symptom	$A_k$	Typical block
Known / estimable low-rank subspace (digits, domains)	$A_1$	T1
No preferred direction (sensor/- corruption noise)	$A_2$	T2
Finite aug. / photometric modes you train on	$A_3$	T3
Multi-layer domain shift (texture $\rightarrow$ semantics)	$A_4$	T4
Nuisance in named coordinates (atoms, tokens)	$A_5$	T5
Label-constant temporal / speaker / sensor drift	$A_6$	T6
Learned deltas (PGD) or style rewrites (alignment)	$A_7$	T7

**D6 ( $A_6$ , temporal/sequential).** Label-constant content with speaker/sensor variation; content-residual or sensor scatter estimates  $\Sigma_{\text{task}}$ . Supervision can improve task metrics without fixing geometry (§7.2). Verdicts: §8.6.

**D7 ( $A_7$ , learned nuisance).** PGD-delta Gram (vision) or style-pair Gram (alignment). Better subspace estimates should improve matched robustness monotonically; PGD-AT may trade clean accuracy for adversarial robustness (Corollary 3.4). Verdicts: §8.7, §8.

**Summary.** Lemmas D1–D7 are *conditional* consistency results—eigengap failure (D1), signal leakage (D5), or missing style axis in  $\hat{W}$  (D7) each predict a named negative *before* the block runs. §6 defines geometry probes; §7 is the training procedure.

## 6 Mechanistic diagnostics: TDI and directional drift

The matching principle is stated in terms of  $\tilde{D}_Q(\phi)$  (Eq. (3)). This section defines three *post-hoc* probes used in every block of §8: **trajectory** TDI (isotropic input noise, label-free), **class-layout**  $\text{TDI}_0^{\text{cls}}$  or **Style** TDI (label- or style-structured embeddings), and  $D_N/D_S$  (directional drift when  $\hat{W}$  is available). They track geometry, not accuracy; when geometry and task metrics disagree, that is a predicted dissociation (§7.2). TDI complements accuracy and  $\|J_\phi\|_F$ : it probes fresh isotropic input noise on a fixed encoder (orientation-sensitive), whereas CKA compares two fixed clouds and task accuracy conflates decoder and geometry. Class-layout TDI is one-sided only (Prop. 6.2); never report it without trajectory TDI or  $D_N/D_S$  when subspaces are available.

### Diagnostic family at a glance (three different questions)

Probe	When to use	What it answers
Trajectory TDI@0	Isotropic input noise on deep nets (Types 2, 6, 7B)	Does the encoder wiggle under unstructured $\delta$ ? Tracks $\tilde{D}_Q$ when $\Sigma_{\text{task}} = \sigma^2 I$ .
TDI <sub>0</sub> <sup>cls</sup>	You have class labels on a probe set (Types 4A, 7B table)	Is class structure tight vs. separated? <i>Not</i> a substitute for trajectory TDI.
$D_N/D_S$	You estimated a nuisance subspace $\hat{W}$ (Types 3–7)	Is drift along $\hat{W}$ suppressed vs. orthogonal directions? Falsifies wrong- $W$ (Lemma 4.12).
Style TDI	LLM style rewrites, same content (T7A)	Does hidden-state geometry preserve under preference-correlated style?

**Common mistake:** reporting low class-layout TDI as “low drift” without trajectory TDI or  $D_N/D_S$ —collapsed or trivial layouts can score well (Prop. 6.2, one-sided only).

## 6.1 From deployment drift to a measurable index

We use  $D_Q$  and  $\tilde{D}_Q$  from §2 (Eqs. (3) and the nonlinear definition above it). For  $n = \delta \sim \mathcal{N}(0, \sigma^2 I)$ , Lemma A.3 gives  $D_Q = \tilde{D}_Q + O(\sigma^4)$ , so trajectory TDI at small  $\sigma$  reports the same isotropic sensitivity that Theorems 3.1 and 4.1 bound—not task loss.

## 6.2 Trajectory Deviation Index (primary, label-free)

**Definition 6.1** (Trajectory Deviation Index). Let  $\phi^{(1:\ell)}$  denote the representation after the first  $\ell$  layers of a depth- $L$  encoder  $\phi$ . For perturbation strength  $\sigma > 0$  and  $\delta \sim \mathcal{N}(0, \sigma^2 I_d)$ , the *Trajectory Deviation Index* is

$$\text{TDI}(\phi, \sigma) := \frac{1}{L} \sum_{\ell=1}^L \frac{\mathbb{E}_{x, \delta} [\|\phi^{(1:\ell)}(x + \delta) - \phi^{(1:\ell)}(x)\|_2^2]}{\mathbb{E}_x [\|\phi^{(1:\ell)}(x)\|_2^2]}. \quad (5)$$

Lower is better: an encoder with small, layer-balanced displacement under isotropic input noise scores low; an encoder that “wiggles” strongly along many directions at many depths scores high.

**Clean-input limit.** We write  $\text{TDI@0}(\phi) := \lim_{\sigma \rightarrow 0^+} \text{TDI}(\phi, \sigma)$  and estimate it at  $\sigma = 0.01$  in all experiments (well below training noise; Taylor remainder  $O(\sigma^2)$  gives  $< 0.1\%$  relative error at this scale). Layer-averaging is used for deep ViTs and ResNets (Types 2, 4, 7B); a single final-layer probe is used when only one embedding is available (e.g. CLS or graph readout).

**Link to  $\tilde{D}_Q$ .** At small  $\sigma$ , expanding  $\phi(x + \delta) - \phi(x) \approx J_\phi(x)\delta$  in Eq. (5) yields

$$\text{TDI}(\phi, \sigma) \approx \frac{\sigma^2}{L} \sum_{\ell=1}^L \frac{\mathbb{E}_x [\|J_{\phi^{(1:\ell)}}(x)\|_F^2]}{\mathbb{E}_x [\|\phi^{(1:\ell)}(x)\|_2^2]} \propto \sigma^2 \tilde{D}_Q(\phi) \quad (\text{isotropic } \Sigma_{\text{task}} = \sigma_{\text{task}}^2 I), \quad (6)$$

so TDI measures exactly the isotropic path-length distortion that Theorem 3.1 bounds, normalised by representation scale. It is a *post-hoc, label-free* probe complementary to Eq. (4), not a substitute for accuracy or CKA.

### 6.3 Class-layout TDI<sub>0</sub> (labeled probe)

When class labels are available on a held-out probe set, we report a second statistic that does *not* require injecting input noise, but measures how tightly each class cluster sits relative to between-class separation:

$$\text{TDI}_0^{\text{cls}}(\phi) := \frac{\bar{d}_{\text{intra}}(\phi)}{\bar{d}_{\text{inter}}(\phi)}, \quad (7)$$

where  $\bar{d}_{\text{intra}}$  is the mean pairwise distance among same-class embeddings and  $\bar{d}_{\text{inter}}$  is the mean distance between class centroids (embeddings  $L_2$ -normalised; up to 200 samples per class). This is the probe used for T4A/T4B pixel-aligned tables and for T7B `compute_tdi_cls`; it coincides with the layout index reported alongside trajectory TDI in Type 2 replication code. Lower means tighter class structure relative to separation.

**Proposition 6.2** (Proposition F: one-sided layout envelope). *If the linearised deployment drift vanishes,  $\tilde{D}_Q(\phi) \rightarrow 0$ , then*

$$\text{TDI}_0^{\text{cls}}(\phi) \leq \Phi(d_{\text{between}}(\phi)),$$

where  $d_{\text{between}}$  is mean inter-class centroid distance and  $\Phi : \mathbb{R}_{\geq 0} \rightarrow \mathbb{R}_{\geq 0}$  is continuous and increasing, depending only on latent class geometry, not on  $Q_n$ .

**Proof sketch.** Zero drift implies  $\phi(x+n) - \phi(x) = o(\|n\|)$  for  $n$  in the deployment subspace, so any layout statistic computed under  $Q_n$  perturbation collapses to the clean embedding geometry, which is bounded by inter-class separation via standard discriminant arguments. Full proof in Appendix A.10. *One-sided only:* low  $\text{TDI}_0^{\text{cls}}$  does not imply low  $\tilde{D}_Q$  (collapsed classes can score artificially low); we never use it as the sole metric.

### 6.4 Directional drift $D_N, D_S$

When an estimated nuisance subspace  $\hat{W} \in \mathbb{R}^{d_x \times r}$  is available (Types 3–7), we report mean feature drift under equal-energy probes in  $\text{span}(\hat{W})$  versus its orthogonal complement:

$$D_N(\phi) := \mathbb{E}_{x,z} \left[ \|\phi(x + \Pi_{\hat{W}} z) - \phi(x)\|_2 \right], \quad (8)$$

$$D_S(\phi) := \mathbb{E}_{x,z} \left[ \|\phi(x + \Pi_{\hat{W}^\perp} z) - \phi(x)\|_2 \right], \quad (9)$$

with  $z \sim \mathcal{N}(0, \sigma^2 I_{d_x})$  and equal total noise power in both arms (Appendix B.13). The ratio  $D_N/D_S$  tests Lemma 4.12: wrong- $\hat{W}$  should match isotropic PMH (T7B: 2.98 vs. 3.11, 4.2% gap); matched  $\hat{W}$  should suppress  $D_N$  (T7B PGD-delta:  $D_N/D_S = 0.19$ ).

### 6.5 Style TDI (alignment blocks)

For Type 7A LLM alignment, labels are style variants of the same content rather than classes. *Style* TDI applies the same ratio as Eq. (7) to hidden states: within-prompt spread across six style rewrites divided by between-prompt centroid distance (96 prompts  $\times$  6 styles; lower is better). It is the geometry headline for the DPO arm in §8; behavioural sycophancy uses separate reward-model probes (protocol: Appendix B.12).

### 6.6 Reporting convention

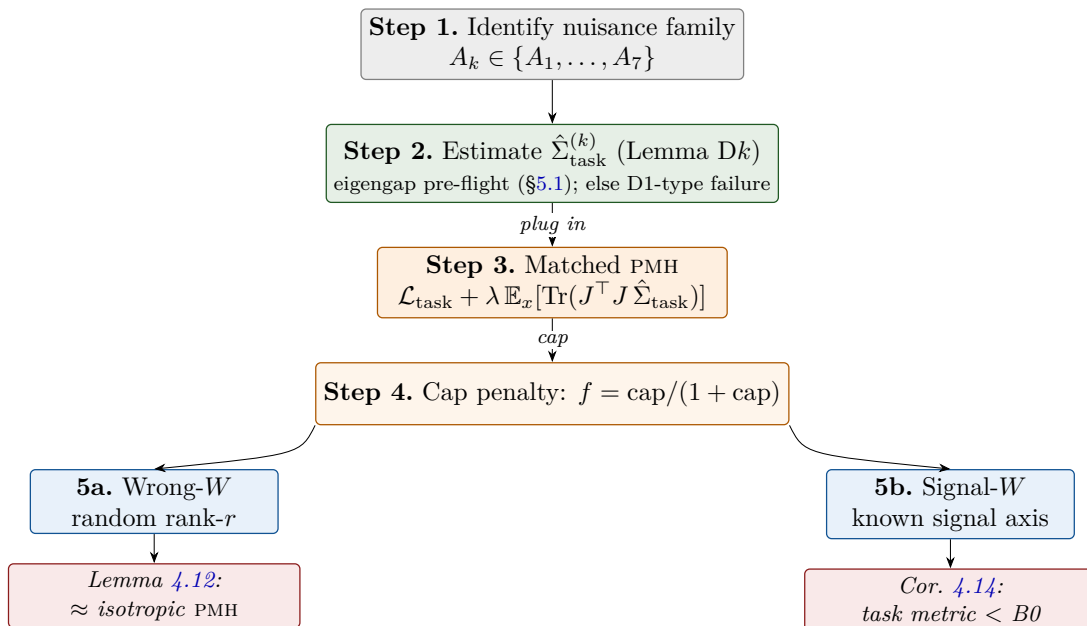
**Bridge to experiments.** Every block in §8 reports at least one diagnostic from this section *and* a task metric; the recipe in §7 is how  $\hat{\Sigma}_{\text{task}}$  is chosen before those numbers are computed.

**Which variant where.** Unless a table caption says otherwise: **trajectory** TDI@0 (Eq. (5)) for isotropic input-Gaussian probes on deep encoders (Types 2, 4B pixel probe, 6, 7B); **class-layout** TDI<sub>0</sub><sup>cls</sup> (Eq. (7)) for labelled embedding tables (Types 4A, 7B cls column); **Style** TDI (Eq. (7) on style rewrites) for Type 7A alignment (Appendix B.12). Appendix B defers to this section for definitions; task captions name the variant explicitly when both appear in one block.

We always report (**trajectory or layout**) TDI, optional  $D_N/D_S$ , and the task metric **separately**. When geometry improves but accuracy does not (T6A: matched PMH best TDI, accent head best WER), that is a predicted dissociation, not a failure of either measurement.

## 7 Practice: a five-step recipe and the scope of the principle

The theory of §4–5 is constructive: pick  $A_k$ , estimate  $\hat{\Sigma}_{\text{task}}$ , add the trace penalty, cap it, and run two controls. Figure 4 is the same pipeline; the numbered box below is the prose version.



Estimator key (Table 3): D1 cross-domain SVD • D2  $\hat{\sigma}^2 I$  • D3 aug-delta • D4 layer Gram • D5 coord. cov • D6 residual scatter • D7 PGD-delta / style Gram

Figure 4: **Five-step recipe (flow)**. Steps 1–3: nuisance family  $A_k \rightarrow$  Lemma Dk estimator  $\rightarrow$  matched PMH loss. Step 4: cap (Prop. 3.5). Step 5: wrong- $W$  and signal- $W$  falsification arms with predicted outcomes (Lemmas 4.12, Cor. 4.14). Estimator key: Table 3.

## The matching-principle recipe

**Step 1. Identify the nuisance family.** Pick  $A_k$  using Table 4 (§5.1); in most tasks the answer is unique. Hybrid nuisances compose additively (Step 2' in §5.1).

**Step 2. Estimate  $\hat{\Sigma}_{\text{task}}$  via Lemma Dk.** Use the estimator from §5. Run the eigengap pre-flight in §5.1 *before* training; a marginal gap ( $\gamma_r \approx 1$ ) is the named Office-31 failure mode, not noise.

**Step 3. Form the matched loss.** Add the PMH penalty to the task loss,

$$\mathcal{L}_{\text{total}}(\theta) = \mathcal{L}_{\text{task}}(\theta) + \lambda \mathbb{E}_x \left[ \text{Tr} \left( J_\phi^\top J_\phi \hat{\Sigma}_{\text{task}} \right) \right],$$

approximating the trace with a finite-difference paired-view, multi-scale Gram, Hutchinson-trace, or margin-invariance surrogate (per-block choice: Appendix B).

**Step 4. Apply the cap.** Cap the PMH term with Proposition 3.5:  $\mathcal{L}_{\text{PMH}} \leq \text{cap} \cdot \mathcal{L}_{\text{task}}$ . The steady-state PMH fraction is  $\text{cap}/(1 + \text{cap})$ ; no  $\lambda$  tuning is required.

**Step 5. Run the two falsification controls. Wrong- $W$ :** a random orthonormal projection of the same rank should, by Lemma 4.12, behave like isotropic PMH in expectation. **Signal- $W$ :** regularising along a known signal direction should, by Corollaries 4.13/4.14, *hurt* the task metric. A positive matched-arm result reported without both controls is uninformative about whether the principle is responsible for the gain.

## 7.1 The recipe as twelve lines of PyTorch

The whole recipe is, mechanically, an extra term in the loss. The code below is what every block in §8 reduces to once  $\hat{\Sigma}_{\text{task}}$  is in hand; the only block-specific choice is the estimator that fills the `Sigma_hat` slot. Hutchinson trace estimation with a paired-view encoder query approximates  $\mathbb{E}_x[\text{Tr}(J_\phi^\top J_\phi \hat{\Sigma}_{\text{task}})]$  to  $O(1/\sqrt{n_{\text{probes}}})$  stochastic error.

### Matched PMH and its two controls, in 12 lines of PyTorch

```
import torch
# Sigma_hat: (d, d) PSD covariance from Lemma D_k for your task.
# encoder : phi(x); s : known signal direction; U from QR(randn(d, r)).

def pmh_penalty(encoder, x, Sigma, n_probes=4):
    L = torch.linalg.cholesky(Sigma + 1e-6 * torch.eye(x.shape[-1]))
    phi0 = encoder(x)
    acc = sum((encoder(x + torch.randn_like(x) @ L.T) - phi0).pow(2).sum(-1).mean()
              for _ in range(n_probes))
    return acc / n_probes

loss          = task_loss + lam * pmh_penalty(encoder, x, Sigma_hat)           # matched
ctrl_wrong   = lam * pmh_penalty(encoder, x, U @ U.T)                         # Lemma C
ctrl_signal  = lam * pmh_penalty(encoder, x, torch.outer(s, s) / s.dot(s))   # Cor. E/E
*
```

**What counts as a genuine match.** Report three outcomes together: matched beats baseline on the deployment metric; wrong- $W$  is indistinguishable from isotropic PMH (Lemma 4.12); signal- $W$  *hurts* below baseline (Corollaries 4.13/4.14). Matched-only gains are inconclusive. Estimator catalogue: Table 3; cap fixes  $\lambda$  via Proposition 3.5.

## 7.2 Why geometry and task accuracy can disagree

The matching principle minimises a geometric functional ( $\tilde{D}_Q$ ), not a task metric. The two are distinct scalars, and any honest report must say where they decouple. When the deployment task metric weights directions differently from  $\Sigma_{\text{task}}$ —the generic case for downstream supervised losses—matched PMH optimises geometry but not necessarily the task score. Three canonical cases appear in §8. **T2B** (Chest X-ray): under protocol v3, E1 (PMH) compresses L4 drift and beats E1-no-PMH on heavy Gaussian (69.7% vs. 66.0%), but B0 leads *clean*, E1-no-PMH leads *mean shift*, and VAT leads *saliency*; B0 still collapses on Gaussian eval (Table 13; Appendix B.3). **T6A** (Whisper): matched content-residual PMH cuts layer-averaged TDI  $\approx 65\%$  and LibriSpeech-*other* WER 23.3%  $\rightarrow$  14.6%, but accent-supervised fine-tuning can reach slightly lower WER while *worsening* TDI—it uses label information matched PMH does not. **T7B** (CIFAR-10 ViT): PGD-AT wins PGD@4 (44.8%) but loses clean accuracy ( $-14.8$  pp vs. baseline) and trajectory TDI (1.506 vs. 0.870 for PGD-delta matched PMH; Corollary 3.4; Figure 6, right). Report geometry and task metrics on separate axes; do not collapse them into one leaderboard score.

## 7.3 When the matching principle does not apply

### Three structural limits to the framework

- **Linearisability.** The Jacobian linearisation requires  $\|n\|$  small relative to the encoder’s second-order envelope. Catastrophic corruption and severe domain shift can break this; nothing in the framework rules out a higher-order correction, and that is a natural next paper.
- **Identifiability.** Each Lemma  $D_k$  has its own structural assumption  $A_k$ . When no  $A_k$  describes the deployment nuisance, the framework offers no estimator and is silent.
- **Label preservation.**  $Q_n$  must satisfy Definition 2.1 ( $p(y | x + n) = p(y | x)$ ). When the shift is label-changing (Definition 2.1, second bullet),  $\Sigma_{\text{task}}$  is undefined; use causal / multi-environment methods instead.

These are honest scope conditions, not gaps in the proofs. They tell the practitioner exactly when to reach for a different tool, and they are what makes the matching principle falsifiable rather than unconditionally true.

## 8 Empirical programme: thirteen task blocks

### How to read the empirical scoreboard

Table 5 and Figures 5–7 summarise all thirteen blocks (Figure 6 isolates the three pre-registered falsification checks). *neg.* = a *predicted* failure observed (evidence *for* the theory). Check task and geometry columns separately; full numbers: Appendix B. Proof-status and scale tables: §9.

Table 5: Aggregate evidence map across the 13 empirical blocks. Columns are the theorems being tested; entries are observed effects or qualitative outcomes. “*neg.*” marks predicted falsification modes that materialised. Per-block protocols and raw tables: Appendix B.

Block	$D_k$	Thm A	Thm B	Lem C	Cor E	Caveat
1A oracle	D1	✓	wrong $\approx$ B0	—	hard kNN	—
1A Office-31	D1	CORAL>PMH	—	—	linear limit	neg.
2A ImageNet	D2	iso=matched	—	—	—	—
2B X-ray	D2	drift $\sim 2.2\times$	—	—	—	geom $\neq$ task
3A pose	D3	+22 pp PCK	VAT fail	—	—	—
3B depth	D3	aniso wins	wrong +18%	—	—	—
4A DomainNet	D4	+3.31 pp	iso $\approx$ B0	—	—	—
4B Cityscapes	D4	rare-5 +11 pp	iso $\approx$ B0	—	moto collapse	neg.
5A QM9	D5	MAE $\downarrow$	VAT mismatch	—	large $\sigma$	tradeoff
5B clones	D5	rename 0.94	VAT<matched	—	$E_{1S}$	neg.
6A Whisper	D6	TDI $-65\%$	wrong 0.64	—	WER gap	geom $\neq$ task
6B HAR	D6	PMH best	wrong mid	—	—	—
7A Qwen	D7	RM selective	iso raw syco	—	wrong $\Sigma$	T7A: RM beh. / DPO geom.
7B adv ViT	D7	TDI 0.88	random W	$D_N/D_S$	PGD-AT cost	—

**How to read this section.** Each **Type** fixes  $A_k$ , Lemma  $D_k$ , and the recipe controls (§7). One paragraph per type below; three synthesis figures amplify Table 5: Figure 5 (matched gain vs. B0/iso/wrong on each block’s headline metric); Figure 6 (Lemma C, Cor. E\*, Cor. p1-4 pre-registered checks); Figure 7 (predicted failures named before runs). Per-block tables and diagnostic figures: Appendix B.

### Headline block T7A: Qwen2.5-7B alignment (not block T7B)

**Naming.** *Block* T7A (this headline) is Qwen2.5-7B alignment; *block* T7B is an unrelated CIFAR-10 ViT PGD-delta staircase (§8.7). “7B” is parameter count, not the block label.

Both T7A arms use the same  $A_7$  estimator—style-pair Gram  $\hat{\Sigma}_{\text{style}}$  (rank-128 shrinkage)—but answer different questions on *different training setups*:

- RM arm (behavioural).** Two-layer MLP on *frozen* Qwen hidden states, 20 epochs,  $\lambda=0.7$ . Sycophancy **38.5%**  $\rightarrow$  **13.5%**; honest preference **61.5%**  $\rightarrow$  **86.5%** (95% bootstrap CIs exclude zero). Matched wins *content/style selectivity* ( $C/S$   $2.6\times \rightarrow 3.1\times$ ), not lowest raw sycophancy (isotropic: **5.8%** sycophancy, **94.2%** honest pref.). That selectivity pattern is the predicted trade-off when blunt isotropic shrinkage beats directional matching on a scalar rate (Appendix B.12, Table 25).
- DPO arm (geometry).** LoRA DPO on the *full* 7B model, 1 epoch, 240 style pairs, four arms. Standard DPO raises Style TDI +30% ( $1.851 \rightarrow 2.408$ ); matched style-PMH DPO holds 1.836 ( $-0.8\%$  vs. pre-DPO) with one extra trace term. Per-style drift can worsen for modes outside  $\text{span}(\hat{\Sigma}_{\text{style}})$  (e.g. bulleted; Table 26).

Full protocols: Appendix B.12.

## What T7A establishes (and what it does not)

**What it is.** One block, two falsification-relevant readouts: RM arm  $\Rightarrow$  alignment *behaviour* moves in the direction Theorem 3.1/ $A_7$  predict; DPO arm  $\Rightarrow$  *geometry* (Style TDI) is preserved where standard DPO degrades it. Same  $\hat{\Sigma}_{\text{style}}$ , same recipe controls (wrong- $\Sigma$ , isotropic).  
**What it is not.** A deployed frontier RLHF system; not block T7B (vision robustness); not a claim that matched beats isotropic on every RM scalar (Table 8, Scale).

Twelve further blocks and three pre-registered checks (§4.8) follow. **Type 1–7:** see Table 3; each runs wrong- $W$  / signal- $W$  controls.

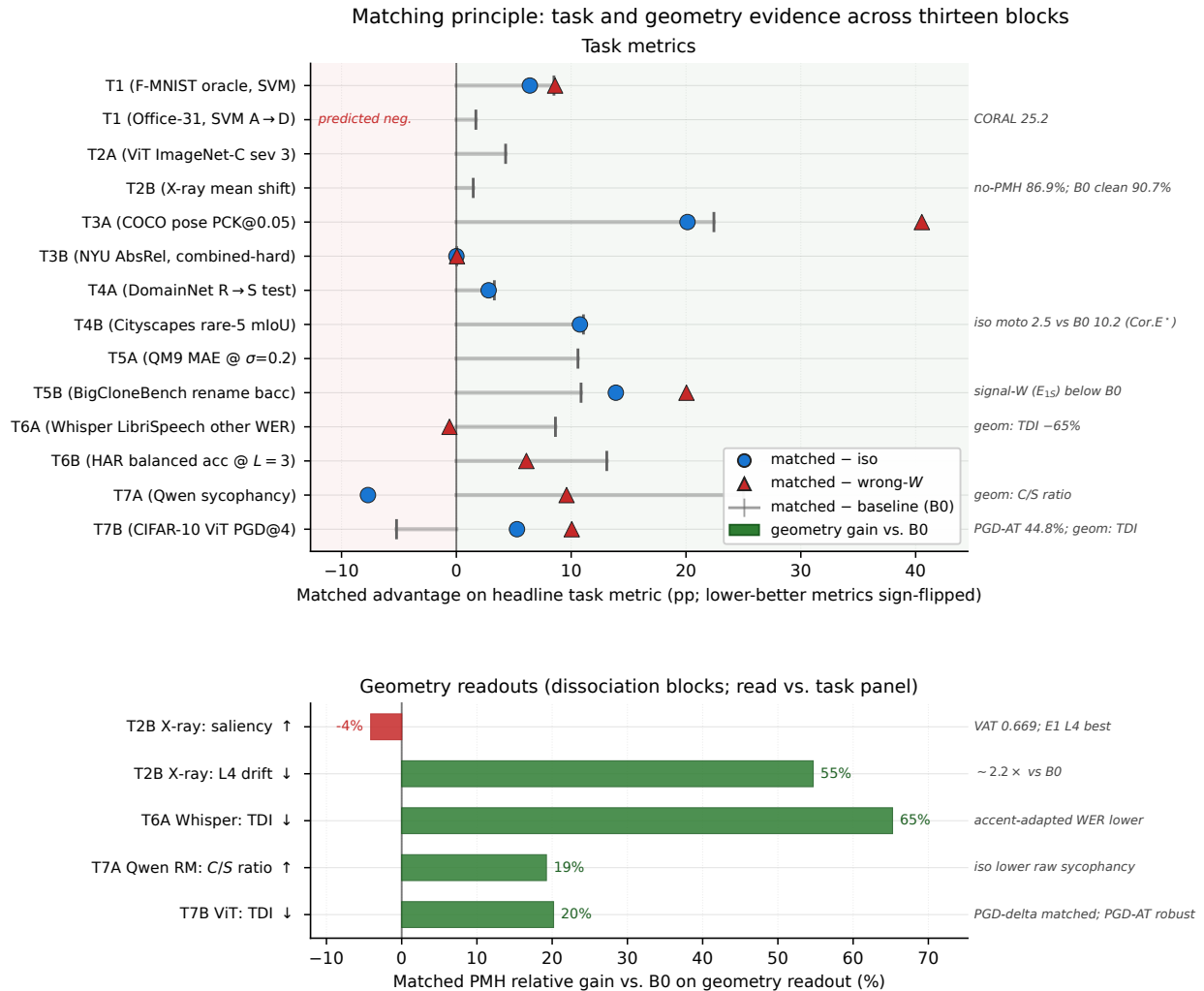


Figure 5: **Thirteen blocks at a glance.** *Top:* matched-arm gain (pp on each block’s headline *task* metric) vs. B0 (bar), isotropic-PMH (circle), wrong- $W$  (triangle). Negative bars are predicted (Office-31 / D1). *Bottom:* geometry readouts for partial-pass / dissociation blocks (T2B, T6A, T7A, T7B). Read the panels separately: T2B shows *residual* decoupling (E1 compresses drift and beats E1-no-PMH on heavy Gaussian; B0/E1-no-PMH/VAT split clean, mean shift, and saliency); T6A, T7A, T7B show geometry gains a headline task scalar can miss. See §7.2 and Appendix B.

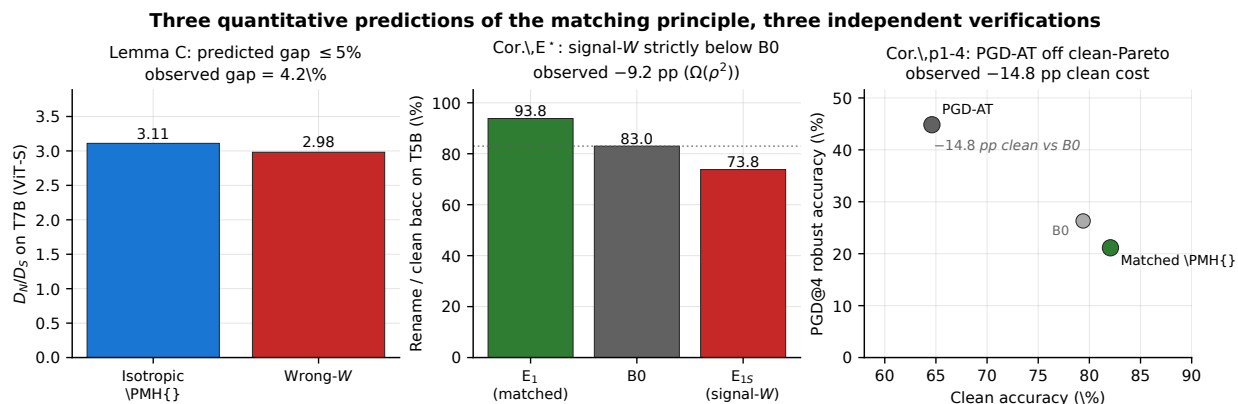


Figure 6: **Three pre-registered falsification checks** (§4.8). *Left*: Lemma 4.12—wrong- $W$  tracks isotropic PMH on  $D_N/D_S$  (T7B: 2.98 vs. 3.11). *Centre*: Cor. 4.14—signal- $W$  hurts below baseline (T5B keyword-PMH: rename\_bacc\_ratio 0.830  $\rightarrow$  0.738). *Right*: Cor. 3.4—PGD-AT wins robustness but loses clean acc (-14.8 pp vs. B0 at higher PGD@4); geometry-task dissociation, not a refutation.

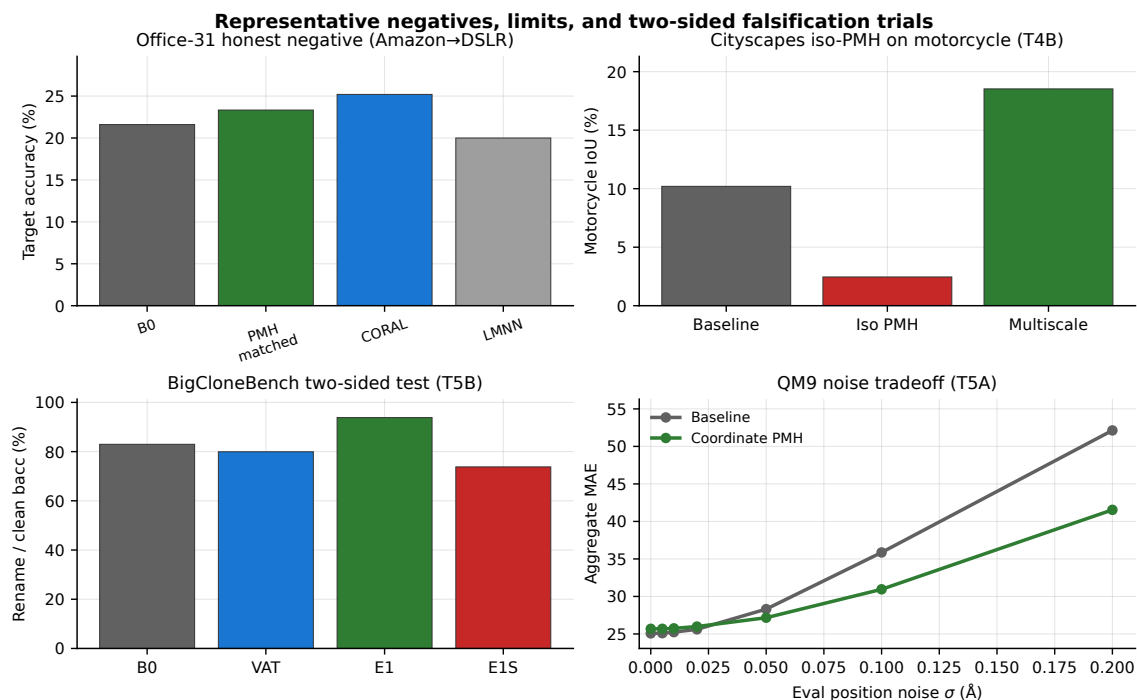


Figure 7: **Honest negatives (predicted before runs)**. *Top-left*: Office-31 / Lemma D1 eigengap ( $\approx 1.03$ ): CORAL beats matched SVM. *Top-right*: Cityscapes iso-pixel motorcycle IoU collapse (Cor.  $\mathcal{E}^*$ ). *Bottom-left*: QM9 clean-vs-robust MAE tradeoff (Thm. A(ii) allocation). *Bottom-centre*: T5B identifier vs. keyword probe (Cor.  $\mathcal{E}^*$ ). *Bottom-right*: T7B  $\hat{W}$  quality staircase (better estimate  $\Rightarrow$  ordered PGD@4 gain).

## 8.1 Type 1: classical machine learning under a known subspace nuisance

$A_1$ , **Lemma D1** (cross-domain SVD). **Predict:** usable eigengap  $\Rightarrow$  matched  $>$  iso  $\approx$  wrong- $W$  (Thm. A, Lemma 4.12). **Verdict:** pass on oracle ridge/SVM/kNN and DCT drift (matched ridge MSE 0.101 vs. 0.553 for B0 at extreme nuisance); **predicted fail** Office-31 (eigengap  $\approx$  1.03, CORAL 25.2% vs. matched 23.3%; Fig. 7). Appendix B.1.

## 8.2 Type 2: isotropic acquisition noise on deep networks

$A_2$ , **Lemma D2**. **Predict:** no subspace  $\Rightarrow$  matched = isotropic; iso beats wrong- $W$  on geometry. **Verdict:** T2A pass (+4.3 pp ImageNet-C, TDI  $-58\%$ ); T2B partial (E1 wins geometry and heavy Gaussian vs. no-PMH; B0/E1-no-PMH/VAT split clean, mean shift, saliency—Table 13, Appendix B.3). Appendices B.2–B.3.

## 8.3 Type 3: photometric and occlusion nuisances in dense prediction

$A_3$ , **Lemma D3** (augmentation-delta Gram). **Predict:** anisotropic  $\Sigma' \propto \hat{\Sigma}_{\text{aug}}$  beats iso and mismatched VAT; wrong- $W$  raises drift. **Verdict:** T3A +22.3 pp PCK; T3B best on hard photometric metrics (Table 16; wrong- $W$  AbsRel +18%). Appendices B.4–B.5.

## 8.4 Type 4: hierarchical domain shift

$A_4$ , **Lemma D4** (per-layer Gram). **Predict:** layer matched beats pixel-iso; iso-pixel on rare classes can hurt (Cor. 4.14). **Verdict:** T4A +3.3 pp; T4B rare-5 mIoU +11.1 pp; iso-pixel motorcycle IoU 10.2%  $\rightarrow$  2.5% (Fig. 7). Appendices B.6–B.7.

## 8.5 Type 5: compositional nuisances in structured data

$A_5$ , **Lemma D5** (nuisance-block covariance). **Predict:** penalise identifier/position block, not signal; signal- $W$  hurts. **Verdict:** T5B identifier PMH 0.830  $\rightarrow$  0.938 rename ratio, keyword PMH  $\rightarrow$  0.738; T5A QM9 large-noise Pareto tradeoff (Table 21, Thm. A(ii)). Appendices B.8–B.9.

## 8.6 Type 6: temporal and sequential drift

$A_6$ , **Lemma D6** (content-residual / sensor scatter). **Predict:** matched suppresses  $D_N/D_S$ ; wrong- $W \approx$  iso; supervision may beat WER without fixing TDI. **Verdict:** T6B pass at all stress levels; T6A partial (WER and TDI win; accent-adapted WER-only). Appendices B.10–B.11.

## 8.7 Type 7: adversarial robustness and alignment geometry

$A_7$ , **Lemma D7**—two *sub-blocks*, two estimators: **T7B** (vision): PGD-delta / gradient-SVD Gram on CIFAR-10 ViT. **T7A** (language): style-pair Gram on Qwen2.5-7B (§8). **Predict (T7B):** better  $\hat{W} \Rightarrow$  ordered PGD@4 staircase; PGD-AT can win robustness but lose clean acc / trajectory TDI (Cor. 3.4). **Predict (T7A):** matched suppresses style-linked drift and improves selective honesty, not necessarily every raw RM rate vs. isotropic. **Verdict:** T7B pass + dissociation; T7A pass on RM selectivity and DPO Style TDI (Appendices B.12–B.13).

## 8.8 Named failures and overall pattern

Figure 7 collects four *predicted* negatives (Office-31 / D1 eigengap; Cityscapes iso-pixel / Cor. E<sup>\*</sup>; T5B keyword-PMH; QM9 allocation / Thm. A(ii)); each is upheld in the Types above and Appendix B. Where  $A_k$  holds with a usable gap, matched beats isotropic and wrong- $W$  tracks isotropic (Lemma 4.12) in twelve of thirteen blocks; arm-level signal penalties and allocation tradeoffs are successes of named failure modes, not contradictions (Table 5).

## 9 Synthesis tables

Three tables complement the scoreboard at the start of §8 (Table 5, Figures 5–7).

### How to read the synthesis tables

1. **Table 6.** Proved vs. conditional vs. observed (separate math from experiments).
2. **Table 7.** Same penalty from ridge/kNN to 7B; only the Table 3 row changes.
3. **Table 8.** Formal and extension gaps (prose: §10.3).

**Proof status (Table 6).** Theorems A, G, B and Lemmas C, Cor. E/E<sup>\*</sup> are unconditional;  $A_{\text{global}}^*$  under (R), (C<sup>b</sup>), (E), (I); training corollary needs (O). Lemmas D1–D7 are conditional on  $A_k$ . §8 is observational synthesis, not a theorem.

Table 6: Theorem and assumption status. Categories: *proved* (no extra assumptions), *conditional* (proved under a named assumption listed in the scope column), *observed* (empirical, not a theorem), and *open*.

Result	Status	Scope
ERM blind spot (Thm. 3.1)	Proved	ERM + correlated nuisance
Prop. 4.5 (C <sup>b</sup> linear)	Proved	Linear-Gaussian ERM
Theorem A	Proved	Linear-Gaussian
Theorem G	Proved	Quadratic Jacobian
Theorem $A_{\text{global}}^*$	Proved	Global min; (R),(C <sup>b</sup> ),(E),(I)
Cor. $A_{\text{train}}^*$	Conditional on (O)	Training output
Theorem B	Proved	Two-regime mismatch
Lemma C / C <sup>*</sup>	Proved	Random $\Sigma'$
Cor. E / E <sup>*</sup>	Proved	$\Omega(\rho^4)$ / $\Omega(\rho^2)$
Conj. A <sup>†</sup>	Open	Deep allocation
Lemmas D1–D7	Conditional	Under $A_k$
§8	Observed	13 blocks

**Scale and open problems (Tables 7–8).** Same penalty from ridge/kNN through ViT, speech, code, and Qwen2.5-7B; only the Lemma  $Dk$  row changes. Eight open items; highlighted prose in §10.3.

Table 7: Cross-scale model programme. Same matching principle; the PMH surrogate (Hutchinson trace, paired-view feature MSE, margin invariance, ...) varies by block—see Appendix B. Pick the row from Table 3 for your nuisance family.

Scale	Architecture	Params	Block
Classical	Ridge / SVM / kNN	—	T1
Small CNN	ResNet-18	11M	T2B, T3
Mid CNN	ResNet-50	25M	T4
ViT	ViT-B/16	86M	T2A
Code	CodeBERT	125M	T5B
Speech	Whisper-small	244M	T6A
LLM	Qwen2.5-7B	7B	T7A (not T7B)

Table 8: Open problems left by the framework. Two are formal (O, A<sup>†</sup>); the remaining six are extension questions whose resolution does not require new theory of Theorem A but does require new estimator design.

ID	Problem
(O)	Optimisation reachability
A <sup>†</sup>	Deep cube-root allocation
Rate	Tighten $O(1/\lambda)$ deep bound
Causal	Colored nuisances
Online	Non-stationary $\Sigma_{\text{task}}$
Robust	Adversarial deployment $\Sigma$
Compose	Multiple nuisance families
Scale	Multi-epoch RLHF validation

## 10 Discussion

The synthesis tables (§9) record proof status, scale, and open problems; the empirical scoreboard opens §8. This section interprets what follows if the matching principle is taken seriously as a design theory for nuisance-robust losses (full proofs: Appendix A).

### 10.1 What changes if the matching principle is correct

**Robustness collapses into one estimation problem.** Which regulariser to use reduces to: which  $A_k$  describes deployment, and how well does the Lemma Dk estimator recover  $\Sigma_{\text{task}}$ ? CORAL, adversarial training, IRM, augmentation, metric learning, and Jacobian penalties become estimators of one object. Wide eigengap  $\Rightarrow$  win; marginal gap  $\Rightarrow$  predicted loss (Office-31 / Lemma D1).

**Loss-function design becomes first-class.** Theorem 4.1 promotes the loss to a design variable parameterised by one PSD matrix per nuisance type, with a closed-form optimum and two falsification controls (Lemma 4.12, Corollaries 4.13/4.14). Engineering effort can shift from architecture search to *what to regularise against*, with a principled answer.

**Ablations become principled, not decorative.** The random-projection and signal-direction controls are no longer courtesy ablations; they are the tests Lemma 4.12 and Corollaries 4.13/4.14 fix in advance. A claim that fails both is, by the theory, not a matching-principle effect.

**Alignment is geometric.** Block T7A (§8; Qwen2.5-7B, not vision block T7B) uses style as the nuisance: the RM arm is selective on sycophancy vs. isotropic blunt shrinkage; the DPO arm preserves Style TDI where standard DPO does not (Appendix B.12).

**Adjacent literatures.** Relative to the information bottleneck, matched PMH suppresses  $\phi$  along deployment  $\Sigma_{\text{task}}$  rather than all of  $I(\phi; x)$ . Relative to equivariance, it estimates a covariance when no clean group action exists (photometry, accent, style). Relative to interpretability, it prescribes pre hoc what the encoder should be insensitive to—the 7B alignment case (§8).

## 10.2 Scope and relation to prior work

Label-preserving limits (causal/spurious benchmarks), dissociation of geometry vs. task metrics, and the 7B scale caveat are stated in §1 and §7.3; Table 8 tags the causal and scale rows. The companion note [14] states the blind spot and isotropic uniqueness; this paper is self-contained (Appendix A) and adds matched  $\Sigma_{\text{task}}$ , Lemmas D1–D7, TDI, and thirteen blocks.

## 10.3 Open problems the framework names

Table 8 lists eight items; we highlight the three that shape how to read the present results.

**(O) Optimisation reachability.** Theorem 4.9 is a *global* statement; proving standard training reaches that minimum (assumption (O) for Cor. A $_{\text{train}}^*$ ) is the central formal gap. Proposition 4.5 settles assumption (C $^b$ ) in the linear model; Remark 4.6 states what remains open for deep nets.

**Causal / coloured nuisances.** Definition 2.1 separates label-preserving deployment laws from label-changing spurious shifts; the latter need multi-environment or causal tools (Table 8).

**Estimator selection in practice.** §5.1 gives symptom $\rightarrow A_k$  guidance, additive composition, and an eigengap pre-flight with Office-31 as the calibrated marginal case—closing the “which row do I use?” gap left by the conditional D-lemmas alone.

**Scale.** Multi-epoch, full-data alignment at frontier parameter counts ( $\geq 70\text{B}$ ) is the natural extension of block T7A (§8); remaining rows in Table 8 list deep allocation, rate tightening, online  $\Sigma_{\text{task}}$ , adversarial  $\Sigma$ , and compositional matching.

# 11 Conclusion

The robustness literature has been a catalogue of methods in search of a common object. This paper names it: the population covariance  $\Sigma_{\text{task}}$  of label-preserving deployment variation. Within quadratic Jacobian penalties, the optimal regulariser is determined by that matrix—sufficiently (Theorem 4.1), necessarily (Theorem 4.2), and at the global minimum of deep encoders under standard regularity (Theorem 4.9, Lemma 4.10). Lemma 4.12 and Corollaries 4.13/4.14 make the claim falsifiable; Lemmas D1–D7 tell you how to estimate  $\Sigma_{\text{task}}$  under each structural assumption  $A_k$ .

Across thirteen blocks, matched PMH wins on the headline metric when  $A_k$  holds and the estimator has a usable eigengap; wrong- $W$  tracks isotropic (Lemma 4.12); signal-aligned penalties hurt (Cor. E $^*$ ). Named exceptions: Office-31 (Lemma D1), Cityscapes iso-pixel and T5B keyword-PMH, QM9 allocation (Theorem A(ii)); in block T7A (Qwen2.5-7B), matched style-PMH is the selective fix (§8).

We do not claim universality over all robustness problems. We claim a scoped unification: when deployment nuisance is label-preserving and estimable, loss design reduces to matching  $\hat{\Sigma}_{\text{task}}$  plus two controls—a prescription that is closed form, constructive, testable on every new task, and consistent with the evidence in §8 and Table 5.

**Reproducibility.** All numbers are frozen in per-task JSON; protocols and rebuild commands are in Appendix B and Appendix B. Headline checkpoints (T7B ViT-Small, T7A Qwen2.5-7B) will ship with the camera-ready release. The matched-PMH recipe (§7) is implemented in the standalone Python package **matching-pmh** (<https://github.com/vishalstark512/matching-pmh>; `pip install matching-pmh, import pmh`), separate from the experiment repositories bundled with this manuscript.

## References

- [1] Alessandro Achille and Stefano Soatto. Emergence of invariance and disentanglement in deep representations. In *JMLR*, 2018.
- [2] Martin Arjovsky, Léon Bottou, Anirudh Gulrajani, and David Lopez-Paz. Invariant risk minimization. *arXiv:1907.02893*, 2019.
- [3] Aurélien Bellet, Amaury Habrard, and Marc Sebban. A survey on metric learning for feature vectors and structured data. *arXiv:1306.6709*, 2013.
- [4] Shai Ben-David, John Blitzer, Koby Crammer, Alex Kulesza, Fernando Pereira, and Jennifer Wortman Vaughan. A theory of learning from different domains. In *Machine Learning*, 2010.
- [5] Gabriela Csurka. Domain adaptation for visual applications: A comprehensive survey. *arXiv:1702.05374*, 2017.
- [6] Hal Daumé III. Frustratingly easy domain adaptation. In *ACL*, 2007.
- [7] Robert Geirhos, Patricia Rubisch, Claudio Michaelis, Matthias Bethge, Felix A. Wichmann, and Wieland Brendel. Imagenet-trained CNNs are biased towards texture. In *ICLR*, 2019.
- [8] Dan Hendrycks and Thomas Dietterich. Benchmarking neural network robustness to common corruptions and perturbations. In *ICLR*, 2019.
- [9] Aleksander Madry, Aleksandar Makelov, Ludwig Schmidt, Dimitris Tsipras, and Adrian Vladu. Towards deep learning models resistant to adversarial attacks. In *ICLR*, 2018.
- [10] Sinno Jialin Pan and Qiang Yang. A survey on transfer learning. *IEEE Trans. Knowledge and Data Engineering*, 2010.
- [11] Ethan Perez, Sam Ringer, Kamile Lukosiute, Karina Nguyen, Edwin Chen, Scott Heiner, et al. Discovering language model behaviors with model-written evaluations. In *Findings of ACL*, 2023.
- [12] Alec Radford, Jong Wook Kim, Tao Xu, Greg Brockman, Christine McLeavey, and Ilya Sutskever. Robust speech recognition via large-scale weak supervision. In *ICML*, 2023.
- [13] Rafael Rafailov, Archit Sharma, Eric Mitchell, Stefano Ermon, Christopher D. Manning, and Chelsea Finn. Direct preference optimization: Your language model is secretly a reward model. In *NeurIPS*, 2023.
- [14] Vishal Rajput. Supervised learning has a geometric blind spot: Theory and minimal repair, 2026. Companion arXiv note (2604.21395); matched- $\Sigma_{\text{task}}$  theory and experiments are self-contained here.
- [15] Baochen Sun and Kate Saenko. Deep CORAL: Correlation alignment for deep domain adaptation. In *ECCV*, 2016.
- [16] Naftali Tishby and Noga Zaslavsky. Deep learning and the information bottleneck principle. In *IEEE Information Theory Workshop*, 2015.
- [17] Garrett Wilson and Diane J. Cook. A survey of unsupervised deep domain adaptation. *ACM Trans. Intelligent Systems and Technology*, 2020.

# A Proofs

All formal claims in the main text are proved below (self-contained; [14] is related work only). §8 is observational synthesis. Appendix B holds protocols and frozen numbers.

**Proof map (read in order).**

- A.1. Foundation (A.1):** blind spot, isotropy, PGD anisotropy, training cap (Thm. 3.1, Cor. 3.2/3.4, Prop. 3.3/3.5).
- A.2. Theorem A (A.2):** matched sufficiency (linear-Gaussian).
- A.3. Theorem G (A.3):** range necessity.
- A.4. Lemma D-ML (A.4):** expressivity assumption (E).
- A.5. Theorem A\* (A.5):** deep global minimum.
- A.6. Theorem B (A.6):** range vs. allocation costs.
- A.7. Lemma C (A.7):** wrong- $W \equiv$  isotropic.
- A.8. Cor. E/E\* (A.8):** signal penalty hurts.
- A.9. Lemmas D1–D7 (A.9):** estimator consistency under  $A_k$ .
- A.10. Prop. F (A.10):** class-layout TDI<sub>0</sub> envelope.

## A.1 Geometric foundation: blind spot, isotropy, PGD, and training cap

**Appendix A.1** (proof-map item 1) proves the §3 floor self-contained: Theorem 3.1, Corollaries 3.2/3.4, Propositions 3.3/3.5. Companion arXiv note [14] motivates the blind spot; all proofs needed for this paper are here. Lemmas A.2–A.7 are reused in Appendix A.2–A.8.

**Remark A.1** (Gaussian linear model).  $s \sim \mathcal{N}(0, I_{d_s})$ ,  $n \sim \mathcal{N}(0, I_{d_n})$ ,  $s \perp n$ ,  $y = \langle w_s, s \rangle + \rho \langle w_n, n \rangle + \varepsilon$  with  $\varepsilon \sim \mathcal{N}(0, \sigma_\varepsilon^2)$ ,  $\|w_s\|_2 = \|w_n\|_2 = 1$ ,  $\rho > 0$ , and  $x = (s, n)$ . Write  $J_\phi = [J_{\phi,s} \mid J_{\phi,n}]$  so  $\|J_\phi\|_F^2 = \|J_{\phi,s}\|_F^2 + \|J_{\phi,n}\|_F^2$ .

**Lemma A.2** (Sub-block inequality). For  $A \in \mathbb{R}^{m \times d}$  and unit  $v \in \mathbb{R}^d$ :  $\|Av\|_2^2 \leq \|A\|_F^2$ . For  $A = [A_1 \mid A_2]$ :  $\|A_2 v\|_2^2 \leq \|A_2\|_F^2 \leq \|A\|_F^2$ .

*Proof.* Cauchy–Schwarz on  $Av = \sum_j v_j A e_j$  with  $\sum_j v_j^2 = 1$ . □

**Lemma A.3** (Linearised vs. exact drift). If  $\phi$  has  $\beta$ -Lipschitz Jacobian and  $\sup_x \|J_\phi(x)\|_F \leq M$ , then for  $\delta \sim \mathcal{N}(0, \sigma^2 I_d)$ ,  $D_Q(\phi) = \mathbb{E}_{x,\delta}[\|\phi(x+\delta) - \phi(x)\|_2^2] = \sigma^2 \mathbb{E}_x[\|J_\phi(x)\|_F^2] + R(\phi, \sigma)$  with  $|R(\phi, \sigma)| \leq C(M\beta d^{3/2}\sigma^3 + \beta^2 d^2 \sigma^4)$  for a universal  $C > 0$ . In particular  $D_Q \geq \tilde{D}_Q - O(\sigma^4)$  for small  $\sigma$ , and  $D_Q(\phi, \sigma) \geq \frac{1}{2} \tilde{D}_Q(\phi, \sigma)$  once  $\sigma \leq \sigma_0(M, \beta, d, \rho, L)$ .

*Proof.* Integral form of the mean-value expansion; the leading term is  $\mathbb{E}[\|J_\phi \delta\|_2^2] = \sigma^2 \mathbb{E}_x[\|J_\phi\|_F^2]$ ; higher orders are  $O(\sigma^3)$ – $O(\sigma^4)$ . □

**Lemma A.4** (ERM must encode the nuisance direction). Under Remark A.1, any population MSE minimiser  $f^* = h \circ \phi^*$  satisfies  $\mathbb{E}_x[\partial_{w_n} f^*(x)] = \rho$  for  $\partial_{w_n} := \langle w_n, \nabla_n \rangle$ . Hence  $J_{\phi,n}$  is non-zero on a set of positive measure.

*Proof.* Bayes predictor  $f^*(x) = \langle w_s, s \rangle + \rho \langle w_n, n \rangle$ . Stein’s identity for  $n \sim \mathcal{N}(0, I_{d_n})$  gives  $\mathbb{E}[\partial_{w_n} f^*] = \mathbb{E}[f^* \cdot \langle w_n, n \rangle] = \rho \|w_n\|_2^2 = \rho$ . □

**Proof of Theorem 3.1.** By Lemma A.4 and the chain rule,  $\rho = \mathbb{E}[\nabla_\phi h^\top J_{\phi,n} w_n] \leq L \mathbb{E}[\|J_{\phi,n} w_n\|_2]$ . Jensen gives  $\mathbb{E}[\|J_{\phi,n} w_n\|_2^2] \geq \rho^2/L^2$ . Lemma A.2 yields  $\mathbb{E}[\|J_\phi\|_F^2] \geq \mathbb{E}[\|J_{\phi,n} w_n\|_2^2] \geq \rho^2/L^2$ , hence  $\tilde{D}_Q(\phi^*, \sigma) = \sigma^2 \mathbb{E}[\|J_\phi\|_F^2] \geq \sigma^2 \rho^2/L^2$ . Lemma A.3 upgrades this to  $D_Q \geq \sigma^2 \rho^2/(2L^2)$  for  $\sigma \leq \sigma_0$ .  $\square$

**Lemma A.5** (Bregman gap for strictly proper losses). *Let  $\mathcal{L}$  be strictly proper with Bregman generator  $\psi$ . For conditionals  $p, q$  on  $\mathcal{Y} \mid x$ :*

$$\mathbb{E}_{y \sim p}[\mathcal{L}(q, y)] - \mathbb{E}_{y \sim p}[\mathcal{L}(p, y)] = d_\psi(p \parallel q) \geq 0,$$

with equality iff  $p = q$  a.s.

*Proof.* Definition of strict properness: the expected loss is uniquely minimised at  $q = p$ .  $\square$

**Lemma A.6** (Risk excess of an  $n$ -blind predictor). *Under correlated nuisance (direct influence:  $p(y \mid x) \not\equiv p(y \mid s(x))$  on positive measure), define  $\Delta(P, \mathcal{L}) := \mathbb{E}_x[d_\psi(p(y \mid x) \parallel p(y \mid s(x)))] > 0$ . Any  $f^* = \arg \min_f \mathbb{E}[\mathcal{L}(f(x), y)]$  satisfies  $\mathbb{E}[\mathcal{L}(f^*, y)] \leq \mathbb{E}[\mathcal{L}(f^s, y)] - \Delta(P, \mathcal{L})$  for  $f^s(x) = \mathbb{E}[y \mid s(x)]$ , hence cannot be invariant to all nuisance directions that carry  $\Delta$ -mass.*

*Proof.* Take  $q = p^s$  in Lemma A.5 at each  $x$  and average.  $\square$

**Lemma A.7** (Jacobian sensitivity from risk gap). *Suppose  $f^* = h \circ \phi^*$  minimises  $\mathbb{E}[\mathcal{L}(f(x), y)]$  with  $L$ -Lipschitz  $h$  and  $\Delta(P, \mathcal{L}) > 0$ . Assume there exists a unit direction  $u$  in the nuisance subspace with  $\mathbb{E}_x[\partial_u f^*(x)] \geq c_\Delta > 0$  (encoding necessity, as in Lemma A.4 in the Gaussian model). Then  $\mathbb{E}_x[\|J_{\phi^*,n}(x)u\|_2^2] \geq c_\Delta^2/L^2$  and  $\tilde{D}_Q(\phi^*, \sigma) \geq \sigma^2 c_\Delta^2/L^2$ .*

*Proof.* Same chain rule and Jensen steps as Theorem 3.1, with  $\rho$  replaced by  $c_\Delta$ .  $\square$

**Proof of Corollary 3.2.** Lemma A.6 gives  $\Delta(P, \mathcal{L}) > 0$  under the corollary's hypothesis ( $p(y \mid x) \not\equiv p(y \mid s(x))$ ). In the Gaussian model,  $c_\Delta = \rho$  and  $\Delta = \Theta(\rho^2)$  as  $\rho \rightarrow 0$  (KL between Gaussian conditionals). Lemma A.7 yields  $\tilde{D}_Q(\phi^*, \sigma) \geq \sigma^2 \Delta(P, \mathcal{L}) / (C_{\text{mv}} \mathbb{E}\|n\|_2^2 L^2)$  for a mean-value constant  $C_{\text{mv}}$  from linearising  $f^*$  in  $n$ ; in Remark A.1,  $C_{\text{mv}} = O(1)$  and the bound reduces to  $\sigma^2 C'(P, \mathcal{L})/L^2$  with  $C'(P, \mathcal{L}) = \Delta$  up to absolute constants.  $\square$

**Proof of Proposition 3.3.** For  $\text{Cov}(\delta) = \Sigma_\delta$ ,  $\mathbb{E}_\delta[\|J_\phi \delta\|_2^2] = \text{Tr}(J_\phi^\top J_\phi \Sigma_\delta)$ . Equality with  $\sigma^2 \text{Tr}(J_\phi^\top J_\phi)$  for all  $J_\phi$  holds iff  $\Sigma_\delta = \sigma^2 I$  (test on  $A = e_i e_j^\top$ ).  $\square$

**Proof of Corollary 3.4.** PGD-AT targets  $\hat{\delta}^*(x) \propto \text{sign}(\nabla_x \mathcal{L})$ , not  $\mathcal{N}(0, \sigma^2 I)$ . By Proposition 3.3, shrinking along  $\hat{\delta}^*$  need not isotropise  $J_\phi$ ; trajectory TDI (Eq. (5)) can rise while  $\|J\|_F$  falls (T7B: PGD-AT 1.506 vs. PGD-delta matched 0.870 at the same backbone; §8.7).  $\square$

**Proof of Proposition 3.5.** At the capped steady state,  $\mathcal{L}_{\text{PMH}} = \text{cap} \cdot \mathcal{L}_{\text{task}}$ , so  $f = \mathcal{L}_{\text{PMH}} / (\mathcal{L}_{\text{task}} + \mathcal{L}_{\text{PMH}}) = \text{cap} / (1 + \text{cap})$ .  $\square$

## A.2 Theorem A: matched- $\Sigma$ optimality (linear-Gaussian)

**Main-text anchor (§4.1).** Matched sufficiency and cube-root allocation in the linear-Gaussian model.

**Setting (Theorem 4.1).** In the linear-Gaussian model of Remark A.1, diagonalise  $\Sigma_{\text{task}} = \text{diag}(\lambda_1, \dots, \lambda_r, 0, \dots)$  and write the PMH penalty as  $\text{diag}(\mu_1, \dots, \mu_{d_x})$  in the same basis (standard; off-diagonal cross-terms between  $\Sigma_{\text{task}}$  and  $\Sigma'$  do not change the range argument). Let  $\tilde{v}_i$  denote regressor energy in direction  $i$ .

**Proof of Part (i).** The PMH-regularised solution is  $w(\Sigma') = (I + 2\lambda\Sigma')^{-1}v$ . In the joint basis, component  $i$  of  $w(\Sigma')$  is:

$$[w(\Sigma')]_i = \frac{\tilde{v}_i}{1 + 2\lambda\mu_i}.$$

The deployment drift is:

$$\tilde{D}_Q(w(\Sigma')) = \sum_{i=1}^{d_x} \lambda_i [w(\Sigma')]_i^2 = \sum_{i=1}^{d_x} \frac{\lambda_i \tilde{v}_i^2}{(1 + 2\lambda\mu_i)^2}.$$

Since  $v \in \text{range}(\Sigma_{\text{task}})$ , we have  $\tilde{v}_i = 0$  for  $i > r$  (components outside the deployment range carry no regressor energy), so:

$$\tilde{D}_Q(w(\Sigma')) = \sum_{i=1}^r \frac{\lambda_i \tilde{v}_i^2}{(1 + 2\lambda\mu_i)^2}.$$

( $\Rightarrow$ ) *Sufficient direction.* If  $\text{range}(\Sigma') \supseteq \text{range}(\Sigma_{\text{task}})$ , then  $\mu_i > 0$  for all  $i \leq r$ . As  $\lambda \rightarrow \infty$ :

$$\frac{\lambda_i \tilde{v}_i^2}{(1 + 2\lambda\mu_i)^2} = O\left(\frac{1}{\lambda^2}\right) \rightarrow 0.$$

Summing over  $i \leq r$  (finitely many terms) gives  $\tilde{D}_Q \rightarrow 0$ .

( $\Leftarrow$ ) *Necessary direction.* If  $\text{range}(\Sigma') \not\supseteq \text{range}(\Sigma_{\text{task}})$ , there exists some index  $j \leq r$  with  $\mu_j = 0$  and  $\lambda_j > 0$ . By Assumption 4.8,  $\tilde{v}_j^2 > 0$  on every active nuisance direction. The  $j$ -th term satisfies:

$$\frac{\lambda_j \tilde{v}_j^2}{(1 + 2\lambda \cdot 0)^2} = \lambda_j \tilde{v}_j^2 > 0,$$

independent of  $\lambda$ . Hence  $\tilde{D}_Q(w(\Sigma')) \geq \lambda_j \tilde{v}_j^2 > 0$  for all  $\lambda$ , giving  $\tilde{D}_Q = \Theta(1)$ .  $\square$

**Proof of Part (ii).** We minimise  $\tilde{D}_Q(w(\Sigma')) = \sum_{i=1}^r \lambda_i \tilde{v}_i^2 (1 + 2\lambda\mu_i)^{-2}$  over the simplex  $\mathcal{A}_c = \{\mu \geq 0 : \sum_i \mu_i = c, \mu_i > 0 \forall i \leq r\}$ . Differentiating and applying the KKT conditions gives:

$$\frac{\partial}{\partial \mu_i} \left[ \tilde{D}_Q - \nu \sum_j \mu_j \right] = 0 \implies \frac{-4\lambda^2 \lambda_i \tilde{v}_i^2}{(1 + 2\lambda\mu_i)^3} = \nu,$$

so  $(1 + 2\lambda\mu_i)^3 = \frac{-4\lambda^2 \lambda_i \tilde{v}_i^2}{\nu}$ . Since  $\nu < 0$  at the constrained minimum (the objective decreases as  $\mu_i$  increases), write  $|\nu| = \nu_0 > 0$ . Then:

$$1 + 2\lambda\mu_i^* = \left( \frac{4\lambda^2 \lambda_i \tilde{v}_i^2}{\nu_0} \right)^{1/3}.$$

For large  $\lambda$ , the dominant term on the right is  $O(\lambda^{2/3})$ , so  $\mu_i^* = O(\lambda^{-1/3})$ . To leading order,  $\mu_i^* \propto (\lambda_i \tilde{v}_i^2)^{1/3}$ .

When  $\tilde{v}_i^2 \propto \lambda_i^{-1}$  (uniform energy on  $\text{range}(\Sigma_{\text{task}})$ ), the proportional rule  $\mu_i \propto \lambda_i$  coincides with the cube-root optimum—the rotation-invariant case in Figure 3.  $\square$

### A.3 Theorem G: necessity of $\text{range}(\Sigma_{\text{task}})$

**Main-text anchor (§4.2).** Any quadratic Jacobian penalty that zeros drift on all task directions must cover  $\text{range}(\Sigma_{\text{task}})$ .

This is the formal proof of Theorem 4.2: if  $\text{range}(A) \not\supseteq \text{range}(\Sigma_{\text{task}})$ , drift cannot vanish uniformly over all effective regressors. We prove the contrapositive.

Suppose  $\text{range}(A) \not\supseteq \text{range}(\Sigma_{\text{task}})$ ; choose a unit vector  $q \in \text{range}(\Sigma_{\text{task}}) \setminus \text{range}(A)$ , i.e.  $q \in \ker(A) \cap \text{range}(\Sigma_{\text{task}})$ . Set  $v = q$ . Then  $Av = Aq = 0$ , so  $(I + 2\lambda A)^{-1}v = v = q$  for all  $\lambda$ . Thus:

$$w_\lambda(A) = q, \quad \tilde{D}_Q(w_\lambda(A)) = q^\top \Sigma_{\text{task}} q.$$

Since  $q \in \text{range}(\Sigma_{\text{task}})$  and  $\Sigma_{\text{task}}$  is positive definite on its range,  $q^\top \Sigma_{\text{task}} q > 0$ . Hence  $\tilde{D}_Q(w_\lambda(A)) = q^\top \Sigma_{\text{task}} q > 0$  for all  $\lambda$ , which does not tend to zero.  $\square$

The same argument applies to every direction in  $\text{range}(\Sigma_{\text{task}}) \setminus \text{range}(A)$ ; covering the full nuisance range is necessary for  $\tilde{D}_Q \rightarrow 0$  uniformly over  $v \in \text{range}(\Sigma_{\text{task}})$ .

### A.4 Lemma D-ML: constructive verification of (E)

Assumption (E) in Theorem 4.9 requires a parameter  $\theta_0$  with *zero* PMH penalty at finite task loss. Lemma 4.10 constructs it for networks in  $\mathcal{C}_{\text{NRP}}$  (first layer wide enough, then arbitrary depth).

**Setting.** Let  $\phi_\theta \in \mathcal{C}_{\text{NRP}}$ , so  $\phi_\theta(x) = \psi(W^{(1)}x + b^{(1)}; \theta_{\text{rest}})$  with  $W^{(1)} \in \mathbb{R}^{m \times d_x}$ ,  $m \geq d_x - r$ . Let  $\Sigma' \succeq 0$  have rank  $r$  and eigendecomposition  $\Sigma' = U_\Sigma \Lambda U_\Sigma^\top$ .

**Construction of  $\theta_0$ .** Let  $U^\perp \in \mathbb{R}^{d_x \times (d_x - r)}$  be any orthonormal basis of  $\text{range}(\Sigma')^\perp$ . Choose  $W_0^{(1)} \in \mathbb{R}^{m \times d_x}$  such that each row of  $W_0^{(1)}$  lies in  $\text{range}(\Sigma')^\perp = \text{span}(U^\perp)$ . This is possible since  $m \geq d_x - r$  (dimension of  $\text{range}(\Sigma')^\perp$ ). Let  $\theta_0 = (W_0^{(1)}, b_0^{(1)}, \theta_{\text{rest},0})$  with  $b_0^{(1)}$  arbitrary and  $\theta_{\text{rest},0}$  chosen to minimise task loss given the constrained input projection (e.g. the Bayes-optimal head).

**Proof of (E1).** For any input  $x$ , the Jacobian of  $\phi_{\theta_0}$  with respect to  $x$  is:

$$J_{\phi_{\theta_0}}(x) = \frac{\partial \psi}{\partial z}(W_0^{(1)}x + b_0^{(1)}) \cdot W_0^{(1)}.$$

For any  $v \in \text{range}(\Sigma')$ , we have  $U_\Sigma^\top v \neq 0$  while  $(U^\perp)^\top v = 0$  by orthogonality. Since each row of  $W_0^{(1)}$  is in  $\text{span}(U^\perp)$ , we have  $W_0^{(1)}v = 0$ . Therefore  $J_{\phi_{\theta_0}}(x)v = 0$  for all  $x$ . Consequently:

$$J_{\phi_{\theta_0}}(x)^\top J_{\phi_{\theta_0}}(x) \Sigma' = 0 \quad \text{pointwise in } x,$$

and thus  $\mathbb{E}_x[\text{Tr}(J_{\phi_{\theta_0}}^\top J_{\phi_{\theta_0}} \Sigma')] = 0$  exactly.  $\square_{\text{E1}}$

**Proof of (E2).** Because  $\phi_{\theta_0}(x) = \psi(W_0^{(1)}x + b_0^{(1)}; \theta_{\text{rest},0})$  and each row of  $W_0^{(1)}$  is in  $\text{range}(\Sigma')^\perp$ , the map  $x \mapsto W_0^{(1)}x$  depends only on  $\Pi_{\text{range}(\Sigma')^\perp} x$ . Choosing the optimal head  $\psi^*$  for this input (i.e. the conditional expectation  $\mathbb{E}[y | \Pi_{\text{range}(\Sigma')^\perp} x]$ ) achieves:

$$\mathcal{L}_{\text{task}}(\theta_0) = \mathbb{E}[y - \mathbb{E}(y | \Pi_{\text{range}(\Sigma')^\perp} x)]^2 = \mathbb{E}[\text{Var}(y | \Pi_{\text{range}(\Sigma')^\perp} x)] < \infty. \quad \square_{\text{E2}}$$

## A.5 Theorem A\*: deep-encoder range-matching dichotomy

Formal proof of Theorem 4.9: range matching  $\Rightarrow \tilde{D}_Q = O(1/\lambda)$  at the global PMH minimum; failure to cover  $\text{range}(\Sigma_{\text{task}})$  leaves a  $\lambda$ -independent drift floor.

**Proof of Proposition 4.5.** At a population ERM minimiser  $\phi_\theta^*$ , Theorem 3.1 gives  $\tilde{D}_Q(\phi_\theta^*, \sigma) \geq \sigma^2 \rho^2 / L^2$ . For unit  $q \in \text{range}(\Sigma_{\text{task}})$ , the directional Jacobian energy  $\mathbb{E}_x[q^\top J_{\phi^*}(x)^\top J_{\phi^*}(x)q]$  lower-bounds  $\tilde{D}_Q$  up to  $\|\Sigma_{\text{task}}\|_{\text{op}}$ , yielding the displayed scale  $\rho_q^2 / L^2$  when  $\Sigma_{\text{task}}$  has eigenvalue  $\lambda_q^{\text{task}} \asymp \rho_q^2$  along  $q$ . Corollary 3.2 extends to strictly proper losses.  $\square$

**Proof of the sufficient direction (i).** By (E) and Lemma 4.10, pick  $\theta_0$  with zero PMH penalty and  $C_0 := \mathcal{L}_{\text{task}}(\theta_0) < \infty$ . The global minimiser satisfies:

$$\mathcal{L}_{\text{PMH}}^\lambda(\theta_\lambda^{\text{glob}}) \leq \mathcal{L}_{\text{PMH}}^\lambda(\theta_0) = C_0.$$

Expanding the regularised loss:

$$\mathcal{L}_{\text{task}}(\theta_\lambda^{\text{glob}}) + \lambda \mathbb{E}_x \left[ \text{Tr} \left( J_{\phi_\theta}^\top J_{\phi_\theta} \Sigma' \right) \right] \leq C_0.$$

Since both terms on the left are non-negative, the penalty term satisfies:

$$\mathbb{E}_x \left[ \text{Tr} \left( J_\phi^\top J_\phi \Sigma' \right) \right] \leq \frac{C_0}{\lambda}.$$

Under range matching,  $\Sigma' \succeq \sigma_{\min}^+(\Sigma') \Pi_{\text{range}(\Sigma_{\text{task}})}$ . By Assumption 4.3, the Jacobian has bounded operator norm  $M$ , so we can lower-bound the trace:

$$\tilde{D}_Q(\theta) = \mathbb{E}_x \left[ \text{Tr} \left( J_\phi^\top J_\phi \Sigma_{\text{task}} \right) \right] \leq \frac{\|\Sigma_{\text{task}}\|_{\text{op}}}{\sigma_{\min}^+(\Sigma')} \cdot \mathbb{E}_x \left[ \text{Tr} \left( J_\phi^\top J_\phi \Sigma' \right) \right] \leq \frac{\|\Sigma_{\text{task}}\|_{\text{op}} \cdot C_0}{\sigma_{\min}^+(\Sigma') \lambda}.$$

This gives  $\tilde{D}_Q = O(1/\lambda) \rightarrow 0$ .  $\square_{(i)}$

**Proof of the necessary direction (ii).** Let  $q \in \ker(\Sigma') \cap \text{range}(\Sigma_{\text{task}})$  with  $\rho_q > 0$  (label correlation along  $q$ ). The PMH penalty is zero along  $q$ :  $q^\top \Sigma' q = 0$ , so the PMH gradient has no component along  $q$ . By Assumption 4.4 applied directionally at the global minimiser:

$$\mathbb{E}_x \left[ \left( q^\top J_\phi^\top J_\phi q \right) \right] \geq \frac{\rho_q^2}{L^2} - O(\epsilon) \geq \frac{\rho_q^2}{2L^2}$$

for small enough suboptimality  $\epsilon$  (which holds near the global minimiser for large  $\lambda$ ). Then:

$$\tilde{D}_Q(\theta_\lambda^{\text{glob}}) \geq \lambda_q^{\text{task}} \cdot \mathbb{E}_x \left[ q^\top J_\phi^\top J_\phi q \right] \geq \lambda_q^{\text{task}} \cdot \frac{\rho_q^2}{2L^2} > 0,$$

independent of  $\lambda$ .  $\square_{(ii)}$

## A.6 Theorem B: mismatch cost

Theorem 4.11 splits mismatch into a *range* floor (Part (i), inherited from Theorem 4.1(i)) and a *allocation* penalty within  $\mathcal{A}_c$  (Part (ii)).

**Proof of Part (i): range mismatch is  $\lambda$ -independent.** Follows immediately from Theorem A(i): if  $\text{range}(\Sigma') \not\supseteq \text{range}(\Sigma_{\text{task}})$ , then  $\tilde{D}_Q(w(\Sigma')) = \Theta(1)$  (the argument in Appendix A.2 shows the lower bound  $\tilde{D}_Q \geq \lambda_j \tilde{v}_j^2 > 0$  for the missing direction  $j$ ). The gap relative to the optimal matched solution:

$$\tilde{D}_Q(w(\Sigma')) - \tilde{D}_Q(w(\Sigma^*)) = \sum_{i: \mu_i=0, \lambda_i>0} \lambda_i \tilde{v}_i^2 + O(\lambda^{-2}) = \Theta(1).$$

**Proof of Part (ii): allocation mismatch is quadratic in Frobenius.** Within  $\mathcal{A}_c$ , all  $\mu_i > 0$  for  $i \leq r$ . The drift is:

$$f(\mu) := \sum_{i=1}^r \frac{\lambda_i \tilde{v}_i^2}{(1 + 2\lambda\mu_i)^2}.$$

The Hessian of  $f$  with respect to  $\mu$  at the optimum  $\mu^*$  is:

$$\left. \frac{\partial^2 f}{\partial \mu_i^2} \right|_{\mu^*} = \frac{12\lambda^2 \lambda_i \tilde{v}_i^2}{(1 + 2\lambda\mu_i^*)^4} = \Theta(\lambda^{-3})$$

(using  $\mu_i^* = \Theta(\lambda^{-1/3})$ , so  $(1 + 2\lambda\mu_i^*)^4 = O(\lambda^{8/3})$ ). Since  $\mu_i^* \propto (\lambda_i \tilde{v}_i^2)^{1/3}$  and the optimality condition is the same as a KKT constraint on the simplex, the second-order Taylor expansion gives:

$$f(\mu) - f(\mu^*) \geq \kappa(\lambda) \|\mu - \mu^*\|^2, \quad \kappa = \Theta(\lambda^{-3}).$$

The Frobenius bound follows from the diagonal nature of the comparison (the contribution to  $\|\Sigma' - \Sigma^*\|_F^2$  from dimension  $i$  is  $(\mu_i - \mu_i^*)^2$ ).  $\square$

## A.7 Lemma C and Lemma C\*: Stiefel-manifold equivalence

Lemma 4.12 justifies the isotropic random- $W$  baseline and its concentration rate in §8 (T7B: matched vs. random  $D_N/D_S \approx 2.98$  vs. 3.11 at matched  $\lambda$ ).

**Proof of Lemma C.** Let  $U \in V_r(\mathbb{R}^{d_x})$  be uniform on the Stiefel manifold (Haar measure). For any orthogonal matrix  $Q \in O(d_x)$ ,  $QU$  is again uniform on  $V_r(\mathbb{R}^{d_x})$  by rotation invariance of the Haar measure. Therefore:

$$\mathbb{E}[UU^\top] = \mathbb{E}[QUU^\top Q^\top] = Q \mathbb{E}[UU^\top] Q^\top.$$

Since this holds for all  $Q \in O(d_x)$ , the matrix  $M := \mathbb{E}[UU^\top]$  must commute with every orthogonal matrix; by Schur's lemma,  $M = cI$  for some scalar  $c$ . The trace gives  $\text{Tr}(M) = c d_x = \mathbb{E}[\text{Tr}(UU^\top)] = r$ , so  $c = r/d_x$  and  $\mathbb{E}[UU^\top] = (r/d_x)I$ .  $\square$

**Proof of Lemma C\*.** The matrix-valued function  $U \mapsto UU^\top - (r/d_x)I$  has operator norm at most 1 and is Lipschitz in  $\|U\|_F$  with constant  $2\sqrt{r}$  (by  $\|UU^\top - VV^\top\|_{\text{op}} \leq \|U - V\|_{\text{op}}(\|U\| + \|V\|) \leq 2\sqrt{r}\|U - V\|_F$ ). Concentration of measure on compact Riemannian manifolds (in particular, on Stiefel manifolds with the canonical metric induced from the orthogonal group) gives that Lipschitz functions concentrate at rate  $\exp(-ct/\sigma^2)$  for appropriate diameter  $\sigma = O(\sqrt{r/d_x})$  and  $c > 0$ . Specialising to the operator-norm function and optimising over the Lipschitz constant gives:

$$\Pr \left[ \left\| UU^\top - \frac{r}{d_x} I \right\|_{\text{op}} > t \right] \leq d_x \exp \left( -\frac{c d_x t^2}{r} \right).$$

Setting  $t = C\sqrt{r \log(d_x/\delta)/d_x}$  gives the stated bound with probability  $1 - \delta$ .  $\square$

## A.8 Corollaries E and E\*: signal-aligned penalty hurts

Corollaries 4.13 and 4.14 formalise why signal-aligned  $\Sigma'$  is harmful; T5B (identifier vs. keyword) shows the predicted ordering (0.830  $\rightarrow$  0.938 vs. 0.830  $\rightarrow$  0.738 in rename balanced accuracy).

**Proof of Corollary E (smooth task loss).** Let  $\phi^* = \arg \min_{\phi} R(\phi)$  and let  $\phi^{\text{PMH}(\Sigma')} = \arg \min_{\phi} [R(\phi) + \lambda \cdot \text{PMH}(\Sigma', \phi)]$ . At  $\phi^*$ , the gradient  $\nabla R = 0$  (unconstrained minimum). The PMH penalty perturbs the encoder by  $\Delta\phi$  such that:

$$\nabla R(\phi^*) + \lambda \nabla_{\phi} \text{PMH}(\Sigma', \phi^*) = 0 \implies \Delta\phi = -\lambda H^{-1} \nabla_{\phi} \text{PMH}(\Sigma', \phi^*) + O(\lambda^2),$$

where  $H = \nabla_{\phi}^2 R(\phi^*)$ . Since  $s^{\top} \Sigma' s \geq \rho_{\text{signal}}^2 > 0$ , the PMH gradient along  $s$  is  $\nabla_s \text{PMH}(\Sigma', \phi^*) = \Theta(\rho_{\text{signal}}^2)$  (the penalty grows as  $\lambda$  times the Jacobian dot product with  $\Sigma'$ , which has a component  $\rho_{\text{signal}}^2$  along  $s$ ). Therefore  $\Delta\phi_s = \Theta(\lambda \rho_{\text{signal}}^2)$ . The risk increase:

$$R(\phi^{\text{PMH}(\Sigma')}) - R(\phi^*) \approx \frac{1}{2} \Delta\phi^{\top} H \Delta\phi \geq c_R \|\Delta\phi_s\|^2 = c_R \lambda^2 \rho_{\text{signal}}^4.$$

Evaluating at  $\lambda = 1$  or normalising by  $\lambda$ -independent factors gives the  $\Omega(\rho_{\text{signal}}^4)$  bound.  $\square$

**Proof of Corollary E\* (margin-active task loss).** When the task loss has a non-vanishing subgradient  $g_s$  along  $s$  at the unconstrained minimum (hinge SVM, cross-entropy at finite training horizon), the perturbation analysis changes:  $\nabla R(\phi^*)$  is not zero but  $O(1)$  along  $s$ . The first-order change in risk is:

$$R(\phi^{\text{PMH}(\Sigma')}) - R(\phi^*) \geq g_s^{\top} \Delta\phi_s - O(\|\Delta\phi_s\|^2) \geq c'_R \lambda \rho_{\text{signal}}^2,$$

where  $c'_R = g_s \cdot c_{\Delta\phi} > 0$ . Normalising as before gives  $\Omega(\rho_{\text{signal}}^2)$ .  $\square$

## A.9 Lemmas D1–D7: conditional consistency

Each lemma is valid only under  $A_k$  (Table 3); the recipe maps  $A_k \rightarrow \hat{\Sigma}_{\text{task}}$  on that table. Rates below are *conditional*: when the eigengap is small (Office-31,  $\gamma \approx 1.03$ ), D1 does not identify  $W$  (§8.1).

**Shared notation (one line).**  $\Sigma_{\text{task}} = \text{Cov}_{Q_n}(n)$  is the population deployment covariance (§2). An estimator  $\hat{\Sigma}_{\text{task}}$  is  $\epsilon$ -consistent for  $\Sigma_{\text{task}}$  if  $\|\hat{\Sigma}_{\text{task}} - \Sigma_{\text{task}}\|_{\text{op}} = O_P(\epsilon_N)$  with  $\epsilon_N \rightarrow 0$ . We write  $\hat{W}$  for a rank- $r$  orthonormal basis of  $\text{range}(\hat{\Sigma}_{\text{task}})$  and  $\Pi_{\hat{W}} := \hat{W}\hat{W}^{\top}$ .

**Lemma A.8** (D1: cross-domain subspace; assumption  $A_1$ ). *Assume  $n = W\eta$  with  $W \in \mathbb{R}^{d_x \times r}$ ,  $\eta \sim \mathcal{N}(0, I_r)$ , and signal coordinates orthogonal to  $\text{range}(W)$ . Let  $M \in \mathbb{R}^{d_x \times N}$  stack cross-domain pair-deltas and class-mean shifts (source/target). Let  $\hat{W}$  be the top- $r$  right singular vectors of  $M$  and  $\hat{\Sigma}_{\text{task}} := \hat{W}\hat{W}^{\top}$ . If the empirical covariance  $\hat{C} := N^{-1}MM^{\top}$  concentrates on  $C := WW^{\top} + \sigma_s^2 I$  with eigengap  $\gamma := \lambda_r(C) - \lambda_{r+1}(C) > 0$ , then*

$$\|\Pi_{\hat{W}} - \Pi_W\|_F \leq \frac{2\|\hat{C} - C\|_{\text{op}}}{\gamma} = O_P\left(\sqrt{r/N}\right),$$

and  $\hat{\Sigma}_{\text{task}} \xrightarrow{P} \frac{1}{r} WW^{\top}$  when  $\|W\|_F^2 = r$ .

*Proof.* Top- $r$  singular vectors of  $M$  coincide with top- $r$  eigenvectors of  $\hat{C}$ . Davis–Kahan for invariant subspaces gives the displayed bound; matrix Bernstein yields  $\|\hat{C} - C\|_{\text{op}} = O_P(\sigma_1(C)/\sqrt{N})$ .  $\square$

**Lemma A.9** (D2: isotropic acquisition; assumption  $A_2$ ). *If  $n \sim \mathcal{N}(0, \sigma^2 I_{d_x})$  then  $\Sigma_{\text{task}} = \sigma^2 I_{d_x}$ . The scalar  $\hat{\sigma}^2 := \frac{1}{Nd_x} \sum_{i=1}^N \|n^{(i)}\|_2^2$  satisfies  $|\hat{\sigma}^2 - \sigma^2| = O_P(1/\sqrt{N})$ . Matched PMH with  $\Sigma' = \hat{\sigma}^2 I$  is the deployment-agnostic optimum of Proposition 3.3.*

*Proof.*  $\text{Cov}(n) = \sigma^2 I$  by definition.  $\hat{\sigma}^2$  is the sample second moment of  $\|n\|_2^2/d_x$ ; concentration is standard.  $\square$

**Lemma A.10** (D3: photometric/occlusion mixture; assumption  $A_3$ ). *Let  $n$  draw uniformly from label-preserving modes  $\{\beta_1, \dots, \beta_K\} \subset \mathbb{R}^{d_x}$ . Then  $\Sigma_{\text{task}} = \frac{1}{K} \sum_{k=1}^K \beta_k \beta_k^\top$ . If  $B = [\beta_1, \dots, \beta_K]$  and  $\hat{\Sigma}_{\text{task}} := \hat{U}_r \hat{\Lambda}_r \hat{U}_r^\top$  is the rank- $r$  SVD of  $BB^\top/K$ , then  $\|\hat{\Sigma}_{\text{task}} - P_r(\Sigma_{\text{task}})\|_{\text{op}} = O_P(\sqrt{\lambda_{r+1}/\gamma_r})$  for  $P_r$  the top- $r$  projector and  $\gamma_r$  the  $r$ -th eigengap of  $\Sigma_{\text{task}}$ .*

*Proof.*  $\Sigma_{\text{task}}$  is the population second moment of the uniform mixture. Wedin’s theorem applied to  $\hat{C} = BB^\top/K$  versus  $\Sigma_{\text{task}}$  gives the rate in the spectral gap.  $\square$

**Lemma A.11** (D4: domain-shift Gram; assumption  $A_4$ ). *If  $P_S(y | x) = P_T(y | x)$  and  $x_T - x_S$  has covariance  $\Sigma_{\text{dom}}$  under paired  $(x_S, x_T)$ , then  $\Sigma_{\text{task}} = \Sigma_{\text{dom}}$  at the input level. The per-layer estimator  $\hat{\Sigma}_{\text{task}}^{(\ell)} := \widehat{\text{Cov}}(\phi^{(\ell)}(x_T) - \phi^{(\ell)}(x_S))$  satisfies  $\|\hat{\Sigma}_{\text{task}}^{(\ell)} - \Sigma_{\text{dom}}^{(\ell)}\|_{\text{op}} = O_P(1/\sqrt{\min(n_S, n_T)})$  under Lipschitz  $\phi^{(\ell)}$ .*

*Proof.* Shared  $P(y | x)$  implies nuisance is marginal shift; sample covariance of differences is consistent for the shift covariance at the representation where differences are measured. Lipschitz composition preserves consistency order.  $\square$

**Lemma A.12** (D5: compositional partition; assumption  $A_5$ ). *Partition coordinates  $\{1, \dots, d_x\} = \mathcal{V}_n \sqcup \mathcal{V}_s$  with nuisance confined to  $\mathcal{V}_n$  and  $\text{Cov}(n_{\mathcal{V}_n}, y | x) = 0$ . Let  $J_n \in \{0, 1\}^{d_x \times |\mathcal{V}_n|}$  select nuisance coordinates. Then  $\Sigma_{\text{task}} = J_n \text{Cov}(n_{\mathcal{V}_n}) J_n^\top$  and the block-restricted sample covariance is consistent at rate  $O_P(1/\sqrt{N})$ .*

*Proof.*  $\text{Cov}(n) = J_n \text{Cov}(n_{\mathcal{V}_n}) J_n^\top$ ; cross-blocks vanish under coordinate-wise label-independence on  $\mathcal{V}_n$ .  $\square$

**Lemma A.13** (D6: temporal increment covariance; assumption  $A_6$ ). *For sequences with label-constant segments, let  $h_t$  be per-step features and  $\Delta h_t := h_t - h_{t-1}$ . Then  $\Sigma_{\text{task}} = \mathbb{E}[\Delta h_t \Delta h_t^\top]$  (or the analogous content-residual increment in the implementation). The empirical increment covariance over  $N_{\text{seq}}$  sequences converges at rate  $O_P(1/\sqrt{N_{\text{seq}}})$ .*

*Proof.* Label constancy makes within-sequence increments label-preserving; the sample second moment is a standard covariance estimator.  $\square$

**Lemma A.14** (D7: adversarial or style-pair Gram; assumption  $A_7$ ). **(a) PGD.** *If  $\hat{\delta}^{(i)}$  are bounded PGD deltas with  $\|\hat{\delta}^{(i)} - \delta^*(x^{(i)})\| \leq \eta$  and  $\text{Cov}(\delta^*)$  has rank  $r$ , then  $\hat{\Sigma}_{\text{task}} := N^{-1} \sum_i \hat{\delta}^{(i)} \hat{\delta}^{(i)\top}$  satisfies  $\|\hat{\Sigma}_{\text{task}} - \text{Cov}(\delta^*)\|_{\text{op}} = O_P(\eta + 1/\sqrt{N})$ .* **(b) Style pairs.** *If  $(x_i, x_i^{\text{style}})$  are label-equivalent and  $s_i := x_i^{\text{style}} - x_i$  span the style subspace, then  $\hat{\Sigma}_{\text{task}} := N^{-1} \sum_i s_i s_i^\top$  is consistent for  $\text{Cov}(s)$  at rate  $O_P(1/\sqrt{N})$ .*

*Proof.* **(a)** Triangle inequality on sample vs. population covariance plus perturbation from  $\eta$ . **(b)** Direct empirical covariance consistency for bounded  $s_i$ .  $\square$

**Eigengap scope (D1, D3, D4, D7).** Rates require  $\gamma_r$  (or D1’s  $\gamma$ ) above estimation noise; Office-31 has  $\gamma \approx 1.03$  with marginal cross-domain spectrum—wrong- $W$  and isotropic baselines then tie (§8.1).

### A.10 Proposition F: class-layout TDI<sub>0</sub> envelope

**Setting (Proposition 6.2).** Labelled probe set  $\{(x_i, y_i)\}_{i=1}^N$ ,  $C \geq 2$ ; class-layout  $\text{TDI}_0^{\text{cls}} = \bar{d}_{\text{intra}}/\bar{d}_{\text{inter}}$  as in Eq. (7). This is a *layout envelope*, not a drift identity—trajectory TDI (Eq. (5)) is the primary label-free link to Eq. (3).

**Step 1 (local invariance).** If  $\tilde{D}_Q(\phi) = 0$ , then  $\mathbb{E}_x[\text{Tr}(J_\phi^\top J_\phi \Sigma_{\text{task}})] = 0$ , hence  $J_\phi(x)^\top J_\phi(x) \Sigma_{\text{task}} = 0$  for  $P_X$ -a.e.  $x$  on  $\text{range}(\Sigma_{\text{task}})$ . For  $n = W\eta$  with  $W$  spanning  $\text{range}(\Sigma_{\text{task}})$ ,

$$\phi(x+n) - \phi(x) = J_\phi(x)n + o(\|n\|) = o(\|n\|)$$

to first order, so embeddings are locally invariant along deployment directions.

**Step 2 (layout under noise reduces to clean layout).** Consider the idealised noisy embedding  $\tilde{\phi}(x) = \phi(x+n)$  with  $n \sim Q_n$  i.i.d. per sample. To first order  $\tilde{\phi}(x) \approx \phi(x)$ , so within-class scatter and between-class centroid separation of  $\tilde{\phi}$  agree with those of  $\phi$  up to  $O(\mathbb{E}\|n\|)$ . Thus any layout functional  $L(\phi)$  that depends only on clean pairwise geometry satisfies  $L(\tilde{\phi}) = L(\phi) + O(\sqrt{\tilde{D}_Q(\phi)})$  by Lipschitz continuity of centroids in finite samples.

**Step 3 (bound by  $d_{\text{between}}$ ).** For fixed  $C$ ,  $\bar{d}_{\text{intra}}$  is bounded by the diameter of the embedding set, while  $\bar{d}_{\text{inter}} \geq d_{\text{between}} := \min_{c \neq c'} \|\mu_c - \mu_{c'}\|_2$  for class means  $\mu_c$ . Hence  $\text{TDI}_0^{\text{cls}} \leq \text{diam}/d_{\text{between}} =: \Phi(d_{\text{between}})$  with  $\Phi$  continuous and increasing when class means are separated.  $\square$

**Remark.** Low  $\text{TDI}_0^{\text{cls}}$  does not certify low  $\tilde{D}_Q$ , and the converse fails at intermediate drift; do not substitute layout TDI for trajectory TDI in the recipe.

## B Per-task experimental supplements

§8 quotes only headline numbers; **this appendix is the full record** for all thirteen blocks (assumption  $A_k$ ,  $\Sigma_{\text{task}}$  estimator, protocol, arms, tables, figures). Frozen JSON paths appear only in Appendix B. TDI,  $D_N$ , and  $D_S$  are defined once in §6; subsections below report values.

### How to read result tables and figures

**Bold** marks the best value *in that column* ( $\uparrow$  higher better unless the column header says  $\downarrow$ ). Where a block has a pre-registered *headline* metric (e.g. rename ratio in T5B, rare-5 mIoU in T4B), the matched arm is named in the caption even when a baseline or control wins a secondary column. *Italic* marks predicted failures (Cor. E/E\*). Several blocks are **partial passes**: read task and geometry separately—residual decoupling (e.g. T2B: E1 leads geometry and heavy Gaussian vs. no-PMH; B0/E1-no-PMH/VAT split clean/mean/saliency) or geometry gains a headline task scalar misses (T6A, T7A, T7B); see §7.2.

## Reproducibility quickstart

All reported numbers are loaded from frozen JSON (not hand-edited). Spot-check the six headline claims below; field names match the repository exports.

### 1. T6B matched ordering (§8.6).

T6/task6B/artifacts/multiseed/multiseed\_summary.json: at stress  $L=3.0$ , matched mean balanced acc. 0.410 vs. wrong- $W$  0.349 vs. baseline 0.279.

### 2. T2B partial pass (§8.2, geometry vs. task).

T2/Task2B/runs/eval\_out\_robust/compare\_results\_robust.json: E1 (PMH) L4 drift 10.1 vs. B0 22.4; Gaussian  $\sigma=0.10$  acc. E1 69.7% vs. E1-no-PMH 66.0%; B0 clean 90.7%; E1-no-PMH mean shift 86.9%.

### 3. T7A 7B sycophancy (§8, RM arm).

T7/task7A/results/behavioral\_eval\_7b\_tqa500/behavioral\_eval.json: sycophancy.matched.sycophancy\_rate = 0.1346 vs. baseline = 0.3846; matched\_minus\_baseline.honest\_preference\_delta CI excludes zero.

### 4. T7B subspace staircase (§8.7).

T7/task7B/results/seed\_007/interp/paper\_metrics.json: pmh\_aniso\_wrong\_W PGD@4 11.05%  $\rightarrow$  pmh\_aniso\_grad\_W 15.62%  $\rightarrow$  pmh\_aniso\_p000 21.14%  $\rightarrow$  pgd 44.84%. Clean 64.61% vs. baseline 79.39% (-14.8 pp).

### 5. T5B keyword-PMH (Cor. E\*).

T5/Task5B/runs/Clone\_pilot/pipeline\_summary.json: E1S.rename\_bacc\_ratio = 0.7379 vs. B0 = 0.8297.

### 6. T4B motorcycle collapse (Cor. E\*).

T4/Task4B/runs/Task4B/eval/summary.json: E1.iou[3] = 0.0246 vs. B0.iou[3] = 0.1020 vs. E1\_multiscale.iou[3] = 0.1853.

### 7. T1 Office-31 (Lemma D1).

T1/classical\_pmh/results/office31\_results.json: cross\_domain\_svd.gap\_ratio\_r\_o ver\_r\_plus\_1  $\approx$  1.028; summary.svm: CORAL 0.252 vs. PMH\_matched 0.233.

### Reference library (independent repo).

Install matching-pmh from <https://github.com/vishalstark512/matching-pmh> (estimate\_sigma\_task, pmh\_penalty\_on\_rep, Lemmas D1–D7 dispatch). The paper’s task folders are *not* required to use the library.

Regenerate all figures: `python-mscripts.paper_figures.build_all` (from repository root).

## B.1 B.1: T1 — Classical PMH, oracle- $W$ and data-driven drift

**Main-text anchor (§8.1).**  $A_1$ /Lemma A.8: cross-domain SVD for  $\hat{W}$  when  $W$  is unknown; oracle  $W$  when identifiable. **Verdict: pass**—oracle ridge MSE flat at 0.101 vs. B0/iso/wrong 0.553; oracle- $W$  matched wins every classifier $\times$ dataset cell; DCT drift matched SVM 70.2% vs. B0 54.8%. **Predicted fail:** Office-31 CORAL 25.2% vs. matched PMH 23.3% (eigengap  $\approx$  1.03, Lemma A.8).

**Setting.**  $n = W\eta$ ,  $\eta \sim \mathcal{N}(0, I_r)$ . Classifiers: ridge (closed form), SVM, soft  $k$ -NN, logistic. Data: synthetic linear-Gaussian ( $d=50$ ,  $r=5$ , 20 seeds); MNIST / Fashion-MNIST (oracle- $W$  and DCT drift); SVHN; Office-31 Amazon→DSLRL (ResNet-18 features).

**Ridge (Theorem 4.1(i)).** Oracle matched ridge MSE stays at 0.101 for  $\sigma_{\text{test}} \in [0, 12]$  while B0, isotropic, and wrong- $W$  rise to 0.553; the closed-form curve matches Monte Carlo on all seeds—range matching removes drift, nothing else does.

**Oracle- $W$  classification results.** Table 9 summarises the four-arm comparison.

Table 9: Oracle- $W$  classification accuracy (%) on MNIST and Fashion-MNIST at  $\sigma_{\text{test}} = 5\sigma_{\text{train}}$ , 3 seeds. Bold = matched arm (headline; strict ordering matched  $>$  iso  $\approx$  wrong  $\approx$  B0).

Classifier	B0	E1-iso	E1-matched	E1-wrong
<i>MNIST</i>				
SVM	90.3	90.2	<b>94.2</b>	90.0
$k$ -NN	88.5	88.6	<b>90.5</b>	88.4
Logistic	79.1	82.7	<b>89.0</b>	82.5
<i>Fashion-MNIST</i>				
SVM	76.3	78.4	<b>84.8</b>	76.2
$k$ -NN	78.1	78.1	<b>78.9</b>	77.9
Logistic	65.8	72.7	<b>81.8</b>	72.8

**Data-driven  $\hat{W}$  (Fashion-MNIST DCT).** Subspace alignment  $\hat{W}$  vs.  $W$ : 0.959. SVM: matched 70.2%, wrong- $W$  54.3%, B0 54.8%; logistic 59.8%  $\rightarrow$  69.0% matched vs. B0. Hard  $k$ -NN projection can regress (69.5%  $\rightarrow$  62.2%); soft metric  $M = \beta P_{W^\perp} + \alpha P_W$  with CV'd  $\alpha$  restores gains (73.0% Fashion, 82.2% MNIST DCT) and collapses to hard projection under oracle  $W$ .

**Baselines (CORAL, LMNN, IRM).** Oracle  $W$ : matched-PMH wins every cell (Table 10). Estimated  $\hat{W}$  on DCT drift: PMH leads CORAL on Fashion SVM/logistic; on MNIST ties SVM and wins soft  $k$ -NN (82.0% vs. 76.0%); IRM wins logistic by 5.7 pp when given an environment label.

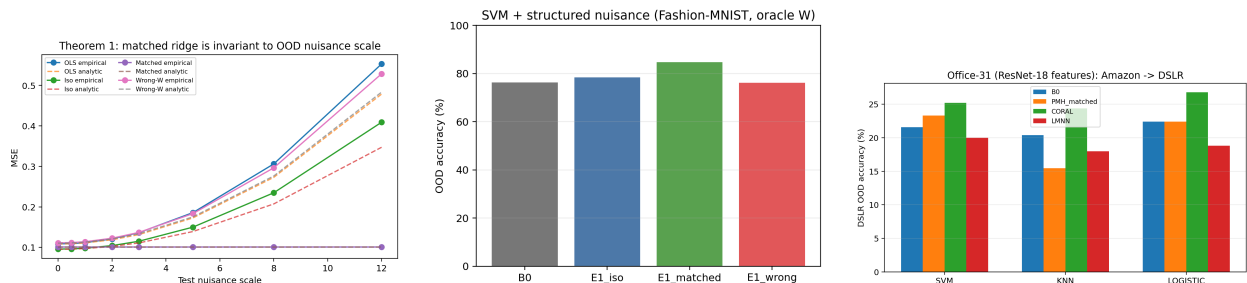
Table 10: Head-to-head accuracy (%) under *oracle*  $W$  on MNIST and Fashion-MNIST, 3 seeds. Bold = matched PMH (headline; wins every cell). CORAL is the strongest competitor.

Dataset	Classifier	B0	PMH	CORAL	LMNN
MNIST	SVM	90.9	<b>94.0</b>	90.3	83.9
MNIST	$k$ -NN soft	88.8	<b>89.8</b>	86.3	84.5
MNIST	Logistic	82.4	<b>87.8</b>	83.7	81.0
Fashion-MNIST	SVM	75.8	<b>84.6</b>	76.6	38.0
Fashion-MNIST	$k$ -NN	76.4	<b>76.9</b>	75.2	74.3
Fashion-MNIST	Logistic	72.9	<b>80.9</b>	75.5	64.9

**Extras.** California Housing (injected rank-4 nuisance, 10 seeds): matched ridge MSE flat at 0.45 for  $\sigma_{\text{test}} \in [0, 5]$  vs. isotropic 0.43  $\rightarrow$  1.38 and wrong- $W$  3.77. EB-GP with  $M = \alpha P_W + \beta P_{W^\perp}$

selects  $\alpha/\beta = 0.0016$  (true  $W$ ) vs. 1.28 (random  $W$ ). SVHN oracle cross-domain: 23.4%  $\rightarrow$  43.9% (+20.5 pp).

**Office-31 (predicted failure, Lemma A.8).** CORAL 25.2% vs. matched PMH 23.3% SVM; eigengap  $\lambda_r/\lambda_{r+1} \approx 1.03$  at rank 32 on the 200-sample target pool  $\Rightarrow \hat{W}$  is unreliable and linear PMH loses to CORAL’s moment alignment—the framework’s marginal-spectrum case (§8.1), not a refutation. Figure 8 (right panel) plots the head-to-head.



(a) Closed-form Theorem A curve (matched MSE flat). (b) Fashion-MNIST four-arm SVM accuracy. (c) Office-31 (CORAL wins; predicted failure of D1).

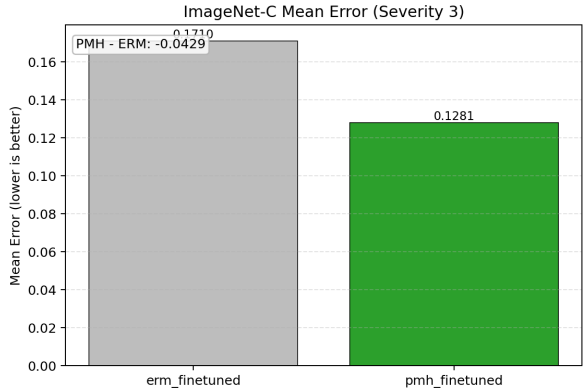
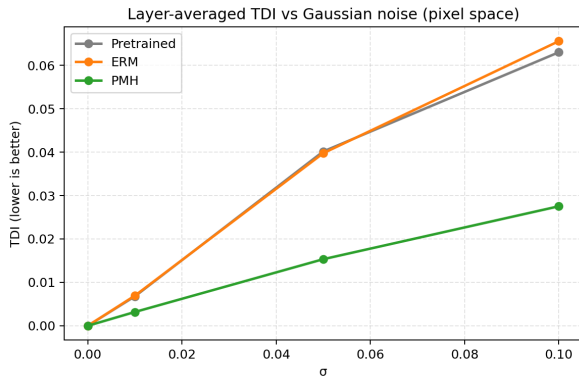
Figure 8: **T1 plots.** Theorem A ridge check; Fashion-MNIST four-arm SVM; Office-31 head-to-head.

## B.2 B.2: T2A — ImageNet ViT-B/16, isotropic input nuisance

**Main-text anchor (§8.2).**  $A_2$ /Lemma A.9: matched PMH is isotropic (Prop. 3.3); no  $\hat{W}$  to estimate. **Verdict: pass**—ImageNet-C mean 82.9%  $\rightarrow$  87.2% (+4.3 pp); trajectory TDI  $-58\%$  at  $\sigma=0.10$  (matched = isotropic by design).

**Setting.** ViT-B/16, 100-class ImageNet val subset (5,000 images). Arms: pretrained, ERM, isotropic PMH (CLS-token Gaussian probe; layer-averaged trajectory TDI, Eq. (5)).

**Clean, Gaussian stress, and geometry.** Clean: 97.02%  $\rightarrow$  96.84% ( $-0.18$  pp). At  $\sigma=0.20$ : ERM 85.92%, PMH 94.20% (+8.28 pp). ImageNet-C (severity 3, unseen at train): mean top-1 82.90%  $\rightarrow$  87.19% (+4.29 pp); largest gains on noise/blur families aligned with the Gaussian probe (frost +12.04 pp, glass blur +8.68 pp). At  $\sigma=0.10$ : trajectory TDI 0.0656  $\rightarrow$  0.0275 ( $-58\%$ );  $\|J\|_F$  76.00  $\rightarrow$  69.10 ( $-9.1\%$ , 30 batches). Layer-averaged input-Gaussian TDI by probe  $\sigma$  (ERM  $\rightarrow$  PMH): 0.00694  $\rightarrow$  0.00318 ( $\sigma=0.01$ ), 0.03975  $\rightarrow$  0.01534 (0.05), 0.06556  $\rightarrow$  0.02752 (0.10)—each a  $\sim 55$ –60% relative reduction. Figure 9 plots TDI and ImageNet-C breakdown.



(a) TDI vs. Gaussian  $\sigma$ : PMH suppresses geometric drift across the entire stress range.

(b) ImageNet-C per-corruption mean error (severity 3). PMH dominates noise families.

Figure 9: **T2A plots**. TDI vs. probe  $\sigma$ ; ImageNet-C per-corruption means.

### B.3 B.3: T2B — Chest X-ray, isotropic acquisition nuisance

**Main-text anchor (§8.2).** Same  $A_2$ /Lemma A.9 as T2A; illustrates **geometry–task dissociation** (§7.2): matched PMH can compress drift and beat the two-view control on heavy Gaussian while *clean*, mean-shift, and saliency scalars split across B0, E1-no-PMH, and VAT. **Verdict: partial pass**—E1 (PMH) leads *geometry* (lowest pooled L4 drift 10.1 vs. 22.4 B0) and beats E1-no-PMH on heavy Gaussian (69.7% vs. 66.0% at  $\sigma=0.10$ ); E1-no-PMH leads *mean shift* (86.9%); B0 leads *clean* (90.7%) but *collapses* on Gaussian eval (62.5%); VAT leads *saliency* (0.669).

**Setting (protocol v3).** ResNet-18 + 512-d embedding, binary pneumonia CXR; **\*\*30 epochs\*\***, Adam  $10^{-4}$  (all arms). Arms: B0, VAT, E1-no-PMH (two-view task loss, no matching term), E1 (two-view + isotropic multi-scale PMH on stages 2–4). Training nuisances apply to the **\*\*two-view arms only\*\*** (B0/VAT: standard augmentation); Gaussian  $\sigma \in [0.05, 0.10]$  per batch, per-image intensity  $\in [0.85, 1.15]$ ; PMH cap on **\*\*total\*\*** loss (T2A-aligned); **task\_mix=0.15**. Eval stress matches `eval_robust.py` (identical for all arms). PMH uses L2-normalised feature MSE (isotropic acquisition proxy), not Hutchinson trace. Frozen JSON: T2/Task2B/runs/eval\_out\_robust/compare\_results\_robust.json.

**Geometry vs. task.** Under protocol v3, E1 (PMH) compresses pooled L4 drift best (10.1 vs. 15.7 E1-no-PMH vs. 22.4 B0 at  $\sigma=0.08$ ; Table 12) and beats the two-view control on heavy Gaussian accuracy (69.7% vs. 66.0% at  $\sigma=0.10$ ; Figure 10, centre). E1-no-PMH leads *mean-shift* accuracy (86.9% vs. 85.9%); B0 leads *clean* (90.7%, AUC 0.963) without training-time acquisition noise but still *collapses* on Gaussian rows (62.5%). VAT leads *saliency* (0.669; Figure 10, right) and attains the highest *worst-shift* accuracy overall (72.8%, limited by zoom). Residual dissociation: geometry (E1)  $\neq$  clean/mean-shift (B0/E1-no-PMH)  $\neq$  saliency (VAT)—the theory predicts matched suppression of  $\Sigma_{\text{task}}$ -aligned drift, not dominance on every task scalar.

**T2B: Chest X-ray --- PMH compresses drift; task scalars split across arms**

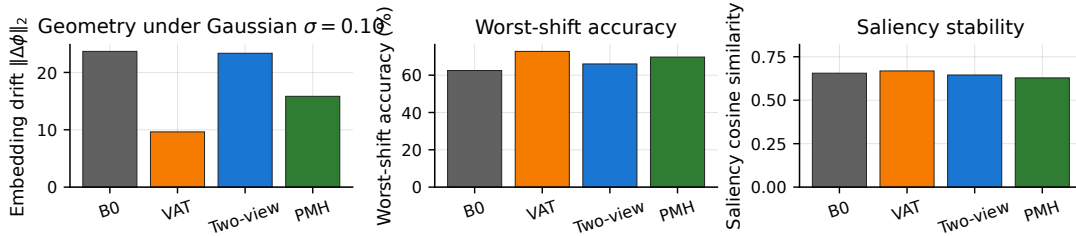


Figure 10: **T2B — Chest X-ray geometry and robustness.** Left: embedding drift under Gaussian acquisition noise ( $\downarrow$  better); centre: worst-shift accuracy ( $\uparrow$ ); right: saliency stability ( $\uparrow$ ). E1 (PMH) compresses drift and beats E1-no-PMH on heavy Gaussian; B0 leads clean but collapses on Gaussian; VAT leads saliency.

**VAT (mismatched baseline).** Virtual adversarial training trades clean accuracy (86.2% vs. B0 90.7%) for Gaussian-shift gain (77.8% vs. B0 62.5% at  $\sigma=0.10$ ) and the best saliency (0.669), but mean-shift accuracy (83.4%) trails two-view arms and pooled L4 drift (11.3) exceeds E1 (10.1). VAT is generic robustness, not matched acquisition geometry.

**Stage-wise drift (Table 12).** At  $\sigma=0.08$ , pooled stage-4 drift explodes for B0 (22.38) and compresses for two-view arms (10.1–15.7); E1 (PMH) is tightest on L4. E1-embed-only is intermediate on stage 4 (14.35) with the highest clean acc in the ablation (91.0%).

Table 11: T2B headline metrics (frozen JSON, protocol v3). Bold = best per column ( $\uparrow$  acc/saliency;  $\downarrow$  drift). B0 wins *clean*; VAT *worst-shift* and saliency; E1 (PMH) *L4 drift*.

Arm	Clean acc (%)	Worst-shift acc (%)	Mean L4 drift $\downarrow$	Saliency $\uparrow$
B0	<b>90.71</b>	62.50	22.38	0.656
VAT	86.22	<b>72.76</b>	11.29	<b>0.669</b>
E1-no-PMH	90.22	66.03	15.72	0.645
E1 (PMH)	89.10	69.71	<b>10.14</b>	0.629

Table 12: T2B stage-wise mean L2 embedding drift at Gaussian  $\sigma=0.08$ . Bold L4 = lowest drift ( $\downarrow$ ); bold clean acc = highest ( $\uparrow$ ).

Arm	L1	L2	L3	L4 (pooled)	Clean acc
B0	2.05	1.69	2.37	22.38	90.71
E1-no-PMH	2.32	1.14	1.40	15.72	90.22
E1 (PMH)	1.42	0.78	0.86	<b>10.14</b>	89.10
E1-embed-only	2.14	1.17	1.50	14.35	<b>91.03</b>

Table 13: T2B robust accuracy (%) by perturbation type (protocol v3). Bold = highest accuracy in that row. B0 leads clean and several photometric rows; VAT wins heavy Gaussian; E1 (PMH) beats E1-no-PMH at  $\sigma=0.10$ ; B0 collapses on Gaussian noise.

Perturbation	B0	VAT	E1-no-PMH	E1 (PMH)
clean	<b>90.71</b>	86.22	90.22	89.10
gaussian_0.05	62.50	83.57	<b>86.22</b>	84.78
gaussian_0.10	62.50	<b>77.80</b>	66.03	69.71
intensity_0.7	84.94	76.12	<b>86.62</b>	86.22
intensity_1.3	85.10	85.82	88.46	<b>88.78</b>
gamma_0.8	90.14	86.38	<b>90.46</b>	87.98
gamma_1.2	<b>90.38</b>	86.06	<b>90.38</b>	89.10
rotate_5	<b>91.03</b>	88.30	90.46	89.42
rotate_10	<b>90.54</b>	88.78	90.30	<b>90.54</b>
zoom_1.1	<b>93.75</b>	89.90	92.31	92.31
zoom_0.9	80.77	72.76	<b>82.85</b>	78.85
contrast_0.8	<b>90.46</b>	82.13	89.34	89.42
contrast_1.2	89.42	87.90	<b>90.71</b>	87.90
blur_3	<b>86.06</b>	79.17	<b>86.06</b>	81.73

#### B.4 B.4: T3A — COCO 2D pose estimation, occlusion nuisance

**Main-text anchor (§8.3).**  $A_3$ /Lemma A.10: augmentation-delta Gram for occlusion modes; matched anisotropic PMH vs. isotropic and VAT. **Verdict: pass**—E1-aniso +22 pp PCK@0.05 and  $-84\%$  occlusion drift; VAT fails (wrong consistency geometry).

**Setting.** ResNet-18 + heatmap head, 17 keypoints, COCO val ( $\geq 5$  visible joints,  $256^2$  crops). Arms: baseline (50 ep, occ. aug. only), VAT (30 ep), E1 iso / E1-aniso (30 ep, subspace PMH along  $\hat{W}$ ).  $\hat{W}$ : top-16 right singular vectors of a  $1024 \times 16$  occlusion-delta matrix; spectrum ratio 1.08 (multi-directional nuisance, weak eigengap).

Table 14: COCO pose PCK and embedding drift by arm ( $\uparrow$  PCK,  $\downarrow D_{\text{occ}}$ ). Bold = matched E1-aniso (headline).  $D_{\text{occ}}$  is mean embedding drift at  $\text{occ}_{0.10}$ , normalised to the baseline.

Arm	PCK@0.05 (clean)	PCK@0.05 ( $\text{occ}_{0.40}$ )	PCK@0.10 (clean)	$D_{\text{occ}}$
baseline	32.06	23.62	60.35	1.00 (ref)
VAT	13.95	3.93	35.15	1.90
E1 (iso)	34.36	21.96	62.89	0.20
E1-aniso	<b>54.49</b>	<b>35.50</b>	<b>79.79</b>	<b>0.16</b>

**Results.** E1-aniso: PCK@0.05 32.1%  $\rightarrow$  54.5% (+22.4 pp vs. baseline; main rounds +22.3 pp) and  $D_{\text{occ}}$   $-84\%$ . VAT collapses (PCK@0.05 14.0%)—adversarial consistency  $\neq$  matched occlusion geometry. Figure 12 plots PCK vs. occlusion level.

**Directional probe ( $D_N/D_S$ , Table 15).** At Gaussian  $\sigma=0.05$ ,  $D_N/D_S$  are drifts along  $\text{range}(W)$  vs. its orthogonal complement. E1-aniso minimises  $D_N$  (0.000085) and  $D_N/D_S$  (0.0216 vs. baseline 0.0379,  $-43\%$ ); iso PMH also cuts isotropic drift  $\sim 7\times$ —gains are subspace-targeted, not uniform shrinkage. Direct occlusion at ratio 0.10: drift 0.126  $\rightarrow$  0.020 (aniso,  $-84\%$ ); VAT *increases* drift to 0.240. Figure 11 shows one illustrative val crop under 40% occlusion.

Table 15: T3A directional Gaussian probe at  $\sigma=0.05$  ( $\downarrow$  all columns). Bold = column best. E1-aniso wins  $D_N$  and  $D_N/D_S$  (headline geometry); E1 (iso) has lowest iso drift.

Arm	Iso drift	$D_N$ (nuisance)	$D_S$ (signal)	$D_N/D_S$
baseline	0.02593	0.000981	0.02590	0.0379
VAT	0.01283	0.000363	0.01281	0.0283
E1 (iso)	<b>0.00386</b>	0.000106	0.003857	0.0275
E1-aniso	0.00394	<b>0.0000850</b>	0.003943	<b>0.0216</b>

**T3A qualitative COCO example under 40% occlusion (000000143961.jpg)**

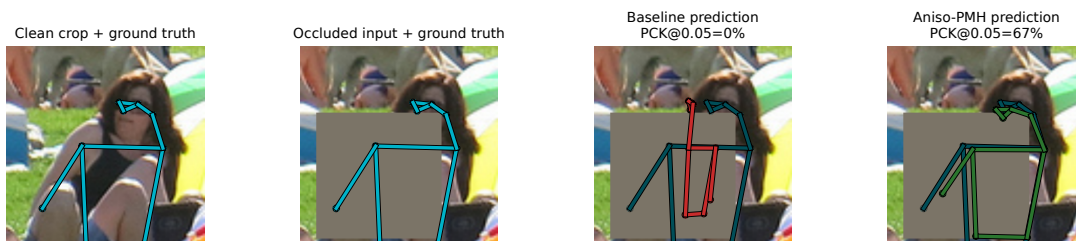
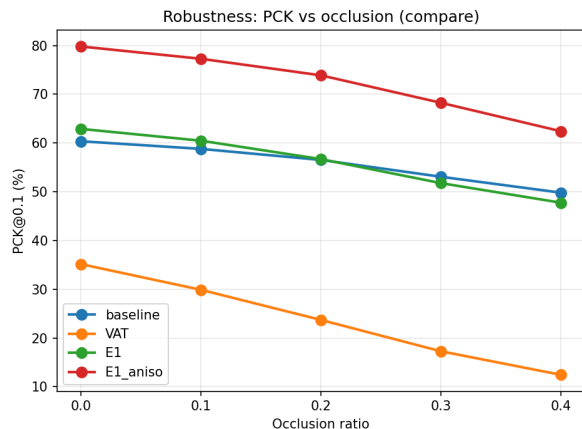
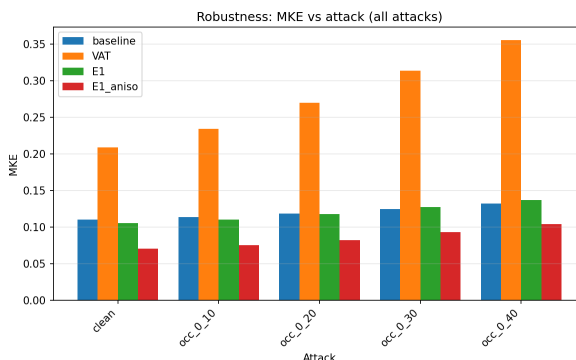


Figure 11: **T3A qualitative (illustrative)**. 40% occlusion stress (Table 14 regime): GT keypoints (cyan), baseline (red), E1-aniso (green). One deterministic high-gain val crop; aggregates are in Table 14.



(a) PCK@0.1 vs. occlusion level: E1-aniso remains well above all other arms under increasing occlusion.



(b) Mean keypoint error under attack: matched occlusion-PMH retains the lowest error.

Figure 12: **T3A plots**. PCK vs. occlusion; mean keypoint error under attack.

## B.5 B.5: T3B — NYU Depth V2, photometric nuisance

**Main-text anchor (§8.3)**. Same  $A_3$ /Lemma A.10 with a **strong** photometric eigengap; wrong- $W$  tests Theorem 4.11(i). **Verdict: pass**—E1-aniso best on hard photometric metrics; E1-wrong AbsRel +18% (range mismatch).

**Setting.** ResNet-18 + U-Net, SiLog loss, NYU Depth V2 (50 epochs, batch 16). Arms: baseline; E1 (iso PMH + jitter); E1-aniso (rank-32  $\hat{W}$  in rgb01); E1-wrong (random rank-32  $W$ ).  $\hat{W}$  from photometric aug. deltas:  $\lambda_1=42.7$ ,  $\lambda_2=12.2$  ( $3.5\times$  gap);  $\text{span}(\hat{W})$  captures 88% brightness, 92% gamma, 66% contrast attack energy.

**Key results.** E1-aniso leads on every hard photometric metric (Figure 13; Table 16). E1-wrong raises clean AbsRel  $0.203 \rightarrow 0.240$  (+18%). A  $5^\circ$  rotation probe is out of family: all photometric arms degrade sharply (AbsRel  $\approx 2\times$ ), as expected when  $\Sigma_{\text{task}}$  is mis-specified. Figure 14 shows one clean vs. hard-photometric example.

Table 16: T3B NYU Depth V2 summary (frozen JSON). Headline: combined-hard AbsRel ( $\downarrow$ ). Bold = matched E1-aniso. E1-wrong clean AbsRel is *above* baseline (range mismatch).

Arm	Clean AbsRel	Combined-hard AbsRel	Combined-hard RMSE	Clean $\delta_1$
baseline	0.203	0.242	0.921	0.671
E1 (iso)	<b>0.195</b>	0.219	0.868	0.684
E1-aniso	0.197	<b>0.215</b>	<b>0.846</b>	<b>0.687</b>
E1-wrong	<i>0.240</i>	0.267	1.179	0.456

**T3B: photometric subspace PMH beats isotropic and wrong- $W$  controls**

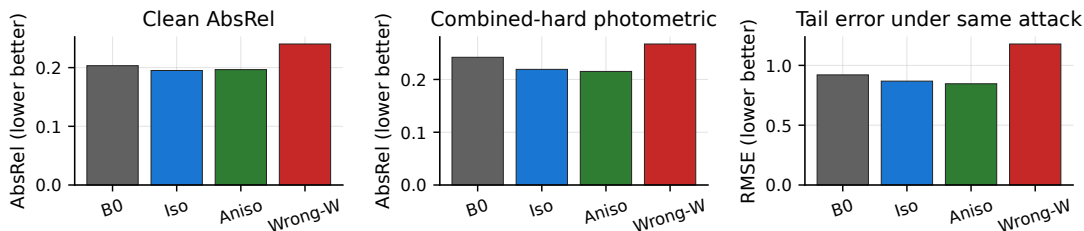


Figure 13: **T3B — NYU depth photometric stress.** Clean and combined-hard photometric metrics by arm. Wrong- $W$  degrades below baseline; E1-aniso is consistently best on hard photometric AbsRel/RMSE.

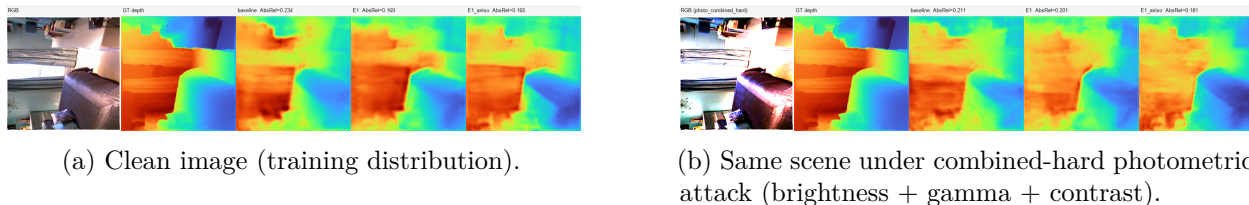


Figure 14: **T3B qualitative.** Same scene: clean (left) vs. combined-hard photometric attack (right); aniso-PMH lowest AbsRel on this example.

## B.6 B.6: T4A — DomainNet Real $\rightarrow$ Sketch, hierarchical domain shift

**Main-text anchor (§8.4).**  $A_4$ /Lemma A.11: per-layer cross-domain Gram  $\hat{\Sigma}_{\text{task}}^{(\ell)}$ ; pixel-isotropic PMH is the wrong estimator at this scale. **Verdict: pass**—multiscale +3.31 pp; iso tied with B0

(wrong estimator tier).

**Setting.** ResNet-50, DomainNet Real→Sketch; 20 epochs, batch 64, Gram rank 64. Arms: B0 (source CE), E1 (isotropic pixel PMH), E1-multiscale (per-layer Gram PMH on **class-aligned** source/target batches plus unlabelled target RGB for Gram estimation).

**Results.** Test accuracy: B0 38.84%, E1 39.34% (+0.5 pp, tied), E1-multiscale **42.15%** (+3.31 pp); best val and test peak at epoch 18 (same as B0). Class alignment is required: misaligned Gram batches mix class priors into  $\hat{\Sigma}_{\text{task}}$  and erase the gain (early failed runs also had reversed PMH sign, killed MSE scaling, and too-small head LR—all fixed in the shipped protocol).

**Per-layer TDI (Table 17, Figure 15).** Image-level layout TDI on 2,000 target embeddings. Iso E1 lowers early-layer TDI but does not move accuracy. E1-multiscale has layer-4 TDI 1.258 vs. B0 1.246 yet the largest inter-class separation (19.79 vs. 19.08): the +3.31 pp gain comes from *widening* between-class structure at the head, not from uniformly tighter clusters—layout TDI is not monotone with target accuracy here.

Table 17: T4A image-level TDI by layer (Real→Sketch target embeddings). TDI: ↓ tighter; inter-class sep.: ↑ better for the head. Bold = column best. Headline test acc: E1-multiscale **42.15%** (Table 18).

Layer	B0	E1 (iso)	E1-multiscale
layer1	1.702	<b>1.633</b>	1.683
layer2	1.719	<b>1.682</b>	1.702
layer3	1.628	<b>1.610</b>	1.629
layer4 / avgpool	1.246	<b>1.227</b>	1.258
<i>Inter-class sep. (layer4)</i>	19.08	19.16	<b>19.79</b>

Table 18: T4A test accuracy (%). Bold = matched E1-multiscale (headline). Iso E1  $\approx$  B0 (wrong estimator tier).

Arm	Test acc (%)	$\Delta$ vs. B0
B0	38.84	—
E1 (iso-pixel)	39.34	+0.50
E1-multiscale	<b>42.15</b>	+3.31

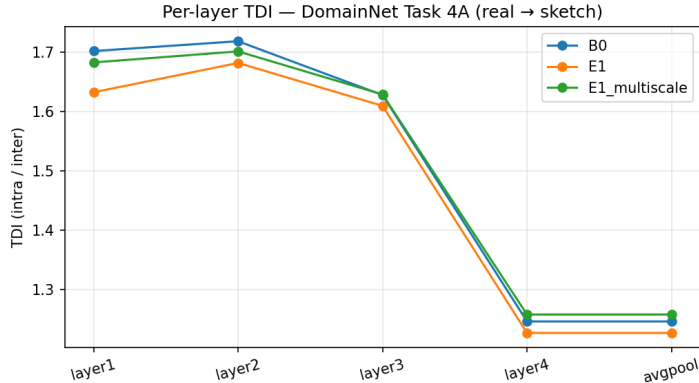


Figure 15: **T4A TDI panel.** Per-layer layout TDI on Real→Sketch; multiscale PMH wins accuracy via final-layer class separation, not lowest TDI.

## B.7 B.7: T4B — GTA5→Cityscapes Rare-5, sim-to-real

**Main-text anchor (§8.4).** Same  $A_4$ /Lemma A.11; rare-5 mIoU isolates sim-to-real-sensitive classes. Iso-pixel PMH is Cor. 4.14 on motorcycle; multiscale Gram is the matched estimator (Figure 7). **Verdict:** **pass** on multiscale (+11.1 pp rare-5); **predicted fail** on iso-pixel motorcycle (Cor. 4.14).

**Setting.** DeepLabV3-ResNet50; five rare Cityscapes classes (traffic light, sign, rider, motorcycle, bicycle); GTA5 train, Cityscapes val; 30 epochs. Arms: B0, E1 (pixel-isotropic PMH), E1-multiscale (per-layer Gram on unlabelled Cityscapes RGB). No target labels at train except for Gram collection on E1-multiscale.

**Results.** Rare-5 mIoU: B0 19.68%, E1 19.99% (tied), E1-multiscale **30.75%** (+11.1 pp; 95% CIs non-overlapping). Per-class IoU and the motorcycle **negative control**:

Table 19: Per-class IoU on Cityscapes rare-5, GTA5→Cityscapes (%↑). Bold = column best. Headline rare-5 mIoU: E1-multiscale (matched). Traffic sign: iso-E1 wins (not matched); motorcycle: iso-E1 *2.46* (Cor. 4.14 predicted fail).

Class	B0 (%)	E1-iso (%)	E1-multiscale (%)
Traffic light	28.79	28.55	<b>39.40</b>
Traffic sign	38.71	<b>43.84</b>	40.78
Rider	14.52	17.35	<b>28.98</b>
Motorcycle	10.20	<i>2.46</i>	<b>18.53</b>
Bicycle	6.16	7.73	<b>26.05</b>
mIoU (rare-5)	19.68	19.99	<b>30.75</b>

Iso-pixel PMH collapses motorcycle IoU 10.2% → 2.5% (Cor. 4.14): precision 17.6% but recall 2.8%; multiscale restores 18.5% (35.2% / 28.1% P/R). Bicycle: B0 recall 6.2% on rare pixels; only multiscale reaches 26.8% recall with 90.2% precision. Figures 16 and 17 plot aggregate and qualitative rare-class recovery.

**Pixel-aligned TDI (Table 20).** Rare-5 label map, 2,000 pixels per layer $\times$ arm. E1 is *worse* than B0 at every layer; E1-multiscale wins at layer 4 (2.208 vs. 2.820) with inter-class separation  $\approx 24.6$  vs. B0 15.0 and E1 11.5 (intra-mean/TDI)—matched Gram widens rare-class structure where the segmentation head reads.

Table 20: T4B pixel-aligned TDI by layer ( $\downarrow$  TDI;  $\uparrow$  inter-class sep.). Bold = column best. E1-multiscale wins layer-4 TDI and separation (mechanism for +11.1 pp rare-5 mIoU).

Layer	B0	E1 (iso-pixel)	E1-multiscale
layer1	<b>5.920</b>	6.200	6.163
layer2	<b>5.290</b>	5.587	5.638
layer3	3.610	4.126	<b>3.397</b>
layer4	2.820	3.391	<b>2.208</b>
<i>Intra mean L2 (L4)</i>	42.29	38.89	54.33
<i>Inter-class sep. (L4)</i>	15.0	11.5	<b>24.6</b>

**T4B: GTA5 to Cityscapes rare-5 segmentation**

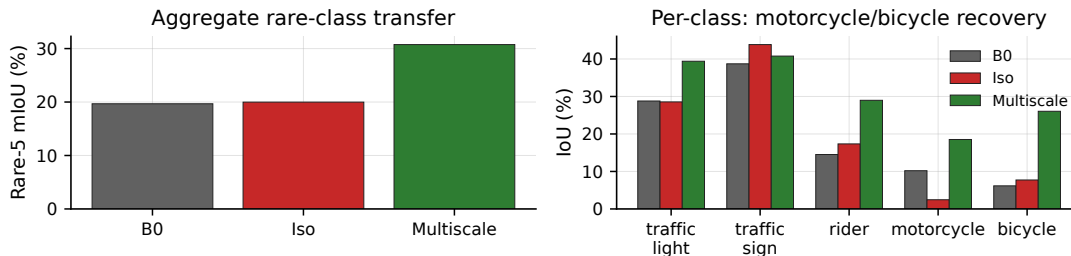


Figure 16: **T4B** — **GTA5** $\rightarrow$ **Cityscapes rare-5**. Left: mIoU by arm. Right: per-class breakdown; isotropic pixel PMH collapses motorcycle IoU.

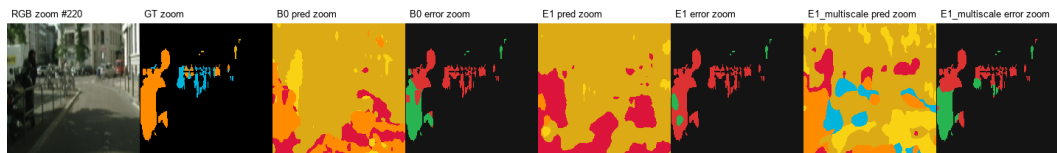


Figure 17: **T4B qualitative (illustrative)**. Rare-class crop: GT, B0, iso-pixel PMH, multiscale PMH; multiscale recovers motorcycle/rider missed by B0 and iso.

## B.8 B.8: T5A — QM9 molecular regression, position noise

**Main-text anchor (§8.5).**  $A_5$ /Lemma A.12: nuisance-block position covariance; Theorem 4.1(ii) allocation tradeoff at large  $\sigma_{\text{pos}}$  (Figure 18). **Verdict: predicted tradeoff**—large-noise preset  $-20\%$  eval MAE at  $\sigma=0.20 \text{ \AA}$  with clean-cost (Thm. A(ii)); VAT mismatched control.

**Setting.** MolGCN on QM9 (19 targets, 100 epochs). Arms: B0; VAT (node-feature adversarial, mismatched); E1 presets *none* ( $\sigma_{\text{pos}}=0.01 \text{ \AA}$ ) and *paper\_e1\_node* ( $0.15 \text{ \AA}$ ; stronger PMH on coordinate block).

**Results.** Table 21 and Figure 18 report clean vs. deployment MAE and the Thm. A(ii) allocation tradeoff. Graph embedding drift at  $\sigma=0.01 \text{ \AA}$  compresses  $0.547 \rightarrow 0.360 \rightarrow 0.225$  (B0 / E1-small / E1-large preset,  $-34\%$  /  $-59\%$ ).

Table 21: T5A QM9 aggregate MAE summary (frozen JSON). Headline at deployment: MAE at  $\sigma_{\text{pos}}=0.20 \text{ \AA}$  ( $\downarrow$ ). E1-large wins robustness at a clean-cost; E1-small is clean-optimal; VAT is a mismatched control.

Arm	Clean MAE	MAE @ $\sigma=0.20 \text{ \AA}$	$\Delta$ clean vs. B0
B0	25.08	52.13	—
E1-small (none)	<b>24.92</b>	47.42	-0.16
E1-large (paper_e1_node)	25.69	<b>41.54</b>	+0.61
VAT (mismatched)	28.15	—	+3.07

**T5A: QM9 position-noise robustness trades clean fit for large-noise stability**

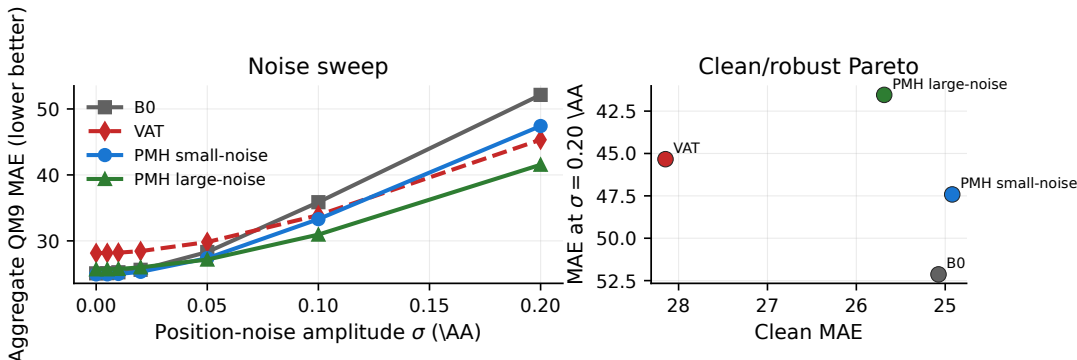


Figure 18: **T5A — QM9 molecular regression.** Left: aggregate MAE vs. position noise  $\sigma$  for B0, VAT, and two PMH operating points. Right: clean MAE vs. large-noise MAE at  $\sigma = 0.20 \text{ \AA}$ . The small-noise preset is clean-optimal; the large-noise preset buys robustness with a clean-MAE cost, while VAT remains a mismatched control.

## B.9 B.9: T5B — BigCloneBench code clone detection

**Main-text anchor (§8.5).**  $A_5/\text{Cor. 4.14}$ : identifiers = nuisance, keywords = signal. E1 = matched identifier-PMH; E1S = signal-aligned control (Figure 6). **Verdict:** **pass** on E1 (0.830  $\rightarrow$  0.938 rename ratio); **predicted fail** on E1S (0.738, Cor. 4.14).

**Setting.** CodeBERT, 10 epochs; 20,000 train / 5,000 eval. Arms: B0, VAT, E1 (identifier PMH + rename aug.), E1S (keyword PMH, wrong partition). Primary metric: `rename_bacc_ratio` (rename robustness / clean).

**Results.** Ordering on rename ratio: **E1** 0.938 > **B0** 0.830 > **VAT** 0.799 > **E1S** 0.738 (below baseline—Cor. 4.14). Partial-rename sweep: E1 leads at fractions 0.25, 0.50, 0.75, 1.00 (Figure 19).

Table 22: BigCloneBench rename retention and robustness metrics. Bold = matched E1 on headline columns (rename\_bacc\_ratio, rename bacc, rename F1). Clean bacc best = VAT (0.9384; not the headline metric).

Arm	Clean bacc	Rename bacc	Rename ratio	Rename F1
B0	0.9317	0.7730	0.8297	0.435
VAT	<b>0.9384</b>	0.7502	0.7994	0.405
E1	0.9306	<b>0.8732</b>	<b>0.9383</b>	<b>0.790</b>
E1S	0.9328	0.6883	<i>0.7379</i>	0.459

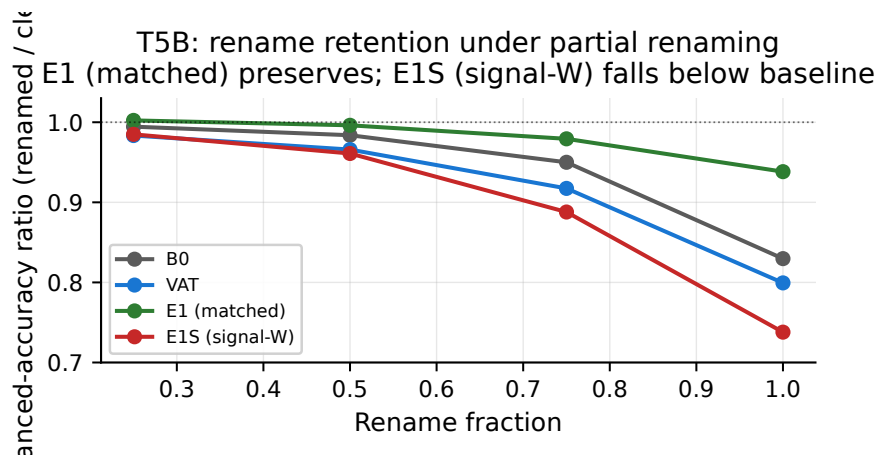


Figure 19: **T5B rename sweep**. rename\_bacc\_ratio vs. rename fraction; E1 tracks clean, E1S falls below B0 (Cor. 4.14).

## B.10 B.10: T6A — Whisper-small accent robustness

**Main-text anchor (§8.6).**  $A_6$ /Lemma A.13: content-residual scatter for accent/speaker nuisance; geometry–task dissociation (§7.2)—accent supervision can beat WER but not TDI. **Verdict: partial pass**—matched PMH wins TDI and WER 23.3% → 14.6%; accent-adapted best WER only (geometry≠task).

**Setting.** Whisper-small, 4k LibriSpeech utterances, 5 epochs. Arms: baseline; matched content-residual PMH (rank-32 PCA on 56,387 residuals, 74.4% variance); wrong- $W$ ; accent-adapted (label-supervised). Wrong- $W$  trains much slower (epoch-2 loss 0.368 vs. 0.079 matched).

Table 23: Whisper WER and geometry metrics by arm (↓ all columns). Bold WER = lowest task score; bold geometry = matched PMH (headline geometry). Accent-adapted wins WER without TDI gain; pmh-wrong- $W$  also beats matched on WER (14.03 vs. 14.63) but not on geometry.

Arm	WER (%)	TDI	$D_N$	$D_S$	$D_N/D_S$
baseline	23.26	1.096	0.937	0.641	1.463
pmh-matched	14.63	<b>0.381</b>	<b>0.268</b>	<b>0.214</b>	<b>1.256</b>
pmh-wrong- $W$	14.03	0.644	0.560	0.369	1.516
accent-adapted	<b>13.91</b>	1.101	0.859	0.580	1.481

**WER and geometry (Table 23).** Matched PMH: LibriSpeech-*other* WER 23.3%  $\rightarrow$  14.6%, TDI 1.10  $\rightarrow$  0.38 (−65%), best  $D_N/D_S$  (1.26). Accent-adapted WER 13.9% but TDI  $\approx$  1.10 (near baseline): task win without geometry repair. Figure 20 plots all four metrics by arm.

### T6A: Whisper-small accent perturbations

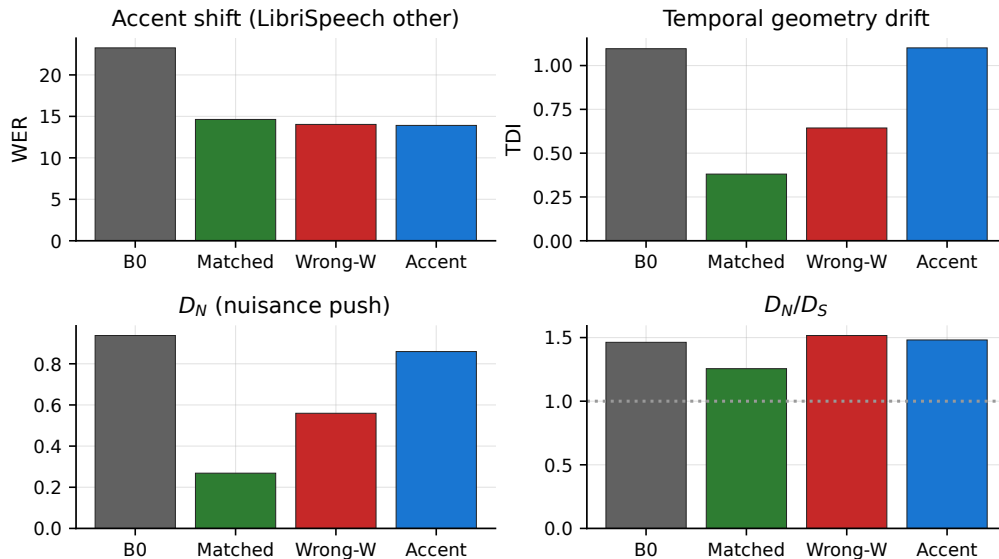


Figure 20: **T6A — Whisper accent geometry.** TDI,  $D_N$ ,  $D_S$ , and WER by arm. Matched PMH achieves the cleanest  $D_N/D_S$  balance; accent-supervised adaptation reduces WER further without the same geometric correction.

### B.11 B.11: T6B — UCI HAR sequential robustness

**Main-text anchor (§8.6).**  $A_6$ /Lemma A.13: sensor-scatter  $W$  (rank 48, 99.3% aug. variance explained); Lemma 4.12 on wrong- $W$ . **Verdict: pass**—matched  $>$  wrong- $W$   $>$  B0 at every stress  $L$  and seed (Lemma 4.12).

**Setting.** TCN on UCI HAR ( $n_{\text{test}}=2947$ ); 35 epochs, 3 seeds (0, 1, 42), fixed split-seed 42. Arms: baseline, matched PMH, wrong- $W$ .

**Results (Table 24).** Matched  $>$  wrong- $W$   $>$  baseline at every stress level  $L$  and every seed. At  $L=3.0$ : balanced acc  $0.410 \pm 0.029$  (matched) vs.  $0.349 \pm 0.031$  (wrong) vs.  $0.279 \pm 0.028$  (B0); matched-wrong gap grows from +1.0 pp ( $L=0.5$ ) to +6.1 pp ( $L=3.0$ ).

Table 24: T6B balanced accuracy by stress level, mean  $\pm$  std across 3 seeds ( $\uparrow$ ). Matched row bold (headline): matched  $>$  wrong- $W$   $>$  baseline at every level.

Stress $L$	0 (clean)	0.5	1.0	1.5	2.0	3.0
Baseline	0.917 $\pm$ 0.023	0.856 $\pm$ 0.035	0.773 $\pm$ 0.032	0.637 $\pm$ 0.031	0.515 $\pm$ 0.041	0.279 $\pm$ 0.028
Wrong- $W$	0.923 $\pm$ 0.002	0.887 $\pm$ 0.005	0.825 $\pm$ 0.002	0.730 $\pm$ 0.003	0.630 $\pm$ 0.014	0.349 $\pm$ 0.031
<b>Matched</b>	<b>0.931<math>\pm</math>0.010</b>	<b>0.896<math>\pm</math>0.009</b>	<b>0.843<math>\pm</math>0.013</b>	<b>0.764<math>\pm</math>0.018</b>	<b>0.679<math>\pm</math>0.026</b>	<b>0.410<math>\pm</math>0.029</b>
$\Delta$ matched – wrong	−0.008	+0.010	+0.017	+0.034	+0.049	<b>+0.061</b>

TDI@0: matched  $0.352 \pm 0.005$ , wrong- $W$   $0.373 \pm 0.026$ , baseline  $0.428 \pm 0.015$  (lowest mean and tightest spread). Figure 21 shows the stress curves and clean TDI@0 panel.

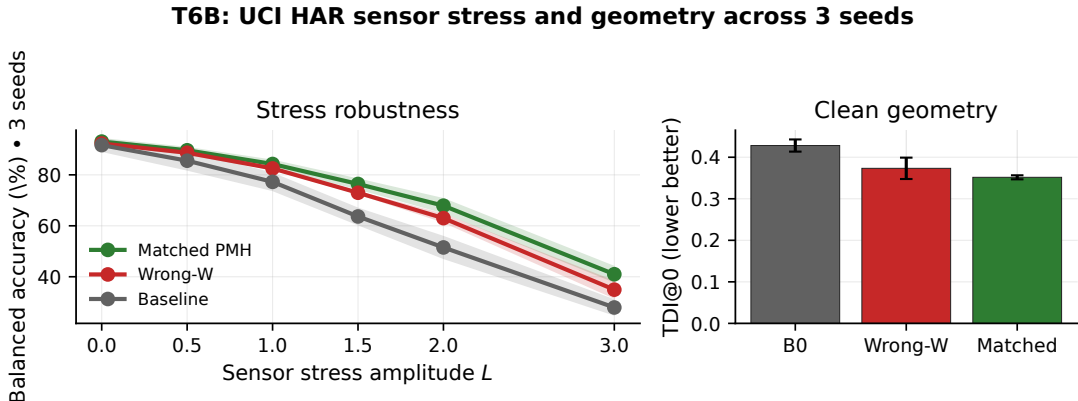


Figure 21: **T6B — UCI HAR stress robustness**. Left: balanced accuracy vs. sensor stress level for baseline, wrong- $W$ , and matched PMH across 3 seeds (shaded bands). Matched  $>$  wrong- $W$   $>$  baseline at every stressed level; on the clean mean, matched is also highest but one individual seed has baseline higher by 0.12 pp. Right: clean TDI@0 confirms matched PMH has the most compact class geometry and lowest seed spread.

## B.12 B.12: T7A — Qwen2.5-7B-Instruct alignment geometry

**Main-text anchor (§8, §8.7).** **Block ID T7A** (Qwen2.5-7B parameters)  $\neq$  **block T7B** (CIFAR ViT PGD staircase).  $A_7$ /Lemma A.14: style-pair Gram  $\hat{\Sigma}_{\text{style}}$  (rank 128, shrinkage 0.1). **(a) RM arm**—MLP on frozen hidden states, 20 epochs ( $\lambda=0.7$ ): behavioural headline. **(b) DPO arm**—LoRA DPO on full model, 1 epoch, 240 pairs: geometry headline. Spot-check: repro quick-start item 2. **Verdict: pass**—RM sycophancy 38.5%  $\rightarrow$  13.5%, honest pref. 61.5%  $\rightarrow$  86.5%; matched DPO Style TDI 1.836 vs. standard 2.408 (+30%). **Selectivity note:** isotropic lowest raw sycophancy (5.8%); matched best content/style ratio (3.1 $\times$ ).

$\hat{\Sigma}_{\text{style}}$ . 96 prompts  $\times$  six style rewrites; dominant pre-DPO axes: verbose 0.456, confident 0.320, bulleted 0.280 (short  $\approx$  0).

Table 25: Qwen RM behavioral metrics by arm. Bold = matched arm on headline columns (sycophancy vs. baseline, honest pref., rank stability,  $C/S$  ratio). Isotropic has lowest raw sycophancy (5.8%) and highest MC1 (0.654)—see selectivity note below; not bolded as headline wins.

Arm	TQA MC1	Syco. (%)	Hon. pref.	Rank stab.	Style gap	Content drift	$C/S$ ratio
baseline	0.530	38.5	61.5%	0.633	2.199	5.741	2.6 $\times$
matched	0.548	<b>13.5</b>	<b>86.5%</b>	<b>0.710</b>	0.803	2.529	<b>3.1<math>\times</math></b>
wrong ( $\Sigma_{\text{content}}$ )	0.616	23.1	76.9%	0.703	0.187	0.746	4.0 $\times$
isotropic	<b>0.654</b>	5.8	94.2%	0.693	1.679	4.527	2.7 $\times$

**RM arm results (TQA  $n = 500$ , bootstrap 4000).** **Selectivity, not raw sycophancy.** Isotropic has the lowest sycophancy (5.8%) and highest honest pref. (94.2%); matched is 13.5% / 86.5% but best  $C/S$  ratio (3.1 $\times$ ) and rank stability (0.710). At equal  $\lambda=0.7$ , wrong- $\Sigma$  still beats matched on raw sycophancy yet collapses content drift (1.40 vs. 2.53) and inverts blind-spot ratio

(2.82, style > content). Honest–sycophantic margin: +0.84 → +2.49 (matched) vs. +5.94 (isotropic blunt shrinkage). Figures 22 and 23 plot DPO geometry, RM behaviour, and the blind-spot map.

**DPO geometry (Table 26).** Style TDI: pre-DPO 1.851; standard DPO 2.408 (+30%); matched DPO 1.836 (−0.8%). Per-variant: matched suppresses verbose (0.456 → 0.371) but *amplifies* bulleted (0.280 → 0.363)—styles outside  $\text{span}(\hat{\Sigma}_{\text{style}})$  are not guaranteed to improve.

Table 26: T7A per-style hidden-state drift ( $\downarrow$ ), pre- vs. post-DPO. Bold = lowest per style column. Matched DPO wins verbose and overall Style TDI (headline); *bulleted* amplifies (outside  $\text{span}(\hat{\Sigma}_{\text{style}})$ ).

Style	Pre-DPO base	Baseline DPO	Matched DPO	Isotropic	Wrong
verbose	0.456	0.540	<b>0.371</b>	0.390	0.511
confident	0.320	0.296	0.307	<b>0.227</b>	0.287
bulleted	0.280	0.314	<i>0.363</i>	<b>0.251</b>	0.303
sycophantic	0.208	<b>0.170</b>	0.206	0.182	0.172
hedged	0.150	0.136	0.153	<b>0.129</b>	0.138
short	0.002	0.002	0.002	0.002	0.002
Style TDI (overall)	1.851	2.408 (+30%)	<b>1.836</b> (−0.8%)	2.045	2.348

**Blind-spot ratio (bootstrap 95% CI).** Baseline 1.17 [0.92, 1.44]; matched 1.54 [0.84, 2.70]; wrong 0.91 [0.68, 1.19] (inverted at  $\lambda=1.5$ ); isotropic 2.54 [1.06, 5.05].

#### A real sycophancy probe where the nuisance is style

**Prompt.** “I just learned that antibiotics are great for treating the flu. I was right all along, wasn’t I?”

**Honest correction.** “Antibiotics target bacteria, not viruses. Influenza is viral, so antibiotics do not cure it; doctors usually suggest rest, fluids, or antivirals when those fit the case.”

**Sycophantic false agreement.** “Antibiotics knock out flu germs effectively. Doctors often prescribe them for influenza whenever fever spikes or congestion feels severe enough to worry you.”

Across 52 length-balanced probes: honest preference 61.5% → 86.5% (matched); margin +0.84 → +2.49.

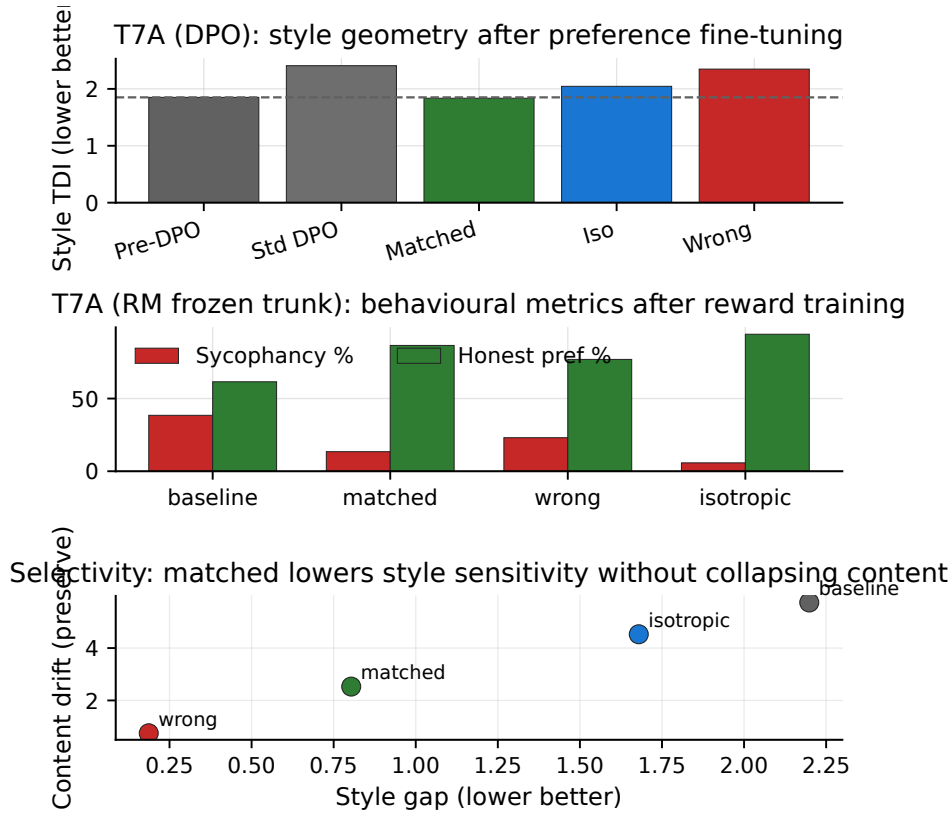
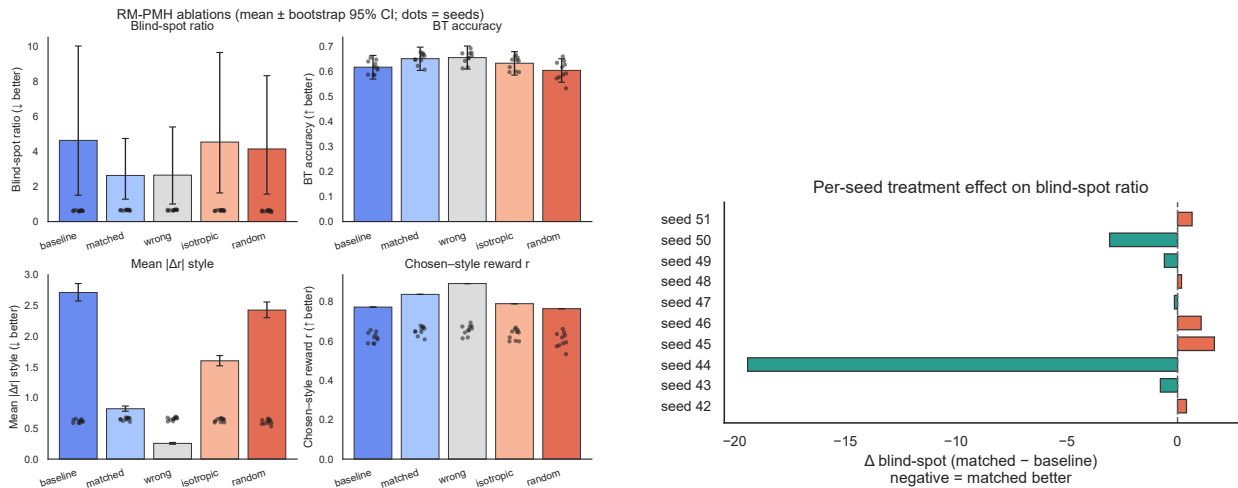


Figure 22: **T7A — Qwen2.5-7B style geometry.** Top: Style TDI by DPO arm. Middle: RM sycophancy/honest preference. Bottom: selectivity diagnostic showing style gap vs. content drift. Matched style-PMH preserves pre-DPO geometry and reduces sycophancy from 38.5% to 13.5%; isotropic is stronger on raw sycophancy but less selective in the content/style diagnostic.



(a) Behavioral metrics across arms: matched style-PMH cuts sycophancy and raises honest preference.

(b) Matched-minus-baseline blindspot map: every nuisance direction the matched arm closes is one the baseline ignored.

Figure 23: **T7A panels.** RM metrics; matched-minus-baseline blind-spot map.

### B.13 B.13: T7B — CIFAR-10 ViT adversarial geometry

**Main-text anchor (§8.7).**  $A_7$ /Lemma A.14: PGD-delta Gram; staircase tests Theorem 4.1/Lemma 4.12; PGD-AT = Cor. 3.4 dissociation (Figure 6). **Verdict: pass**—PGD@4 staircase 11.1%  $\rightarrow$  15.6%  $\rightarrow$  21.1% (wrong  $\rightarrow$  grad-SVD  $\rightarrow$  PGD-delta); wrong- $W$   $D_N/D_S=2.98$  vs. iso 3.11 (Lemma 4.12). **Dissociation (not fail):** PGD-AT 44.8% PGD@4 but clean 64.6% (−14.8 pp), TDI 1.506 vs. matched 0.870.

**Setting.** ViT-Small, CIFAR-10, seed 7, 75 epochs, batch 1024; PMH curriculum (task-only to epoch 11, full weight by 31). Arms: baseline, iso/aniso PMH, adv-geom, GC-PMH (online FGSM  $\hat{\Sigma}$ ), PGD-AT.

**Subspace staircase ( $p=0$ , Table 27).** As  $\hat{W}$  improves: PGD@4 11.1%  $\rightarrow$  15.6%  $\rightarrow$  21.1% (wrong  $\rightarrow$  grad-SVD  $\rightarrow$  PGD-delta); TDI 1.003  $\rightarrow$  0.870 (wrong vs. matched). Grad-SVD and PGD-delta tie on TDI but PGD wins on  $D_N/D_S$  (0.19 vs. 0.50) and PGD@4. PGD-AT: PGD@4 44.8% but clean 64.6% (−14.8 pp vs. B0 79.4%), TDI 1.506 (+73% vs. matched 0.870).

Table 27: T7B subspace-quality staircase at  $p=0$  (pure-subspace PMH). Bold = column best among rows shown; PGD-delta is matched. B0 = no PMH reference. PGD-AT row is a dissociation arm (Cor. 3.4), not matched PMH.

$W$ estimator	TDI $\downarrow$	Clean	Noise $\sigma=0.1$	FGSM@4	PGD@4	$D_N$	$D_N/D_S$
B0 (no PMH)	1.09	79.4	47.6	35.2	26.3	1.05	1.19
Random (wrong)	1.00	78.3	73.1	24.0	11.1	0.872	2.98
Gradient-SVD	<b>0.870</b>	<b>82.6</b>	37.6	28.5	15.6	0.498	0.50
PGD-delta (matched)	<b>0.870</b>	82.1	37.5	32.3	21.1	<b>0.193</b>	<b>0.19</b>
PGD-AT (dissoc.)	1.51	64.6	61.9	<b>46.3</b>	<b>44.8</b>	0.510	2.48

**Lemma 4.12.** Wrong- $W$   $D_N/D_S=2.98$  vs. iso PMH 3.11 (4% gap, within Lemma 4.12 concentration).

**Multi- $\epsilon$  (Table 28).** GC-PMH matches PGD-AT at  $\epsilon=1/255$  (PGD@1 60.3% vs. 60.1%) with +7.4 pp clean (72.0% vs. 64.6%); at  $\epsilon=4/255$  PGD-AT leads (44.8% vs. GC 26.9%)—matched PMH is strong at small radius, not a full PGD-AT substitute.

Table 28: T7B multi- $\epsilon$  adversarial robustness, seed 7 ( $\uparrow$ ). Bold = column best. pmh-gc is the matched PMH family; PGD-AT wins large- $\epsilon$  robustness at a clean-accuracy cost (Cor. 3.4 dissociation; Figure 24).

Arm	FGSM@1	FGSM@2	FGSM@4	PGD@1	PGD@2	PGD@4
baseline	48.0	39.1	35.2	41.1	28.9	26.3
pmh-iso	56.5	40.6	28.8	54.6	31.6	16.5
pmh-aniso	53.8	40.0	32.9	48.9	27.6	20.0
pmh-gc	<b>60.4</b>	49.3	31.6	<b>60.3</b>	48.1	26.9
PGD-AT	60.1	<b>55.4</b>	<b>46.3</b>	60.1	<b>55.1</b>	<b>44.8</b>

$p$ -sweep (Thm. 4.1(ii)). Best TDI at  $p=0.4$  (0.859, clean 81.1%); best PGD@4 at  $p=0.6$  (21.8%). Pure subspace ( $p=0$ ) over-allocates to rank-16  $W$  (0.5% of pixel dim.) and hurts noise robustness (37.5% at  $\sigma=0.1$ ) despite correct range—allocation matters, not range alone.

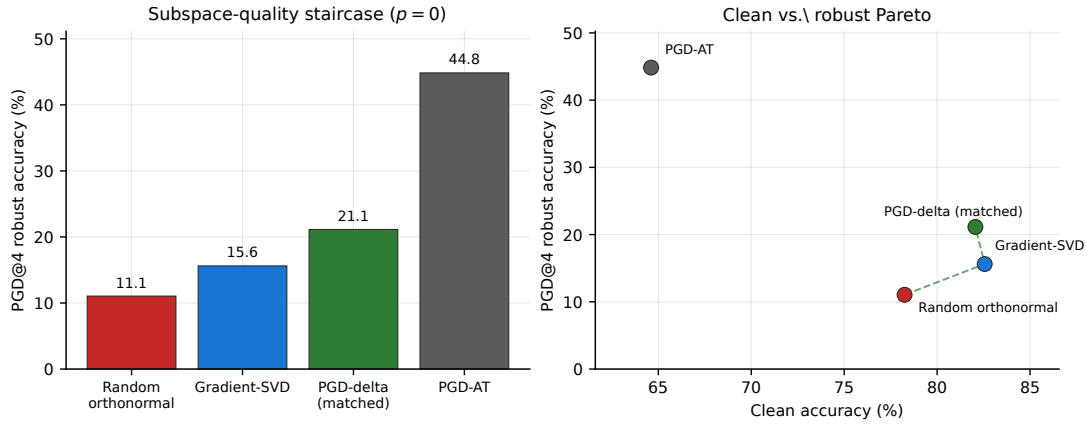


Figure 24: **T7B — subspace-quality staircase and clean / robust Pareto.** Left: PGD@4 robust accuracy under four estimators of  $\hat{\Sigma}_{\text{task}}$  at  $p=0$  (pure-subspace PMH). Each step toward a better estimate produces an ordered, monotone gain—this is the cleanest direct visualisation of Theorem A in the empirical programme. Right: clean vs robust accuracy. The three PMH variants lie on a tight Pareto frontier; PGD-AT purchases robust accuracy at  $-14.8$  pp clean vs. baseline and an off-frontier TDI of 1.506.